Royal Netherlands
Meteorological Institute
Ministry of Infrastructure and the Environment

Trends and related causes in extreme hourly precipitation

Mendy van der Vliet

KNMI Internal Report IR-2016-07

Utrecht University

Faculty of Science

Master thesis

Trends and related causes in extreme hourly precipitation

Author:
Mendy van der Vliet

Supervisor:
Dr. Peter Siegmund (KNMI)
Dr. Willem Jan van de Berg (UU)

October 5, 2016

Universiteit Utrecht

Koninklijk Nederlands
Meteorologisch Instituut
Ministerie van Infrastructuur en Milieu

Acknowledgments

I would like to express my gratitude to my daily supervisor of the Royal Netherlands Meteorological Institute (KNMI), Peter Siegmund, whose patience, guidance and encouragement, helped considerably with my master thesis. I am very grateful that Peter was always willing to make time for me. I appreciate much his assistance in writing this thesis, learning me to report in a clear and concise way. Furthermore, I would like to thank my supervisor from Utrecht University, Willem Jan van de Berg, for keeping me sharp by asking critical questions, and encouraging me during the entire graduation experience. Finally, I would like to thank Aarnoud van Delden for reading my thesis as second supervisor, and being such a helpful master coordinator.

A very special thanks goes to Martin Roth, whose motivation, persistence and expertise, made a true difference to my master thesis. He guided me superbly in the world of statistics and dynamic reporting. By his doing I did not only finished my master thesis, but also learned in an independent manner how to apply trend analysis and how to use R, Knitr, and Version Control System in a smart and interactive way.

I must also acknowledge Jules Beersma, Geert Lenderink, and Gerard van der Schrier, for taking time out from their busy schedules to advice me in multiple stages of my research. I am also grateful to Siebren de Haan for providing me with CAPE data.

Additionally, I would like to thank the KNMI, and especially its director Gerard van der Steenhoven and my department head Albert Klein Tank, because of the motivating and inspiring work ambiance. As an internship I felt completely equal to my (superior) colleagues and was motivated to take part in multiple innovation working groups (e.g. Data Reproducibility, Product Life-cycle Board, KNMI Hackathon and KNMI Connected). The thrust from the KNMI was even that high that I won the KNMI innovation competition, the Dragons Den, as leader of the latter group. I would not been able to do this without the loyal support, criticism, geniusness and jokes of my team members: Alessandro, Suzanne and Andrej.

I would also like to thank Rike Hattem van-Schielen, and Matty Bos, organizing bosses of the Climate Hackathon, and Michiel van Dongen, by supporting me to realize my own project, The Green Tree, a real-time air quality visualization tool. During my bachelor and master I discovered my research passion and talents, but it was only in the end of masters, in the internship at the KNMI, that I discovered my creativity and ambition towards innovation of science.

In conclusion, I recognize that this research would not have been so fun without my roommate and personal assistant, Patrick van den Hoek, and other young colleagues of the KNMI. Last but not least, I am so thankful to Ina, Jako, Lysanne, Rody and Evert, for their financial and emotional support.

Contents

List of Figures

List of Tables

Abstract

The intensity and frequency of (extreme) precipitation are likely affected by climate change. While many studies have focused on trends in extreme daily sums, extreme precipitation often occurs on shorter timescales. The present work aims to assess and understand trends in intensity and frequency of hourly extreme precipitation for 5 stations in the Netherlands (De Bilt, De Kooy, Vlissingen, Maastricht and Eelde) for the period 1958 until 2015.

Robust signals are found in hourly precipitation data with spatial and seasonal variation in magnitude and number of significant trends. Multiple significant trends ($p > 95\%$) for independent 2-day periods show a rapid increase of the (25-5%) highest intensities, a decrease in the frequency of wet hours (of the mean and 50-0.1% wettest 2-days), and a constant to increasing signal in the mean and (10-1% highest) precipitation sums.

Our study confirms previous findings (IPCC, 2013) that the "high" extremes increase in a disproportional way, compared to the yearly mean and "low" extremes.

To explain the observed trends, we studied from theory and by statistical analysis four important factors for extreme precipitation, (i) temperature, (ii) dewpoint temperature, (iii) CAPE and (iv) wind speed. The observed trends in precipitation intensity are likely caused by the increase in temperature, via Clausius-Clapeyron related increase of the atmospheric "moisture-holding capacity". This finding matches well with our observed negative trends in the frequency of wet hours, as warmer air becomes less easily saturated.

Promising for future research is the integration with high-resolution (e.g. satellite and radar) observational data, testing of models' capability to capture extreme precipitation and scaling up the research to larger regions such as Europe.

Chapter 1

Introduction

1.1 Background

One of the meteorological factors affecting our society the most are changes in precipitation (Berg and Haerter, 2013a). In particular the extreme events regarding precipitation give rise to natural hazards such as floods and droughts, of which the impact is determined by the occurrence, magnitude and location (Trenberth and Parsons, 2003; IPCC, 2013).Resultant from extreme precipitation are multiple forms of damage to private and public assets, as well as temporary disruption of social and economic activities (Cramer and Tibig, 2014, p.998) such as traffic or long-term socioeconomic effects related to crop production (Rosenzweig and Bloomfield, 2002; Koetse and Rietveld, 2009). Therefore, the Fourth Assessment Report(AR4) of the Intergovernmental Panel on Climate Change (IPCC) emphasized the importance of understanding the changes of weather extremes in time. As climate change can cause changes in the probability of occurrence or the severity of extreme weather events, it could drive trends in temperature and precipitation extremes (IPCC, 2013).

The AR5 of the IPCC concluded that it is likely that since 1951 there have been in more regions where there have been statistically significant increases in heavy precipitation events (e.g. above the 95ht percentile) than regions where there have been statistically significant decreases (IPCC, 2013). Note that there are strong seasonal and (sub)regional variations in the trends. For Europe, from 1951 to 2010, Besselaar and Buishand (2013) found a median reduction in 5- to 20-year return periods for extreme precipitation events of 21% with a range between 2% and 58% depending on the subregion and season. However, the annual heavy precipitation events have increased globally in a disproportional way compared to mean changes between 1951 and 2003 over various mid-latitude areas, even in regions where a reduction was found in the mean (IPCC, 2013). This difference in changes between mean and extreme precipitation can be explained from the fact that the global-mean precipitation is constrained by the energy budget of the atmosphere, while the extreme events depend in a non-linear way on the moisture availability (Pall and Stone, 2007; IPCC, 2013). With global warming, the moisture-holding capacity of the atmosphere rises. Under the constraint of constant relative humidity, changes in the uppermost quantiles of precipitation are expected to be thermodynamically related to temperature following the Clausius-Clapeyron (CC) equation (approximately 7% increase per degree of warming)(Pall and Stone, 2007). According to multiple studies (Pall and Stone, 2007; Lenderink and Van Meijgaard, 2010; Hardwick Jones and Sharma, 2010; Lenderink and Van Oldenborgh, 2011) this is because the heaviest events are expected when all the moisture in a volume of air is precipitated out.

Changes in temperature, and more directly in dewpoint temperature (as measure of the saturation level of the air) (Lenderink, Meijgaard, and Selten, 2009) can thus be seen as explanatory factors for trends in extremes. Furthermore, vertical instability is important for the formation of

intense rain showers (Monkam, 2002; Adams and Souza, 2009; Loriaux and Siebesma, 2013). Next to temperature, dewpoint temperature and vertical instability, the degree of wind shear can be an important factor for trends in extreme precipitation (Brauer, 2007; Trenberth, 2011). Wind shear can namely influence the intensity of precipitation via the organisation of precipitation systems (Browning, 1964; Sumner, 1988; Weisman and Klemp, 1982; Wingo and Cecil, 2010).

1.2 Relevance of this study

While numerous studies (e.g. Zhang and Niitsoo (2000), Klein Tank et al. (2002), Sen Roy and Balling (2004), Zhai (2005), Buishand and Brandsma (2013), Daniels and Holtslag (2014), and Roth and Jongbloed (2015)) have investigated trends in datasets of daily precipitation sums, trend analysis on datasets of hourly precipitation sums has only been done in recent years (Lenderink and Van Meijgaard, 2008; Sen Roy, 2009; Lenderink and Van Oldenborgh, 2011). In contrast to daily data, hourly data provides the possibility to capture short-lasting, intensive precipitation. Analysis thereof is essential regarding precipitation extremes. On a daily basis, long-lasting, weak stratiform precipitation could add up to a relatively high daily sum, while one single convective extreme precipitation event could produce the the same daily sum (see Chapter 3 for information about cloud types). Thus, the combination of duration and intensity indicates what kind of precipitation mechanism is producing the event in question.

Lenderink and Van Meijgaard (2008), Lenderink and Van Meijgaard (2010), and Lenderink and Van Oldenborgh (2011) studied the relationship between hourly precipitation intensity and temperature and/or dewpoint temperature and found a super Clausius-Clapeyron(CC)-scaling for the Netherlands, Belgium, Switzerland and Hong Kong. Although, scaling beyond that expected from thermodynamic theories is controversial. Haerter and Berg (2009) argued that the scaling is a statistical product of the transition from large-scale to convective precipitation with temperature. Besides, they suggest that studying extremes on an hourly basis instead of a daily basis, implies a shift from more large-scale-dominated rain events to convective-dominated events, because the latter type occurs during a shorter time scale than the former type. Overall, convective precipitation is characterized by higher intensities than stratiform precipitation (Berg and Haerter, 2013a). As convective (large-scale) precipitation occurs more often at high (low) temperature, this could explain the super CC-scaling with temperature (Haerter and Berg, 2009).

Moreover, from the few studies based on hourly precipitation sums almost none of them have considered differentiating trends on season and/or region within the Netherlands and Europe. However, mechanisms behind precipitation extremes are related to the climate at that location and season. For instance, significant trends in daily summer precipitation amounts were restricted to coastal regions, assumedly explained by an increase in the sea surface temperature (Lenderink, Meijgaard, and Selten, 2009). Additionally, Daniels and Holtslag (2014) concluded that the distance to the coast is a more important factor for the seasonal mean precipitation and quantiles of wet-day precipitation amounts than soil type, topography or urbanization.

Next to spatial factors, the time of the year can be important for the type of precipitation. Buishand and Brandsma (2013) found trends over the period 1951-2009 for annual precipitation and seasonal amounts, with the strongest increases in the winter season. This is consistent with the increases found in western and central Europe (Besselaar and Buishand, 2013). For this part of Europe, the relative contribution of the synoptic weather systems is prevalent to winter precipitation, while local thunderstorm-like events dominate summer precipitation . The probability density function of wet events consists of the sum of large-scale and convective precipitation. As both types of precipitation differ in intensity, frequency and duration, it is relevant to study changes differentiating on time scale, season and location.

1.3 Aim and structure of this study

This thesis aims at understanding how extreme hourly precipitation in the Netherlands change in time and what the mechanism is behind these changes. In a threefold approach we investigated this: (i) analyzing seasonal and spatial characteristics of hourly precipitation, (ii) applying trend analysis on 2-day maxima in hourly precipitation intensity, 2-day frequencies of wet hours and 2-day precipitation sums for five stations, and (iii) deriving key variables for changes in extreme precipitation from theory and strength of correlation and thoroughly investigating time related changes for the maxima of the key variables themselves and for their relationships with precipitation maxima. The present work concentrates on five Dutch stations; De Kooy, De Bilt, Eelde, Vlissingen and Maastricht.

This thesis has been divided into 6 chapters. In the first Chapter, the Method Chapter, we describe the type of data used and the data quality. Here, we also explain how we define extremes, how we apply trend analysis and investigate the reason for the observed trends. In Chapter 3, we describe from theory the conditions favorable for the production of extreme precipitation and the different cloud types. This provides us with the basic knowledge required to be able to interpret spatial and seasonal variability in precipitation data, which is studied and reported in Chapter 4. The importance of spatial and seasonal factors is analysed for the intensity and frequency of wet hours and the intensity of extremes. Consequently, we decide that it is relevant to study the trends of hourly precipitation extremes for the five stations in the Netherlands separately instead of bundling the station data to enhance the chance on trend detection. We also defined two key seasons based on the seasonal dependence of the precipitation characteristics. This spatial analysis combined with differentiating on season, provides more detailed and robust knowledge about changes in hourly precipitation.

In Chapter 5, we present the results of trend analysis in precipitation characteristics between 1958-2016 for the five stations. We investigate whether extreme intensities increase or decrease in time. Thereby, we compare these trends to trends in mean intensity and compare the trends in extreme and mean intensities between the different stations. Furthermore, we examine trends in precipitation frequency and study whether we observe trends in the 2-day precipitation sum as excepted as the product of the trends in intensity and frequency. In this trend analysis both ordinary least-square, and quantile regression is applied. Based on how the data is distributed, these regression techniques are used solely or in combination. The significance of all fitted regression slopes is investigated in a 9999 Monte Carlo Permutation test.

The fifth part (Chapter 6) attempts to identify and attribute variables responsible for the detected trends in Chapter 5. We defined key variables based on theory and their strength of correlation with precipitation maxima. Furthermore, time regression is applied on temperature, dewpoint temperature, Convective Available Potential Energy (CAPE) and wind speed to observe if their trends match the trends found for precipitation intensity. Besides, we verify whether the super Clausius-Clapeyron scaling found by Lenderink and Van Meijgaard (2008), Lenderink, Meijgaard, and Selten (2009), and Lenderink and Van Oldenborgh (2011) is present in our hourly data and if it may be attributed to mixing of winter-and-summer-dominated processes only or to the evolution of the climate state in time. Additionally we investigate whether changes in precipitation intensity maxima are the result of changes in the distribution(s) of the key variable(s) and/or whether these are the result of changes in the relationship of precipitation intensity with the key variable(s).

Lastly, we end with a discussion of the research method and results and present the main conclusions (Chapter **??**).

Chapter 2

Method

2.1 Introduction

In this chapter an overview is given of the method involved in this work. Firstly, the type of data used in the present work and its quality is described. Secondly, theory about linear trend analysis and quantile regression is discussed, which forms the basis for Chapter 5. Furthermore, the underlying assumptions of trend analysis are discussed. Moreover, methods of fulfilling the assumption of independence and testing for significance are given. Lastly, we elaborate on how we expanded the general statistical analysis in such a way that the causes behind the detected trends in hourly precipitation can be investigated. This part of the method includes Pearson and Spearman correlations and regression of binned quantiles, of which the results are shown in Chapter 6.

2.2 Data

2.2.1 Time and place

For the first part of this thesis hourly rain gauge data is used from five stations in the Netherlands. Taking into consideration the need for having an as long as possible consistent time series as well as data which is spatially representative for different parts of the country, we were left with data of five stations. These stations are: De Kooy (235), De Bilt (260), Eelde (280), Vlissingen (310) and Maastricht (380), of which the location is shown in Figure 2.1. Coordinates and altitude of the stations are listed in Table 2.1. For each station data is available on hourly resolution of which the following variables are used in this study: time, hourly precipitation sum, duration (defined as the hourly time fraction of precipitation), temperature, dew point temperature, relative humidity, wind strength and CAPE (source data: `http://www.knmi.nl/nederland-nu/klimatologie/uurgegevens`).

As our focus of interest is precipitation extremes and their lifetime is often on the sub-hourly to hourly scale, we have chosen a time period by considering both a high resolution as well as a long enough time span for the detection of trends. For the period from 1958 until 2015 coherent time series for all stations are present, which can be easily compared and simultaneously analysed. Only CAPE data are more restricted in time and place. These CAPE observations are derived from radiosonde measurements at the Bilt in the period 01-03-1993 until 2015 (source: de Haan, 2016), and are not available for the other stations. Moreover, CAPE measurements also differ in temporal resolution, from a mean of 4 per day to 1 per day in the course of time (see Figure 2.2). Days which were thought to be of meteorological interest, have up to 5-6 CAPE measurements per day.

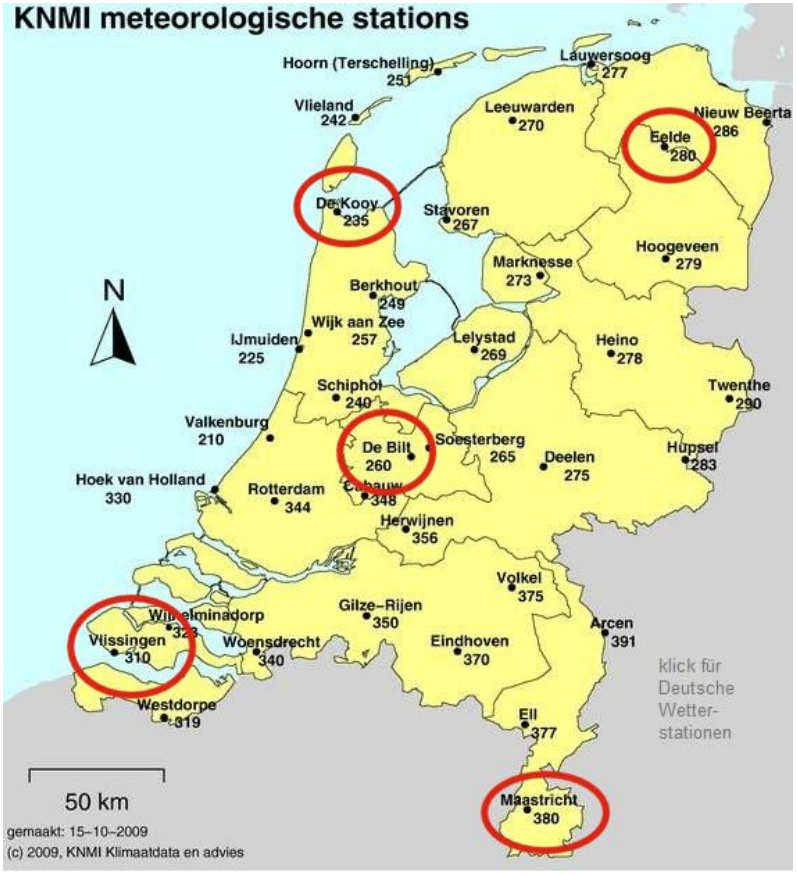

Figure 2.1: A map of the Netherlands showing the locations of the five stations; De Kooy (235), De Bilt (260), Eelde (280), Vlissingen (310) and Maastricht (380).

Table 2.1: Station location and altitude

Station	STN	LON(east)	LAT(north)	ALT (m)
De Kooy	235	4.785	52.924	0.50
De Bilt	260	5.177	52.101	1.90
Eelde	280	6.586	53.125	3.50
Vlissingen	310	3.596	51.442	8.00
Maastricht	380	5.768	50.910	114.00

2.2.2 Type of data and instruments

The variables investigated in this thesis, and their unit, resolution and measurement instrument, are listed in Table 2.2. Precipitation intensity is defined as the mean hourly intensity in mm hr^{-1}, so the accumulated rain amount per hour. CAPE is defined as the amount of energy available for free convection, in Joule/kg, and computed as the amount of work done by the buoyancy force in a parcel of air that is lifted from the lifting condensation level to the level of no buoyancy (Lin, 2007),

$$CAPE = \int_{z_{LCL}}^{z_{LNB}} g(\frac{T - \bar{T}}{\bar{T}})dz \tag{2.1}$$

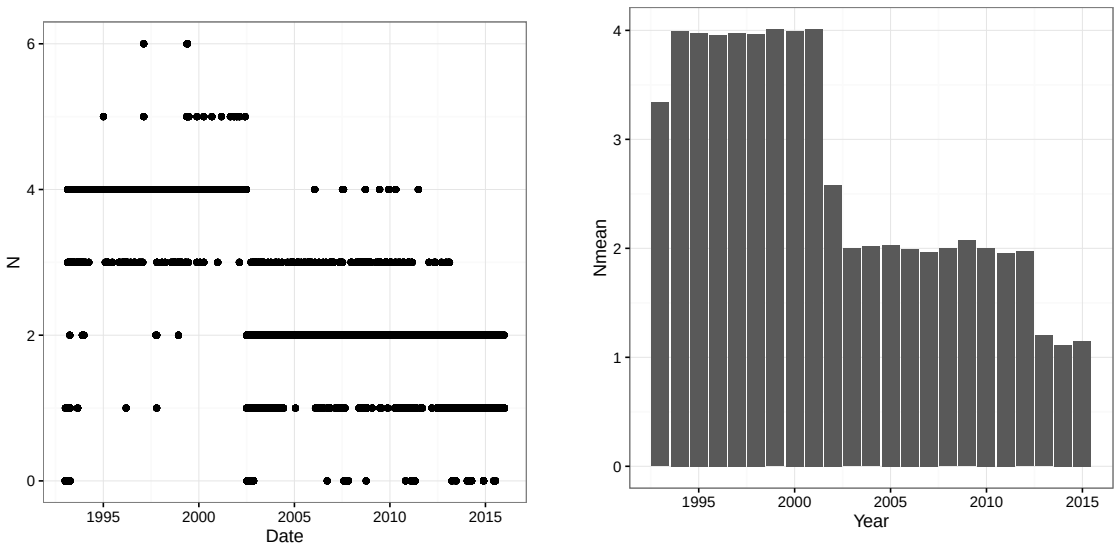

(a) The number of observations (N) per day

(b) The yearly mean number of measurements per day

Figure 2.2: The number of CAPE measurements (N) per day showed as a point cloud in a, and the yearly average per day, represented by bars, in b.

In this equation T is the temperature of the air parcel (the temperature inside the radiosonde), and $\bar{T}$ is the temperature of the environment. Furthermore, g is the gravitational acceleration and z_{LNB} the height at the level of no buoyancy and z_{LCL} the height of the lifted condensation level. For more information about the instruments involved and the exact instrument setup for each variable, see KNMI (2000a, Chapter 14).

Table 2.2: Data characteristics

Name	Unit	Resolution	Instrument
Precipitation	Hourly sum in mm (=liter m^{-2})	0.1 mm	Automatic rain gauge
Duration	part of the hour	0.1 hour	Rain sensor
Temperature	°C	0.1 °C	Electronic KNMI Pt-500 sensor
Dewpoint temperature	°C	0.1 °C	KNMI Pt-500 and E&E33 sensor
CAPE	J kg^{-1}	1 J kg^{-1}	Radiosonde
Relative humidity	%	1 %	E&E33 sensor at 1.5m height)
Wind strength	Hourly mean m/s	0.1 m/s	AWS at 10m height

Until the beginning of the nineties all precipitation measurements were conducted manually with a pluviograph. This is an instrument which measures the amount of water fallen into the rain gauge with the help of a plastic graduated cylinder (KNMI, 2000a, Chapter 6). Between 1963 and 1981 the manual rain gauges of the different stations were replaced by gauges with an orifice, collecting area from 200 cm^2 instead of 400 cm^2, of which the effect is considered to be small (Denkema, 1980; Denkema, 1981; Warmerdam, 1981; Brandsma, 2014). Measurement uncertainties of manual rain gauges may be caused by wind-induced transport of water droplets or snow flakes, evaporation of droplets or loss due to water pouring over (to the graduated cylinder).

These errors can be reduced by choosing a good environment (KNMI, 2000a, Chapter 6).

Since 1991 (Eelde and Maastricht) or 1993 (De Kooy, De Bilt and Vlissingen) the rain measurements are automatized (see Table 2.3). Table 2.3 summarizes the most important historical changes for the five stations regarding precipitation measurements (from `http://projects.knmi.nl/klimatologie/metadata/`). For historical changes of the other meteorological parameters than precipitation, go to the KNMI site (`http://projects.knmi.nl/klimatologie/metadata/`).

Figure 2.3: Example of a manual gauge (with the rim at 0.4 m).

The newer rain gauge automatically registers the height of the float, which is attached to a potentiometer, representing the amount of fallen precipitation (KNMI, 2000a, Chapter 6). Any precipitation fallen in the solid phase is first melted by heating of the funnel, in order to be measured in the liquid phase. An illustration of the so-called KNMI rain gauge is given by Figure 2.4 (for more information see Wauben (2004)). The common setup of an automatic measuring site is the English setup (Figure 2.5). In a comparison study between manual and automatic networks of rain gauges, Brandsma (2014) concluded that automatic rain gauges measure 5-8% less on annual basis (6.5% averaged over the entire period 2001-2013).

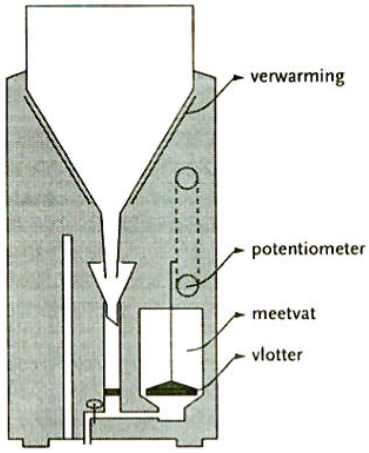

Figure 2.4: The design of an automatic rain gauge (KNMI, 2000a, Chapter 6).

Figure 2.5: An automatic rain gauge of the KNMI in English setting (Brandsma, 2014).

In English setup the gauge is placed on a small concrete box with a drainage tube in the middle of a circular wall with a diameter of 3 meters (Brandsma, 2014). The standard height of both the top of the rain gauge and the wall is 40 cm. See Brandsma (2014) for further details about the material and environment surrounding the pit. The English setup was implemented to prevent wind-induced loss, however in a study of Braak (1945) this is contradicted. Currently, most rain gauges are no longer in the English setup, but situated in an Ott windscreen. Compared to the English set up, Wauben (2004) concluded that the Ott wind screen has a (extra) reduction in the annual mean precipitation of 1.5% (to 6% in windy conditions). For further details about the measurements in temperature, dewpoint temperature, wind direction and wind speed, see KNMI (2000b).

The hourly precipitation data are rounded to 0.1 mm (Table 2.2), except for the hourly pre-

Table 2.3: Historical changes in precipitation data

Orifice area reduction from 400 to 200cm^2		
Station	When	
De Kooy	19720801	
De Bilt	19810401	
Eelde	19730502	
Vlissingen	19620410	
Maastricht	19760701	
Automatic measurement		
Station	When	
De Kooy	19930101	
De Bilt	19930301	
Eelde	19910316	
Vlissingen	19930501	
Maastricht	19910301	
Ott windscreen		
Station	When	
De Kooy	20070426	
De Bilt	20080925	
Eelde	20090518	
Vlissingen	-	
Maastricht	-	
Relocation of instrument		
Station	When	How much
De Kooy	-	-
De Bilt	20080925, 13.00 UT	200 m
Eelde	19730501	750 m
Vlissingen	-	-
Maastricht	20051101	1770 m

cipitation sums of < 0.05 mm. For this study we rounded hourly precipitation sums of < 0.05 mm to 0 in order to have a consistent rounding. This leads to more dry hours ($\pm$ 8% of total amount of hours). For frequency analysis we could argue to include these hours and code them as wet, however for intensity analysis this is not desired. The exact amounts are namely not known. Therefore, we choose for a consistent data set, in which wet hours are defined as hours in which precipitation accumulates to amounts higher than 0.05 mm. Furthermore, we converted the unit from sums (or degrees, speeds) of 0.1 mm (°C, m/s) to sums (or degrees, speeds) of 1 mm (°C, m/s).

Moreover, for some research questions in this thesis we only consider wet hours, days, daily or 2-days maxima. For instance in Chapter 4 we analyse only wet hours, when we are interested in the characteristics of precipitation events. In Chapter 6 we are interested in the correlation between precipitation and other variables. Therefore, when considering daily or 2-day maxima in intensity, we only take into account wet maxima (higher than 0.05 mm/hr). Another reason to investigate the statistics of wet events only, is that these are less dependent on changes in the atmospheric circulation (Lenderink and Van Oldenborgh, 2011), which can be convenient when studying local factors such as moisture availability and CAPE.

2.2.3 Data quality

For trend analysis a high-quality data set is required, especially one whose variability consists solely of changes in weather and climate. This is the definition of an homogeneous climate time series (Freitas and Nunes, 2013). Nonetheless, long instrumental records are rarely homogeneous, for example due to station relocations, changes of rain gauge type, and changes in the rain gauge site (Buishand and Brandsma, 2013; Freitas and Nunes, 2013). As can be deduced from Table 2.3 our data sets also have inhomogeneities. Although much attention has been devoted to homogeneity testing and adjusting for inhomogeneities, methods thereof are not considered here for multiple reasons.

First of all, inventing and applying homogenization tests for hourly data is a time consuming and difficult task and would not fit within the time framework of this thesis. Secondly, there are no existing homogenization programs available on hourly resolution to implement easily. Thirdly, homogenization tests in which neighboring stations are used in pairwise comparison would not be suited here, due to the large spatial distance between the stations. As a matter of fact, there are no other neighboring stations matching in resolution and length of data set.

A possible way of correcting for instrumental errors is by comparing the automatic rain gauges with the hand rain gauges, because we know from Brandsma (2014) that the former measures annually 5-8% lower than the latter (Section 2.2.2). This can be explained by errors in evaporation values due to a warming element in the automatic rain gauge and by a relatively less favorable aerodynamic shape (Smits and Kok, 2004). However, there are several limitations to this correction. First, the timing of manual measurement is less trustworthy, especially in case of extreme precipitation, resulting in large absolute differences. Second, the correction factor as applied by Buishand (1988) (multiplying every hour by the factor, $f = D/P$, with D the daily sum of the manual rain gauge and P the daily sum of the automatic rain gauge) is not valid here. Rain is namely not evenly distributed over the hours, and this kind of errors will be bigger for extreme rain intensities. Third, the manual and automatic rain gauges are often placed further from each other in the course of time (Table 2.3). The larger the distance and the more local the rain events of interest, the smaller the benefit of this correction technique. As intense convective rain events can be very local, this is a serious limitation.

Last, an underestimation of automatic measurements is not that relevant for trends in extremes, when this bias is consistent in time. Then we can still deduce trends. This leads us to the conclusion that the proposed types of correction are not worthwhile to apply on our data. As we can deduce from Table 2.3 some time-wise steps in measurements are expected due to the implementation of different kind of instruments or due to relocation. Therefore, these errors are not consistent over the entire time period.

In order to study possible jumps in our precipitation data, we show the annual means of the hourly precipitation sums (P) in combination with the timing of the important historical changes for every station in Figure 2.6. The regression lines (solid red lines) of the annual means in P are drawn by the *geom_smooth* function of the "ggplot2" package in R, which are in fact estimates of the conditional mean function. In other words, such a regression line is an estimate of the average of the annual means in P conditional on the year (the type of estimator is called LOESS). The gray bands in Figure 2.6 enclosing the regression lines, are plotted by the same R function, and represent the 95% confidence level intervals for the predictions from the smoothed LOESS model.

For De Kooy three important historical changes have taken place, of which the timing is indicated in Figure 2.6a by dashed lines. The dashed purple line is linked to the reduction in the orifice area from 400 to 200 cm^2 in 1972. In Figure 2.6a this effect seems to be negligible, confirming what was stated in Section 2.2.2. The dashed green line represents the change from manual to automatic (electric) measurements in 1993. In this figure it is hard to detect an evident jump in

the data between the period before and after the change. The little bump in the year 1993 is not thought to be the result of the change, as we would expect a long-term shift in the data. In other words, we are seeking for simultaneous occurrence of an historical change with a breakpoint in the annual precipitation means. The dashed blue line in Figure 2.6a relates to the change of setup; since 2007 the rain gauge is located in an Ott windscreen instead of an English setup. This would lead to a decrease in the annual means in P of 1.5%, which could have influenced the breakpoint in the smoothed regression fit around 2007.

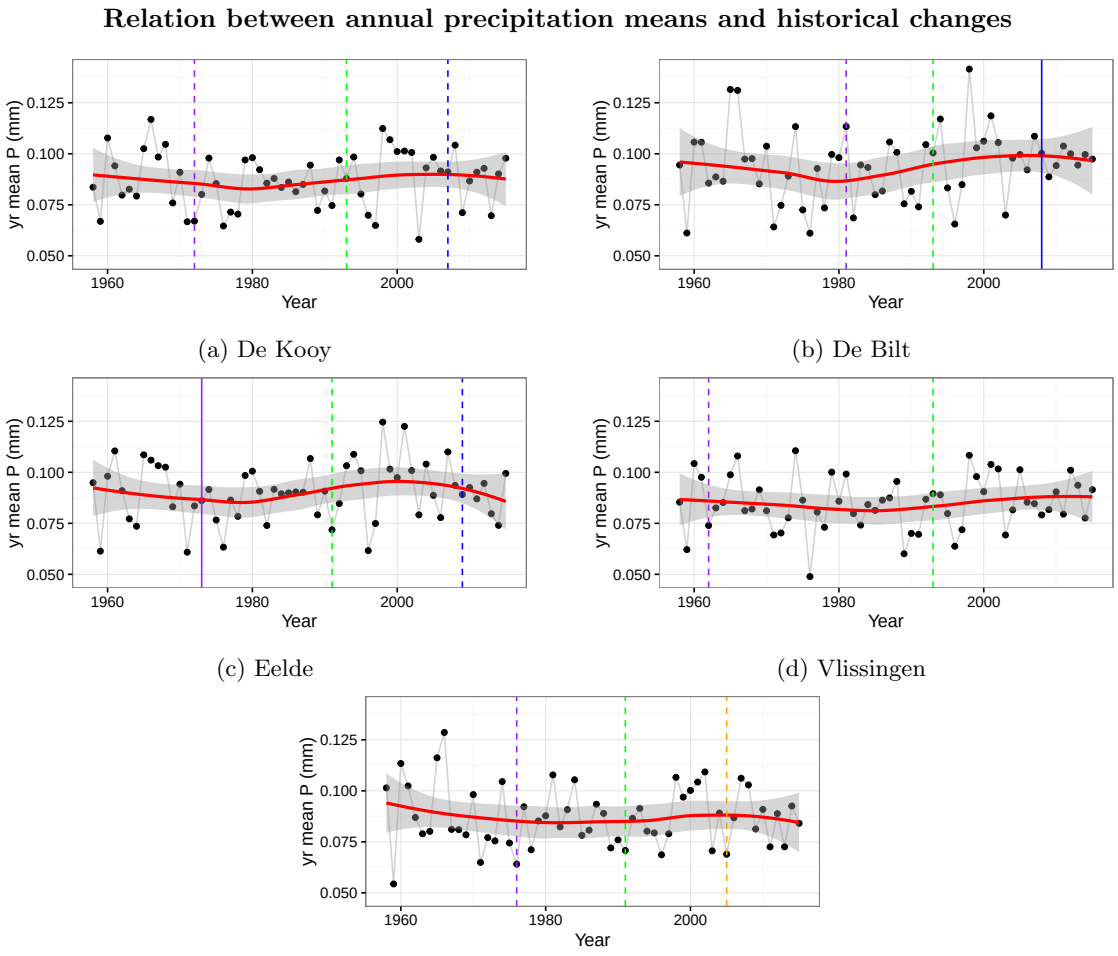

(a) De Kooy

(b) De Bilt

(c) Eelde

(d) Vlissingen

(e) Maastricht

Figure 2.6: The annual means of the hourly precipitation sums (P in mm) of De Kooy (a), De Bilt (b), Eelde (c), Vlissingen (d), and Maastricht (e), from 1958 till 2015. The red line presents a regression fitting of the annual means in P, enclosed by the corresponding 95% confidence interval (gray band). The vertical dashed lines give the timings of important historical changes, the type of change is indicated by the color: orifice area reduction (purple), automatic measurement (green), Ott windscreen (blue), and relocation of the instrument (orange). When one of the changes occurs simultaneously with a relocation a solid line is used instead of a dashed line.

Contrary to a large temporal jump in the year 1982, we do not spot a clear shift in the precipitation data of De Bilt for the reduction in orifice area (Figure 2.6b). The increase in the annual mean loss due to the change from manual to automatic rain gauge can not be deduced from Figure 2.6b. However, for the implementation of the Ott windscreen and simultaneous relocation (200 m) of the station in 2008, we again observe a breakpoint in the smoothed regression line. It is

possible that this change in setup has had an effect on the precipitation measured, although keep in mind that the confidence interval increases at the same time.

None of the historical changes regarding precipitation measurements at Eelde can be linked to breakpoints in the regression of the yearly mean (2.6c). This is interesting regarding the change to the Ott windscreen setup, of which we thought it might have influenced the decreasing trends in annual mean P observed in Figures 2.6a, 2.6b. This is apparently not a consistent relationship. Therefore, it is still possible that this decreasing trend starting the early 2000s has another (f.e. climatic) reason. Note that the uncertainty, expressed by the confidence interval band, is quite high for this time period and station.

Figure 2.6d demonstrates the regression and individual points of the annual precipitation means and two historical changes for the station in Vlissingen. Both the change in orifice area, as well as the implementation of an automatic rain gauge, can not be linked to a breakpoint in the regression of the annual means. What is more striking about Figure 2.6d, is the much less pronounced interdecadal pattern in the annual means in precipitation, compared to the other stations.

The reduction in orifice area (in 1976) and change to an automatic rain gauge (1991) in Maastricht, does not correspond to a clear shift or jump in the annual precipitation means (2.6e). The relocation in 2005, which was the farthest in distance compared to the other stations, goes hand in hand with a breakpoint. However, this is probably the same start (in the early 2000s) of a decreasing trend as for the other stations, which indicates that the mean driver is not related to a change in type of instrument.

Overall, the observed breakpoints in Figure 2.6 do not match the same type of change for every station. Therefore, the effects of changes in type of instrument, setting and/or location are not likely to have caused a significant jump in the hourly precipitation data. Whether the observed interdecadal patterns in Figure 2.6 might be linked to climatic changes (f.e. changes in temperature) will be further investigated in Chapter 6.

2.3 Definition of extremes

A couple of so-called 'extreme indices' are listed in the Fifth Assessment Report of the IPCC, which are widely used in literature. These indices are based on either the probability of occurrence of given quantities or on absolute or percentage threshold exceedances (relative to the climatological reference period), but also some complex definitions about duration, intensity and persistence of extreme events are involved (IPCC, 2013). These extreme indices have been selected on basis of their robust statistical properties, their applicability across a wide range of climate types and extensive data availability over space and time. These indices reflect more "moderate" extremes, as they do not include 1 in 100 year events, but events taking place as often as 5% or 10% of all hours per year (IPCC, 2013).

The indices used in this study are expressions of events occurring $1-45$ times a year, so including "high" to "moderate" precipitation extremes. Accordingly, the annual number of events is large enough to apply meaningful trend analysis on 58 yr time series. Extreme events are defined using the 75, 90, 95, 99, 99.9 %- quantiles, so hours with the highest $25-0.1$ % intensities. Quantiles are cut points partitioning a probability distribution into contiguous intervals, expressed as the values above which $100-\tau$ % (where τ is f.e. 75%, the 75%-quantile) of the highest values are situated. For the entire data set with all hourly values, the 99 and 99.9 %-quantiles express "moderate" extremes occurring 10-85 times a year, whereas dry hours occurring $\pm$ 88% of the time. However, we only apply full trend analysis on data consisting of 2-day maxima (the reason for this will be given in Section 2.4.2). The $75-99.9$ %-quantiles of this data set correspond to $1-45$ times

a year and intensities of $> 2-24$ mm hr^{-1}. Here, the 99 and 99.9 %-quantiles represent the "high" extremes, with frequencies of approximately 0.18 and 2 times per year. The 75, 90, 95 %-quantiles belong to values occurring roughly 10, 18 and 45 times a year. These indices are chosen such that the extremes selected have impacting intensities($> 1.6-6$ mm hr^{-1} for "moderate" extremes and $>$ 8-30 mm/hr for "high" extremes), as well as a high enough occurrence per year for trend analysis.

2.4 Trends

In Chapter 5 trend analysis is applied on intensity and frequency (number of wet hours per day) data for every station. In this section we will explain how we applied trend analysis and on which assumptions it is based. We differentiate between two linear regression techniques: least-square and quantile regressing. Furthermore, we describe how we tested the significance of the observed trends.

2.4.1 Simple linear trend

To detect and quantify historical climate trends, the linear component of the change over time is often estimated. The strengths and weaknesses of this approach are well understood as it is frequently and widely applied (Von Storch and Zwiers, 1999; Wilks, 2011; IPCC, 2013). In linear trend modelling the way in which the trend is dependent on the sampling distribution (Gaussian, lognormal or otherwise) and the residuals on the trend line, has to be considered carefully. Moreover, uncertainty and serial correlation in the data have to be taken into account (Von Storch and Zwiers, 1999; Santer et al., 2008; IPCC, 2013). Two different methods of linear regression are used in this study; fitting a linear regression model by the ordinary least square approach, and by linear quantile regression. The choice for a certain method is based on the sampling distribution and the type of result (e.g. regression of the mean or the extreme part) we are interested in.

Least-square regression fitting

The ordinary least square (OLS) method is a minimization function of the sum of squares of the vertical distance, $\sum (y_i - \beta_0 - \beta_1 x_i)^2$, from the data points to the regression line (Leng et al., 2007). Figure 2.7 illustrates this. The slope of this regression $\hat{\beta_1}$ is given by $\frac{\sum (x_i - \bar{x})(y_i - \bar{y})}{\sum (x_i - \bar{x})^2} = \frac{S_{xy}}{S_y y}$. In a similar way the OLS estimate of X on Y minimizes the horizontal distance between the points and the regression line. The latter is also named the reverse regression. Ordinary least regression is only applicable when only one of two variables is random (Leng et al., 2007).

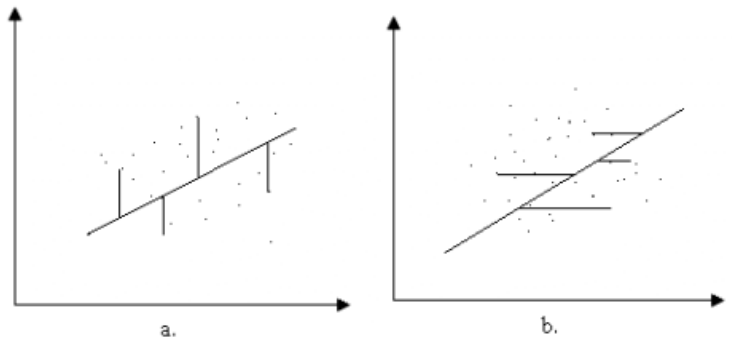

Figure 2.7: Ordinary least square regression, which minimizes the vertical (a) or horizontal (b) distance between the data points and the regression line.

Quantile regression

Multiple studies use linear regression for changes in seasonal or annual quantiles. However, when quantiles are calculated from small samples (i.e. from data per season or year), these can be biased. Therefore, quantile regression is used to overcome this problem (Wasko and Sharma, 2014; Roth and Jongbloed, 2015). Quantile regression can be viewed as an optimization of a linear τ-dependent fit to a certain data set, thereby estimating the τ-th quantiles of the response variable. As described in Koenker and Bassett Jr (1978) and Koenker and Ng (2005) we can describe the minimization problem to obtain the τ-th sample quantile of data series y as function of t as

$$\min_{\beta \in \mathbb{R}} \sum_{t=1}^{T} \left(\sum_{(y_t - \beta) \leq 0} (\tau - 1)(y_t - \beta) + \sum_{(y_t - \beta) > 0} \tau (y_t - \beta) \right) \tag{2.2}$$

where the value of β for which the function is minimal is the estimator. To solve a linear quantile fit, we make the estimator time dependent, $\beta \rightarrow (\beta_0 + \beta_1 * t)$, and rewrite Equation 2.2 to

$$\min_{\beta \in \mathbb{R}} \sum_{t=1}^{T} \left(\sum_{(y_t - \beta) \leq 0} (\tau - 1)(y_t - (\beta_0 + \beta_1 * t)) + \sum_{(y_t - \beta) > 0} \tau (y_t - \beta_0 + \beta_1 * t) \right) \tag{2.3}$$

To illustrate how quantile regression works we plotted Figure 2.8.

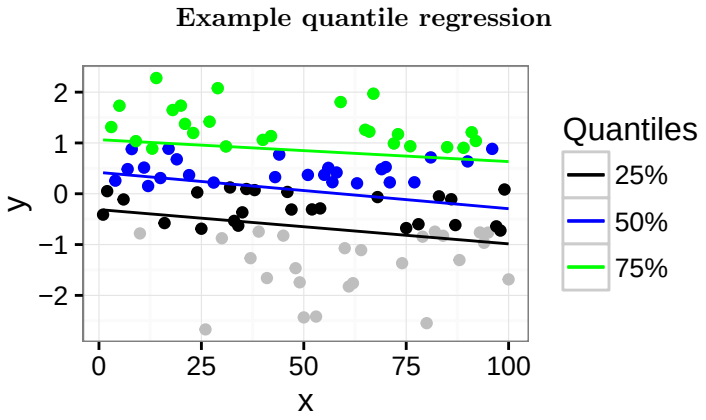

Figure 2.8: For a random data set of 100 values of y for all x (numbers from 1 to 100) the colored lines (black-green) give quantile regression fits with respectively τ = 25, 50, 75%. The dots in black give all values higher than the 25%-quantile. Note, these dots are overplotted by the blue dots which indicate all values higher than the 50%-quantile. The latter dots are also over plot by the green dots giving all values higher than the 75%-quantile.

Complementing the least square method, quantile regression is less sensitive for outliers and therefore a more robust alternative for estimating the main tendency in extremes (Koenker, 2005; Roth and Jongbloed, 2015). Besides, for spatial comparison quantiles are more relevant then counts of exceedance over thresholds (Klein Tank and Können, 2003), as they correspond to the same part of the distribution for all stations. Therefore, quantile regression offers the possibility to investigate better the conditional distribution (τ-% of the data) of the response (Koenker, 2005). Note, that trend estimates of high quantiles can still be noisy due to data scarcity (Roth and Jongbloed, 2015).

Quantile regression was performed using the R package "quantreg" (*Package quantreg: Quantile regression*). The default method for computing quantile regression is a modified version of the Barrodale and Roberts algorithm for l1-regression, described in detail in Koenker and d'Orey (1987) and Koenker and d'Orey (1994). For large data sets (n > 10000) we use Frisch-Newton interior point method ((Koenker, 2005)) to calculate quantile regression.

2.4.2 Time dependency of data

When notable autocorrelation is present, the linear regression estimates may be potentially invalid and inconsistent (*Time-series Analysis*). Autocorrelation is cross-correlation of a signal with itself at different points in time. In other words, hourly values successive in time are dependent on each other. Partial autocorrelations are cross-correlations in time with intermediate autocorrelations removed. Based on the autocorrelation function (acf) and partial autocorrelation function (pacf) repeating time-dependent patterns can be recognized. Koenker (2005, pp.128) stated that the typical independent and identically distributed errors (IID) condition (i.e. the condition that all random variables have the same probability distribution as the others and are mutually independent) is most of the time influencing the regression error terms for both the mean- and quantile regression. Therefore, it is important to correct for autocorrelation when applying quantile regression to detect a trend (Huo et al., 2013). To have a time-independent data set a sampling spacing larger than the significant lags of these patterns can be chosen.

2.4.3 Testing of significance

Whether least square or quantile fits on the independent data are significant, has to be tested. First, we start with an hypothesis of stationarity against a linear trend. In the case of stationarity the fitted value (f.e. of the quantile of interest) is constant over time, i.e.

$$H_0 : Q_i == \beta \tag{2.4}$$

with the time step i, or

$$H_0 : \alpha == 0 \tag{2.5}$$

with α presenting the slope.

This can be tested against the alternative that it is increasing (or decreasing), i.e.

$$H_1 : Q_i \leq Q_n \tag{2.6}$$

or differently formulated as

$$H_1 : Q_i = \alpha_0 + \alpha_1 * i, \alpha_1 > 0 \tag{2.7}$$

with n indicating the nth-time step.

Here, we test whether the slopes of the fitted regression lines are significantly larger than zero. In a 9999-Monte Carlo permutation test we calculate the slopes of 9999 permuted versions of one time series, to compare with the observed slope of one single regression. The corresponding p-value is computed as $p = \frac{\sum \alpha_{obs} > \alpha_{perm}}{N}$, with α_{obs} the slope of the observed fitted values, α_{perm} the slopes of the permuted series and N the number of permutations. By comparing the p-value to the 95% and 99% confidence levels in the distribution of all slopes, the observed regression fits can be assigned a significant positive or non-significant trend. Thereby rejecting or accepting the H_0 hypothesis.

The reason why a permutation test is chosen, is that this is a non-parametric test. Parametric approaches (f.e. z-, t-, or F-test) assume that the data is normally distributed, while a non-parametric (f.e permutation test) can be applied without the assumption that the data follow a normal distribution (Srinivasan ("'Small Area Estimations'")). A permutation (randomization) test is a resampling and exact test, the latter means that it is not defined on basis of parametric assumptions and does not use approximate algorithms. A basic premise of the permutation test is that the observations are exchangeable under the null hypothesis (Srinivasan ("'Small Area Estimations'")), so there should be no difference in location or method of measurement between the data. Although one data set consists of measurements at only one location, we already discussed tiny changes in the measurement settings and location in 58 years. These historical changes appeared to be insignificant in Section 2.2.3, so our assumption holds.

A major disadvantage of permutation tests is that they can be very demanding in computational power, therefore it is worthwhile to use a Monte Carlo permutation test. With this Monte Carlo approach we mean an N-times repeated random sampling (with an specific order), instead of calculating the slope of every possible order of a series of almost 10940 observed values, which would give 10940! outcomes. As the data set consist of so many points, the chance of producing an identical ordered series in 9999-random sampling is extremely low. So, no significant bias is expected from randomly generated duplicated series.

2.5 Causes

A comprehensive four-fold study into the causes of the observed trends is carried out in Chapter 6. First, we identify variables related to the production of (extreme) precipitation from theory. Second, key variables are distinguished based on their correlation matrices and plotting patterns

(precipitation over key variable x). Third, quantile and linear regression in time is carried out on variable(s) which are likely to cause changes in precipitation. Finally, changes in the distribution and in the quantile regression relationship of precipitation over a variable are investigated for each variable by comparison of two time periods. For this part we binned mean hourly precipitation intensity with respect to the explanatory variable(s). In this section we describe how we computed the correlation matrices, and carried out the binning and corresponding analysis.

2.5.1 Pearson and Spearman correlation matrices

The correlations of the key variables are shown in a heat map, which is a correlation matrix in which the cells are colored from blue to red; from strong negative to strong positive correlation, with in between white indicating zero correlation. First, we calculated Pearson correlation coefficients. We computed such a Pearson heat map for 5 different sets of data: (i) all wet hours for precipitation variables (hourly duration, intensity, and sum) and the key variables without CAPE, (ii) wet 2-day maxima of these variables, (iii) wet 2-day maxima in CAPE, (iv) wet daily maxima of variables from (i), (v) wet daily maxima in CAPE.

The Pearson correlation coefficient is also known as the product-moment correlation coefficient and defined as: $r = \frac{\sum z_x z_y}{N}$, where z_x and z_y are the z scores of variables x and y and N the sample size (Cohen and Lea, 2004). The z score is a measure of how many standard deviations an element is from the mean, $z = \frac{X-\mu}{\sigma}$. The Pearson correlation coefficient is 1.0, the highest magnitude, when all samples have the same z score for both variables. In the case the formula reduces to $r = \frac{\sum z^2}{N}$. This always equals 1.0, as the variance of a set of z scores is $\frac{\sum z-\bar{z}^2}{N}$ and always 1, $\bar{z}$ is always 0, so $\frac{\sum z^2}{N} = 1.0$ (Cohen and Lea, 2004). A Pearson correlation coefficient of -1.0 is reached when every sample has the same z score, but with opposite sign. When z scores differ between x and y, the correlation coefficients are of a magnitude between 1.0 and zero.

Pearson correlation assumes normal distributed data and that the data are related to each other in a linear way (Artusi, Verderio, and Marubini, 2002). A restriction to Pearson correlation is its sensitivity to outliers (Chok, 2010).

Second, we also calculated Spearman correlation coefficients, which we applied on data sets (ii), (iii) and (v). Spearman correlation indicates the strength of association between two ranked variables and can be seen as the non-parametric version of the Pearson product-moment correlation (Cohen and Lea, 2004). In contrast to Pearson correlation, Spearman correlation has no assumptions about the way in which data are distributed. The assumptions of Spearman correlations are that data must be at least ordinal and that the variables are related in a monotonically way (Artusi, Verderio, and Marubini, 2002; Cohen and Lea, 2004). A function of a certain relationship can be called monotonic if it is entirely decreasing or increasing. Comparison of Pearson and Spearman correlation coefficients for the same variables indicates whether a relation is more linear or more (monotonically) non-linear.

2.5.2 Binning

Differences in the number of measurements for each unit value of a certain variable can influence the fit between two variables, therefore we consider the distribution of each variable. To reduce this influence we apply binning of hourly mean precipitation intensity in unit value for a certain variable (temperature, dewpoint temperature, CAPE and wind speed). For temperature and dewpoint temperature we use bins of 2 °C. For CAPE a bin size of 50 J/kg is applied and for wind speed a bin size of 2 m/s. The number of observations per bin must be ≥ 200. As we only have CAPE data from 1993 onward we did not apply time comparison of binned mean and quantile

lines for this variable, but only considered the seasonal point clouds and distributions. All bins are differentiated between summer and winter season, and for all variables except CAPE we also differentiated between the period 1958-1986 and the period 1987-2015.

The resolution is limited greatly to binning of the data and differentiating of the measurements on season and time period. Therefore, we use daily maxima of mean hourly intensity and daily maxima of the key variables, instead of 2-day maxima. Wet-only maxima are considered, as we are solely interested in changes in precipitation, not in dryness. Furthermore, we bundle the daily maxima of the five stations, in order to increase the resolution. Besides, we want to study the common relationship, because we observed a robust signal for all stations in increasing precipitation intensity and decreasing frequency of wet hours.

For each bin the mean and the 95,99 %-quantiles are calculated from the binned intensity maxima and lines are fitted through all the means and quantiles. The two periods have a length of 29 years. As climate is classically referred to as the weather of 30 years (WMO), the differences in distribution and binned quantile regression between the two periods can be seen as changes in the climate state.

Chapter 3

Theoretical Background

This chapter presents a theoretical overview of cloud processes and types, and of conditions for precipitation to occur. This will provide the background information needed to interpret the results, especially those reported in Chapter 4 about spatial and seasonal variability in hourly precipitation data. The chapter is divided into four parts. The first part describes briefly how clouds are formed and the second part how precipitation is produced. A description of two cloud types and associated precipitation characteristics forms the third part. The last part highlights conditions of extreme precipitation from large- to small-scale, including processes of synoptic, cyclonic and locally induced precipitation and internal cloud processes.

3.1 The formation of clouds

Prerequisites for cloud formation are: moisture, cloud condensation nuclei (CCN) and initial cooling. In the first place, sufficient moisture in the air is needed to condense out and form precipitation. Although air can be supersaturated with respect to water, surfaces on which condensation can take place are also required (Sumner, 1988, p.44-45). Within a cloud the surfaces on which droplets form are called cloud condensation nuclei (CCNs). If the air contains enough moisture and CCNs, initial cooling of air below its dew-point temperature will lead to (partial) condensation of its water content.

By initial cooling we mean the cooling initiated by an external event that triggers droplets to form, which then may continue to grow despite of the release of heat from condensation of moisture, as a result of processes that will be discussed in Section 3.2. An important external event causing this initial cooling is free or forced convection. In the field of meteorology, convection is commonly used as a term for vertical heat transport associated with an updraft. A more precise definition of convection is: motion or mixing within a fluid, in this case air, thereby causing mixing of energy (heat), momentum and molecules (i.e. water molecules as water vapor) (Krennert, 2016). Free convection in the atmosphere is a result of density-driven rise of warm (light) air currents or thermals (Sumner, 1988, p.44-45). Air can also be forced to rise due to a topographical or frontal barrier or turbulence (Sumner, 1988, p.45).

3.2 Production of precipitation

The presence of CCNs allows water to condense out in saturated conditions. Water preferentially condenses on the bigger aerosols, for which the curvature is less. This is called the curvature or Kelvin effect and can be explained by considering the degree of bonding between the water molecules (Hobbs, 1993; Shulman et al., 1996). This is higher for a flatter surface and therefore

the water vapor pressure is lower (i.e. the tendency of particles to escape from the liquid to the gas phase), compared to a more curved surface. Next to size, an important property of aerosols is hygroscopicity. Many aerosols are hygroscopic, which means that they are able to attract water onto their surfaces (Sumner, 1988, p.50). This allows condensation to take place, even in air that is not completely saturated.

A raindrop has a typical size of about 1000 microns (1.0 mm), while a cloud droplet radius is generally about 20 microns (Sumner, 1988, p.51). However, the growth of cloud droplets towards a size big enough to precipitate out is not only determined by the condensation process. All cloud droplets will be subject to gravity and often collide when moving vertically. Three different terms are used for the collision process, based on the phase of the two particles: coalescence (for liquid on liquid), aggregation (for solid on solid) and accretion (for liquid on solid) (Sumner, 1988, p.109)(Pruppacher, Klett, and Wang, 1998). The mode of collision may determine the form of the precipitation. In general, coalescence produces rain or drizzle, aggregation produces snow, and accretion produces ice pellets and ice grains, or hail(Sumner, 1988, p.110).

Another important mechanism behind rapid growth of cloud particles is called the Wegener-Bergeron-Findeisen process, which is determined by the difference in water vapor pressure above ice and water surfaces. Ice namely has a lower vapor pressure than liquid water as it costs more energy to convert water from a solid to a gas than from a liquid to a gas. Since it is harder for an ice molecule to leave the ice surface as water vapor, the amount of water vapor molecules, and hence the water vapor pressure, is lower above ice. When a mixture of supercooled liquid droplets and ice particles is present in the cloud, differences in water vapor pressure lead to fast evaporation of water and deposition on the ice particles (Sumner, 1988; Hoose et al., 2008). Therefore, ice particles can grow very efficiently.

Next to the Wegener-Bergeron-Findeisen process, possible pathways of particle growth in mixed-phase clouds involve (i) simultaneous evaporation and (ii) simultaneous growth of ice particles and liquid droplets (Korolev, 2007). The pathway of evolution taken by a cloud depends on the local thermodynamic conditions. Simultaneous evaporation may be caused by entrainment and mixing of dry air from the clouds surrounding, whereas simultaneous growth of ice particles and water droplets may result from updrafts or isobaric mixing of saturated with saturated or unsaturated air (Korolev, 2007). The latter can occur after saturation is achieved in the first phase of mixing, when there still is a temperature difference between parts of the cloud (based on the degree of mixing and cloud liquid water content, LWC). This may result in small zones of supersaturation in the cloud where growth of ice and water particles may take place at the same time. A description of the full mechanism can be found in Korolev and Isaac (2000).

It should be stressed that not all clouds generate precipitation. They could, for example, be too short-lived, in which case they are not able to produce large enough particles. It can also be that clouds are too shallow (small vertical extent), which corresponds to less vertical motions and thus less cloud-droplet growth by collision (Sumner, 1988). Moreover, they can be situated too high in the atmosphere, where moisture availability and the degree of vertical motion is small (except for convectional clouds with enough vertical development in all layers) and there is a longer pathway for the falling rain droplets (Sumner, 1988). A longer pathway means a larger possibility to fall through a layer of unsaturated air.

As we only have station data, we can not take into account the changes in CCNs, cloud properties and dynamics, however from Li et al. (2011) we know that changes in precipitation related to changes in concentrations of CCNs depend on the cloud's LWC and on whether the cloud contains ice particles next to liquid particles or not. For regions with increasing CCNs, precipitation frequency increases for deep clouds with high LWC, but decreases for clouds with a low LWC (Li et al., 2011). Furthermore, positive (mainly summer) trends in cloud-top height are detected attributable to aerosol-induced strengthening of upward winds for mixed-phase clouds

with a warm, low base. Please note, monitoring of trends in aerosols, serving as CCNs, are imperfect according to the latest IPCC report (IPCC, 2013). However, we can keep these potential changes in precipitation due to changes in CCNs in mind, when we interpret the results of the trends in precipitation frequency and intensity (which is influenced by the vertical extent of the cloud) in Chapter 5. Besides, we are now able to relate cloud conditions to cloud types. This is relevant because the occurrence of a certain cloud type not only gives a better understanding of the mechanism behind precipitation, but also links to seasonality.

3.3 Cloud types

The following two types of clouds can be distinguished by the way of formation and morphology: (i) clouds originating from convectional activity, mostly cumuliform (non-layered, more "puffy") clouds , and (ii) clouds originating from slower, more widespread ascent or turbulent flow, consisting of mainly stratiform (layered) clouds (Sumner, 1988, p.74). An illustration of cumuliform and stratiform cloud types (including the subclasses) is presented by Figure 3.1.

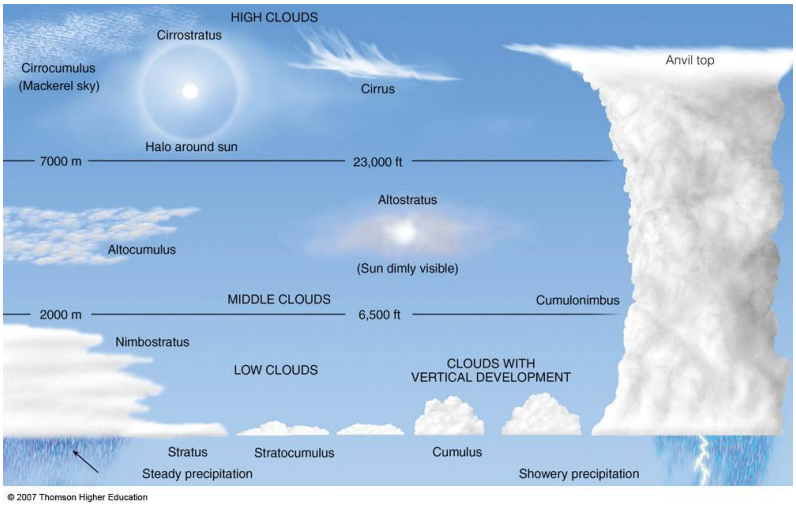

Figure 3.1: A schematic visualization of stratiform (left) and cumuliform clouds and subclasses in these two main types based on height and appearance. Source: Thomson Higher Education (2007).

The first type depends on vertical instability (which can be expressed as CAPE) and moisture availability (which can be expressed as dewpoint temperature). The type of clouds associated with free convection, cumuliform clouds, is dependent on the environmental lapse rate (ELR) and the humidity of the air. Sumner (1988, p.62) states: "Where the ELR is such that positive buoyancy persists through a deep layer of the atmosphere, then convection currents will operate through the layer with their speed and strength related to the magnitude of buoyancy". In this case we have an extremely unstable atmosphere, while the opposite ELR belongs to an extreme stable atmosphere. Convectional precipitation, associated with cumulus and cumulonimbus clouds, operates at small and medium scale (Rangno and Hobbs, 2005). They typically form cells of more intense precipitation over areas of about tens to hundreds of square kilometers (Sumner, 1988). These cells have short lifetimes, as the processes producing them directly (thermal) or indirectly (forced) are generally restricted to the hours of the day when the isolation is strongest.

According to Sumner (1988), most precipitation from convective clouds is produced by the Wegener-Bergeron-Findeisen process, because of the considerable vertical development of the

clouds (therefore exceeding the 0°C isotherm), resulting in very intense precipitation (sometimes in the form of hail or ice pellets). These clouds, formed under conditions of high convectional activity, are characterized by (i) a large vertical extent, (ii) strong differential motion (strong up- and downdrafts), (iii) an internal environment in which ice and supercooled droplets may exist in close proximity and where seeding of the lower part of the cloud takes place by ice from above, and (v) a large potential in producing precipitation of an extremely high intensity at the ground surface (Sumner, 1988). The majority of severe local storms associated with self-perpetuating convectional systems are associated with significant hail production (Sumner, 1988). In contrast to Sumner (1988), Korolev (2007) (as described in Section 3.2) concluded that precipitation formation is also resultant from simultaneous growth of ice particles and water in (super)cooled clouds originating from convectional activity.

The second type of clouds are stratiform clouds. An important driver for formation of these clouds is frontal collision and occlusion. Frontal precipitation is characterized by a meso-scale band along the front. This band can be distinguished in perpendicular direction with respect to the front by a narrow updraft zone near the leading edge of the frontal cloud and a broad zone of stratiform precipitation (Hobbs, Houze Jr, and Matejka, 1975). Frontal clouds can be recognized by their corresponding synoptic settings of low and high pressure areas, temperature fields and resultant wind direction (Sumner, 1988).

Cloud micro-physical data indicate a concentration of 50-500 ice particles per dm^3 in the frontal cloud. These concentrations are too large to be completely explained by Wegener-Bergeron-Findeisen process. From air craft data Hobbs, Houze Jr, and Matejka (1975) found that cloud particles must have grown due to riming (accretion of supercooled water droplets on an ice crystal) and aggregation (sticking together of ice crystals) as well.

Cold fronts, in which colder and denser air forces warmer air to move on top of it, tend to have a much steeper frontal slope. This leads to a more pronounced cumuliform-type of clouds with resultant heavier precipitation (Sumner, 1988). Squall-lines (organisation of cells into a line orientated approximately normal to the direction of movement) with trailing stratiform precipitation typically occur in the form of prefrontal troughs ahead of cold fronts at mid-latitudes (Newton, 1950; Schultz, 2005; Morrison, Thompson, and Tatarskii, 2009). Many studies have described morphological features of squall-lines,which are based on the conceptual model of Biggerstaff and Houze Jr (1991). As mentioned in Morrison, Thompson, and Tatarskii (2009) these include: "an upshear-tilted, multicellular convective region with heavy precipitation and active updraft cell generation along the gust front and a low-level radar reflectivity minimum between the convective and stratiform regions, followed by a region of moderate precipitation in the trailing stratiform region." The region in which the highest intensities in stratiform precipitation are found is downwind of the intensive parts of the convective line. Biggerstaff and Houze Jr (1991) demonstrated that the magnitudes of the relative wind and micro-physical velocity determine the width of the trailing region of stratiform precipitation. Especially, an occlusion of a cold and a warm front can lead to extreme precipitation at the northwest of the low center (Schultz and Vaughan, 2011).

Next to frontal precipitation, stratiform clouds can also be formed due to or effected by turbulence, for example when the cloud layer is radiatively destabilized (Houze Jr, 2014). Orographic barriers may influence more convective, as well as more stratiform precipitation (Sumner, 1988; Houze, 2012), which can give clouds a more wave-like appearance (Sumner, 1988). A study of Basist, Bell, and Meentemeyer (1994) demonstrated that topographic predictors correlate strongly with mean precipitation.

When comparing convective with stratiform precipitation, studies of Berg and Haerter (2013a) and Berg and Haerter (2013b) show that convective (stratiform) precipitation occurs more dominantly at higher (lower) temperature. Therefore, in summer we have relatively more convective rain events compared to the winter, when relatively more stratiform rain events occur. Both types

are also characterized by different spatial scales. The type of large-scale precipitation (>1000 km^2) is more often stratiform than convective, whereas precipitation falling over an area between 20-300 km^2 occurs more often for the convective type than for the stratiform type (Berg and Haerter, 2013a). So in general, on the one hand stratiform precipitation has a bigger horizontal scale, on the other hand convective precipitation has a larger vertical extent (Houze Jr, 1997; Anagnostou, 2004). Another difference between the two precipitation types is the mean intensity, which is higher for convective rain events than for stratiform rain events (Berg and Haerter, 2013a). Finally, convective precipitation can be distinguished from stratiform precipitation by a relatively greater horizontal homogeneity(Anagnostou, 2004). Overall, stratiform precipitation accounts for less intense and homogeneous precipitation, spread out over a larger area, with a smaller vertical extent and dominating at lower temperatures, compared to convective precipitation.

3.4 Conditions for extreme rainfall

Now that we know the basic ingredients for cloud formation and precipitation production and the resultant two main cloud types, we will focus more on the mechanism behind extreme precipitation. As extreme rainfall is caused by processes of different scales, they are listed here from large to small scale.

3.4.1 Synoptic conditions

Large-scale (Grimm and Silva Dias, 1995; Gandu and Silva Dias, 1998; Aceituno, 1989) and meso-scale patterns of convection and precipitation (Velasco and Fritsch, 1987) can be determined by intraseasonal variability and interannual variations such as El Niño Southern Oscillation (ENSO) and related teleconnections (Hoerling and Kumar, 2000; Carvalho, Jones, and Liebmann, 2002). A study of Maddox, Chappell, and Hoxit (1979) found characteristics in the meso-α scale (200-2000 km) environment at the time of extreme precipitation. Among these characteristics are a weak mid-tropospheric, meso-α scale trough, a deep layer of moist tropospheric air, vertical shear of the horizontal wind through the cloud depth and high potential for convective storms and/or cells to develop. Next to extreme precipitation, meso-scale convective complexes are associated with strong winds and large hail (Maddox, Chappell, and Hoxit, 1979). Overall, studying synoptic conditions in interaction with processes on smaller scales is of highest importance. In this study we do not use synoptic data, as we consider point measurements at station level.

3.4.2 Extratropical cyclones

In the winter season extreme precipitation and wind speed are related to extremes in cyclone intensity in subregions of the North Atlantic (Raible et al., 2007). Connections are clearly visible between large-scale atmospheric patterns and extremes in cyclone intensity (Bosart, Bracken, and Seimon, 1998; Bracken and Bosart, 2000), although this does not apply for the summer season. Winter extremes of cyclone intensity are significantly higher in almost all regions, due to a stronger meridional temperature gradient and an increase in lower tropospheric baroclinicity (Raible et al., 2007). Baroclinicity is a measure of how misaligned the gradient of constant pressure is from the gradient of constant density. When the tilt of density surfaces is reduced, potential energy it released. It thereby feeds the kinetic energy of disturbances (Cushman-Roisin and Beckers, 2011). Baroclinicity is, thus, a form of instability and it is the dominant driver for cyclogenesis in the middle latitudes (Cushman-Roisin and Beckers, 2011). As we do not analyse synoptic data the effect of cyclone intensity or baroclinicity will not be taken into account in this thesis.

3.4.3 Locally induced precipitation

In general, the following rule holds: the greater the speed of the uplift, the larger the vertical extent of individual clouds (and the less their horizontal extent), but the heavier the precipitation produced locally. As already mentioned in Section 3.1, free convection occurs when thermals (hot air) are lifted vertically (Sumner, 1988). Precipitation resulting from a strong updraft will fall over a relatively small area, compared to precipitation falling along a gently-sloped front. In general, higher magnitudes of rainfall intensity are maintained over a short duration, while lower magnitudes of rainfall intensity are associated with longer-lasting and spatially more widespread precipitation events (Haerter and Berg, 2009). The precipitation intensity at the core of a convective storm is determined by its size (i.e. bigger storm size corresponds to higher precipitation intensity) (Sumner, 1988).

Favorable conditions for convective storms to occur are (i) conditional or convective instability, (ii) low-level air with a high moisture content, (iii) strong wind shear, (iv) instability release by dynamical processes and (v) dry air above the storm cell(s) (Sumner, 1988). From this we can deduce that in the development of convective storms local conditions interact with synoptic conditions.

Next to free convection, forced convection can also produce precipitation on a local level. Factors regarding forced convection are topography (Basist, Bell, and Meentemeyer, 1994) and local quasi-permanent areas of surface convergence (e.g. along sea- or land-breeze fronts) (Wapler and Lane, 2012). These mostly do not generate precipitation extremes of the same magnitude as convective storms (Sumner, 1988). However, as the type of fronts can be slow-moving or stationary, heavy precipitation can accumulate in a fixed area, but only when there is sufficient uplift or atmospheric moisture. Organisation of cloud cells into linear bands (e.g. squall lines or sea breeze fronts) or spiral arms (e.g. in tropical cyclones) is dependent on large-scale dynamic processes or localized convergence of air near the surface (Sumner, 1988).

3.4.4 Internal dynamic processes in clouds

A single-cell storm is usually short-lived. This is the result of an inbuilt self-destructing mechanism in which the thermal or warm updraft is replaced by the cold downdraft (Sumner, 1988, p.153). A downdraft originates from downward frictional drag imposed on the air by the rain droplets. It is cold because of rapid evaporation of the falling and already cold precipitation (Sumner, 1988, p.153). In longer-lived storms, new cells are formed adjacent to thermals, so that storm-building activity can be transferred from one thermal to the next. Conditional instability of the second kind (unstable air which has the condition to rise a certain vertical distance) may serve this self-enhancing and self-perpetuating process in which the short-lived nature of the individual cumuliform elements or towers contribute to a much longer-lived system (Sumner, 1988, p.153)(Barry and Carleton, 2001, p.490). This may account for the development of convective complexes of cumulonimbus clouds, which can form tropical cyclones. These clouds will possess areas of downdraft and updraft, with similar order of velocities. These areas can be separated by wind shear, allowing for the inflow of warm, moist air into a cell and outflow of dry, cold air (Miller, 2015). See Figure 3.2 for an illustration. The contrast in relative velocity greatly contributes to the intensity of the storm and the violence of precipitation it can produce (Sumner, 1988). Although we do not have high-level measurements of wind velocity, we have measurements of surface wind strength. So, at least the strength of the surface wind speed indicates the potential of producing a stable storm.

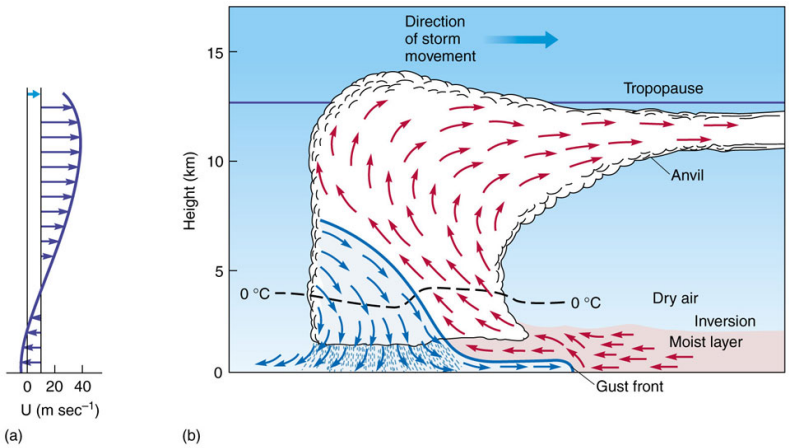

Figure 3.2: A schematic visualization of up and downdraft area's in a storm. On the left side a profile of the horizontal wind, u. Source: `http://geog.ucsb.edu/~joel/g110w07/lecture_notes/thunderstorm/agburt11_13.jpg`.

To summarize, clouds are formed when air with sufficient moisture and hygroscopic CCNs is cooled by an external event, mainly free or forced uplift. Cloud droplets can precipitate out under gravity, when clouds are sufficiently long-lived for cloud droplet to grow big enough due to collision processes. Trends in CCNs are not well monitored and are contrasting depending on the LWC and the homogeneity of the cloud. Although we can not analyse internal cloud processes with our station data, we can link these processes to the two main cloud types, convective or cumuliform clouds and stratiform clouds, and corresponding precipitation characteristics.

Whereas cumuliform clouds are produced by a strong vertical ascent, by free convection, stratiform clouds originate from a slower, more widespread ascent or turbulent flow. Extreme precipitation can be produced on the local, small-scale level by (free) convective storms, which are characterized by vertical instability, low-level moist air, strong wind shear and the cloud dynamics, or to a lesser extent by stationary forced (i.e. frontal and/or topographic) convective systems. Moreover, we can not investigate causes of changes in extreme precipitation on the large-scale level. In order to study the effect of the large-scale setting on precipitation extremes (i.e. the presence of a meso-scale mid-tropospheric trough or extratropical cyclone or the presence of large-scale wind shear), data of a higher spatial resolution is required. However, as we will focus on hourly extreme intensities, this might not be a significant problem. In Section 3.3 we pointed out that stratiform precipitation has a larger scale and is less intense than convective precipitation. In the next chapter (Chapter 4) we will see whether less intense precipitation (dominantly of the stratiform type) can be distinguished from more intense precipitation (dominantly of the convective type) by season. In Chapter 6 we will dive further into the causes of changes in extreme precipitation, in which we will take into account the conditions favorable for extreme precipitation.

Results

The results are presented in several parts. The first part studies the spatial and seasonal variability regarding (extreme) precipitation. In the second part trends in extreme precipitation are investigated. The third part focuses on the causes behind these trends, by studying the relation with temperature, dewpoint temperature, wind direction and strength, CAPE, and weather conditions. The last part extends the current work to European scale.

Chapter 4

Spatial and seasonal variability in precipitation

Prior to analyzing trends in hourly precipitation sums, it is relevant to investigate the spatial and seasonal variability in precipitation. This will provide basic knowledge about spatial dependence of precipitation characteristics. This allows us to determine whether it is relevant to study trends of individual stations separately or whether we can bundle the data for the Netherlands in Chapter 5. can influence the method of trend analysis. By analyzing the seasonal variability we find seasonal dependent characteristics, on basis of which we have defined seasons of interest for the trend analysis.

4.1 Spatial variability

First, the distribution of precipitation data is investigated in three plots, consisting of a probability density function, a conditional density function and a logarithmic frequency point plot for the extreme part of the distribution (Figures 4.1,4.2). The first figure is based on histograms of the different plots, as we use rounded (i.e. not fully continuous) data, and allows us to visualize all stations. Another way of visualizing spatial differences in the distributions, is shown in Figure 4.2a. The third figure (4.2b) zooms in on the extreme part of the intensity spectrum and demonstrates the robustness of the spatial differences observed in Figure 4.2a for the extreme part. For the latter figure we did not choose for a histogram, due to the logarithmic scaling of the x-axis (intensity), as well as the y-axis (intensity).

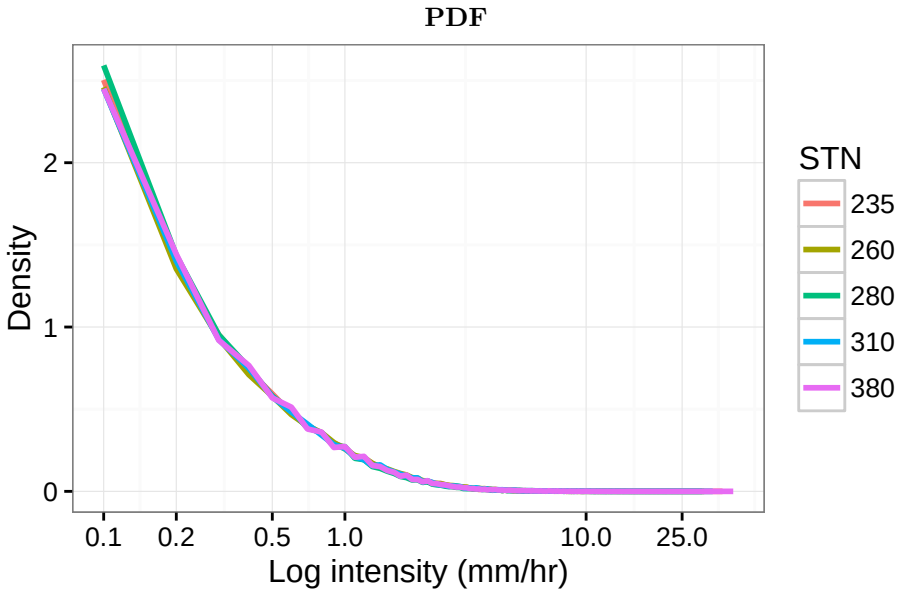

Figure 4.1: The probability density function for all 5 stations: De Kooy (235), De Bilt(260), Eelde(280), Vlissingen (310) and Maastricht (380).

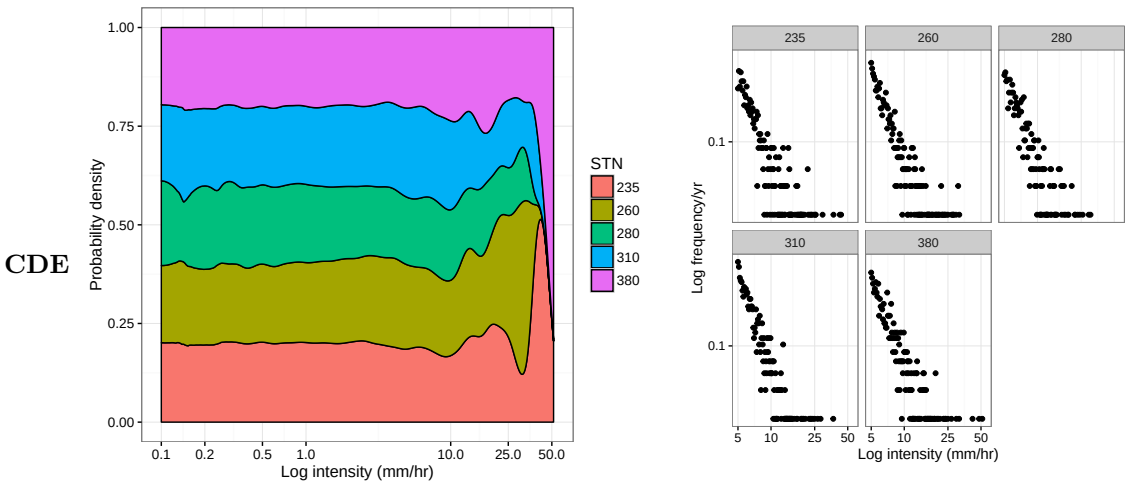

(a) CDE

(b) Distribution of points

Figure 4.2: The conditional density estimate, in other words the estimation of the probability density function conditional on the intensity, for all 5 stations: De Kooy (235), De Bilt(260), Eelde(280), Vlissingen (310) and Maastricht (380) is shown in (a). The frequency of extreme intensities (>5 mm/hr) per year is provided by (b). Both axises of plot (b) are logarithmic, which give rise to steps in the extreme tail.

Figures 4.1 and 4.2 demonstrate that the closer the precipitation intensity (P) is to 0 mm/hr, the higher the frequency. The data is bound at 0 and skewed for positive intensities. Dry hours (P <0.05 mm/hr) are excluded from both figures due to logarithmic conversion, but occur approximately 88% of the time. Out of all the wet hours 25% has a value of 0.1 mm/hr and 15% a value of 0.2 mm/hr. As the data is not fully continuous, due to rounding to 0.1 mm, each probability density function (PDF) in Figure 4.1 is drawn by connecting all bars (mids) of the corresponding histogram. Therefore, Figure 4.1 provides an estimation of a PDF and not the true density per

intensity. However, this plot is clearly visualizing the differences between the five stations. In Figure 4.1 it can be seen that the distributions of the stations are very similar, although there are some minor differences. For example, Eelde has higher frequencies of wet hours corresponding to intensities smaller than 1 mm/hr, compared to the other stations. The extreme tail in Figure 4.2a shows that Eelde also has less high extremes (namely < 30 mm/hr) compared to the other stations. On the contrary, at the station in Maastricht the highest extremes (35-50 mm/hr) in precipitation intensity are measured. Next to Maastricht, De Kooy has relatively high frequencies of extreme events (>30-35 mm/hr) compared to other stations. In the same intensity spectrum Vlissingen also accounts for a large part. These stations are both located at the seaside, so extremes are assumedly not so much confined by the availability of moisture. De Bilt (and Eelde to a lesser extent) has relatively many extreme events at a scale of 25-35 mm/hr. For the interval 0.4-1.2 mm/hr De Bilt has relatively less rain events. From the conditional density estimates for every station in this figure, we can deduced that spatial differences are in general higher for the extreme tail of the precipitation distribution. It is worth noting, that these spatial differences might be influenced by the exponential decrease in the number of data points with increasing intensity (figure 4.2b). Explanations for the spatial differences in extreme precipitation will be further investigated in Chapter 6.

To study in more detail the extreme part of the precipitation distribution, we plotted the violin plots of the annual maxima in precipitation in Figure 4.3. The shape and extent of the violins in this figure clearly shows spatial differences in the distributions of the annual maxima. The stations De Kooy and Maastricht have a larger extent in annual maxima, ranging from 5-50 mm/hr compared to the other stations. The violins of Eelde and Vlissingen have almost the same shape, ranging from 7-30 mm/hr (with one outlier of 36.9 mm/hr for Vlissingen) with a thick "belly" at approximately 12 mm/hr. The red dots, representing all annual maxima, show why some of the violins have a "cut-off" (flat) top and others a "tail" (long and thin) top. A thick belly and a flat top is what we expect for data that is skewed for higher intensities. A flat top is the effect of a lack of outliers (no remarkably high red dots) on the visualization of the violin plots. Keep into mind that each violin plot is based on only 58 points per station, namely the annual maxima between 1958-2015. This results in some randomness in the shape of the distribution.

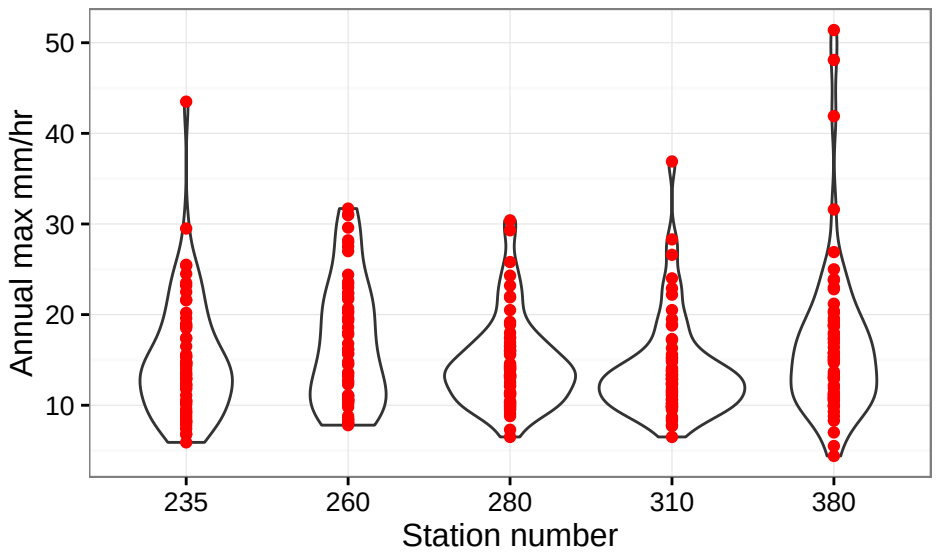

Figure 4.3: Violin plots of annual maximum hourly rainfall

Overall, the distributions of precipitation are skewed for positive intensities and quite similar

in form. Larger spatial differences exist in the extreme tail due to occurrence or lack of outliers. Next to intensity, we can also study other precipitation characteristics. In Figure 4.4 we plotted a pie chart demonstrating the percentage of time that it is raining and a chart diagram showing the total amount of accumulated precipitation per year and per station.

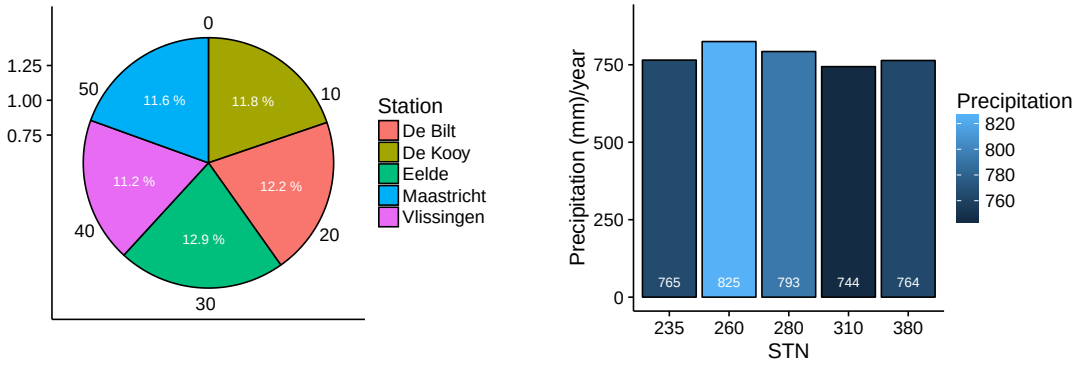

(a) Raining time (%)

(b) Amount of precipitation

Figure 4.4: (a) The fraction of all hours in which precipitation occurs and (b) the annual amount of precipitation per station.

From Figure 4.4 we can deduce that spatial differences exist for the fraction of hours in which precipitation occurs and the amount of precipitation. In Eelde wet hours occur 1.7% more often ($\sim$ 152 hours year^{-1}) compared to Vlissingen, while 11% of precipitation ($\sim$ 81 mm year^{-1}) accumulates more in De Bilt compared to Vlissingen. In general, we observed that it rains more frequently in the more northern and inland stations than in the more southern and coastal stations. In the next section we investigate whether seasonal dependent precipitation characteristics can be recognized.

4.2 Seasonal variability

Stratiform rain events, the dominated type in winter, are characterized by relatively weak-sloping fronts and updrafts and their large scale (Section 3.3). Owing to the large scale of the front, the precipitation will be spread out over a larger area. Therefore, the intensity of this kind of fronts is relatively low and the duration relatively long. Due to the long duration of these large-scale precipitation events, we would expect to observe more hours in winter in which precipitation occurs than in summer. Moreover, temperatures are lower in winter than in summer and cold air requires a lower pressure to reach the same saturation compared to warm air (Section 6.2.1). This may also result in a relatively high winter fraction of wet hours. We analyzed the hourly duration, which is defined as the hourly fraction of time that precipitation occurs, meaned over all wet hours per month in Figure 4.5.

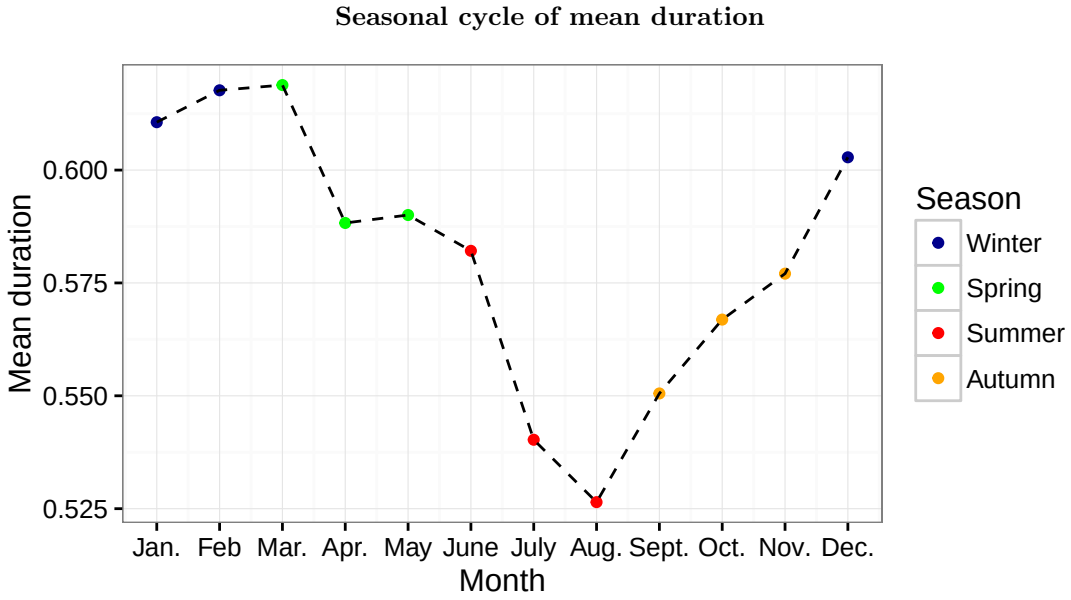

Figure 4.5: Mean duration of all wet hours per month and meaned over 5 stations.

From Figure 4.5 can be concluded that the duration of rain within a wet hour is longest in the months December-March and shortest in July-September. Another characteristic of large-scale winter depressions is their low intensity, which we study by plotting the mean intensity values per month in Figure 4.6a. Next to the intensity, the following figure (Figure 4.6b) gives the fraction of time that precipitation occurs and the monthly precipitation sums in Figure 4.6c. We would expect that the product of a relatively high monthly intensity and relatively high monthly fraction of numbers of wet hours results in high accumulation amounts. The intensity and duration together give indications about the type of precipitation (stratiform versus convective) dominating a certain season.

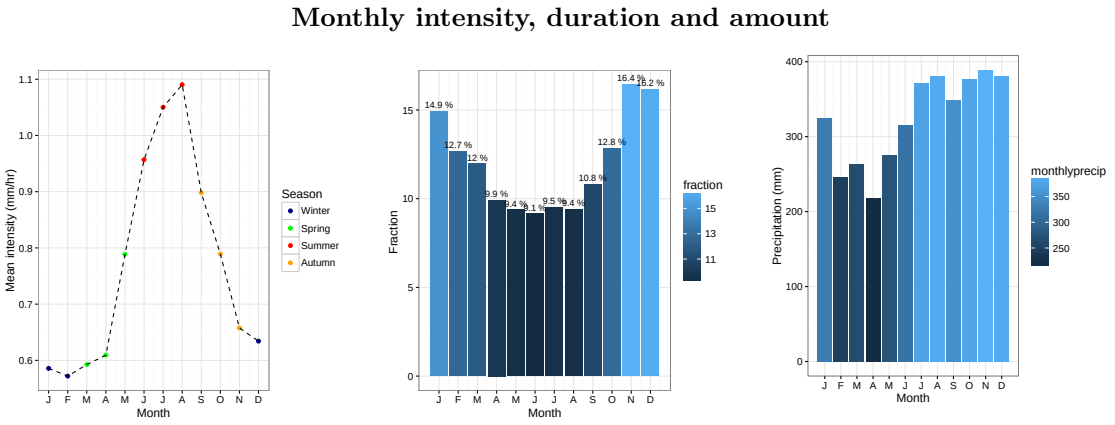

(a) Monthly mean intensity

(b) Monthly fraction wet time

(c) Monthly fraction of total precipitation amount

Figure 4.6: (a) The mean intensity, (b) fraction of the time that precipitation occurs and (c) the annual mean amount of precipitation per month.

From Figure 4.6 we can deduce the relative importance of the mean intensity in wet hours and the fraction of time that precipitation occurs on the total amount of precipitation accumulating per month. The months July till December account for the highest fractions of the total rain amount, approximately 10% per month (Figure 4.6c). In these months the intensity is high (July-September), or the fraction of time that precipitation occurs is high (November-December), or both are just above the mean (October). Moreover, Figure 4.6a shows that the intensity is strongly seasonal dependent, and the theory of weak winter precipitation (here December-April) and intense summer precipitation (June-September) is confirmed by this figure. In November till January it is raining about 4% of the time more than in the months April-September. Figures 4.6a and 4.6b thus demonstrate that precipitation in the winter is spread out more over multiple hours. In other words, in winter it is raining more often, but less intense. Most of the precipitation accumulates in the second half of the year, this arises from a higher mean intensity in autumn than in spring and a higher fraction of wet time in the months November and December. Further, as we are especially interested in impacting rain events, we also investigated the seasonal variability for extreme hourly precipitation, defined as the 95-99.9% quantiles in intensity of wet hours only.

Figure 4.7a shows all monthly maxima in (mean) hourly intensities and how this data is distributed. From this we can deduce that precipitation extremes are season dependent, with intensities between 3-20 mm/hr in December-February compared to much higher intensities in June-August (5-52 mm/hr). So not only the magnitude, but also the variability in magnitude is higher for the summer season compared to the winter season. What is more striking, is that the "belly" of the month September has a significantly higher position (around 13 mm/hr) than the "belly" of May (around 6 mm/hr). The same seasonal pattern is also visible in the monthly quantiles of precipitation intensities (Figure 4.7b), with quantile peaks in the summer season. Moreover, the higher the quantile, the larger the monthly or seasonal difference.

In order to investigate the mean duration of extreme events, we plotted the mean monthly duration (fraction of the hour that precipitation occurs) of all hours with an intensity of > 5 mm/hr (Figure 4.8). A clear seasonal cycle in the mean duration of hourly extremes is visible, with hourly time fraction of > 0.90 for winter months and of approximately 0.80 for summer months. Keep into mind that for the months December-March only $\sim$ 0.1-0.3 % of the wet data (25-75 points) is higher than 5 mm/hr, while for the months June-September this is $\sim$ 1-4 % (250-1000 points)(Figure 4.7b).

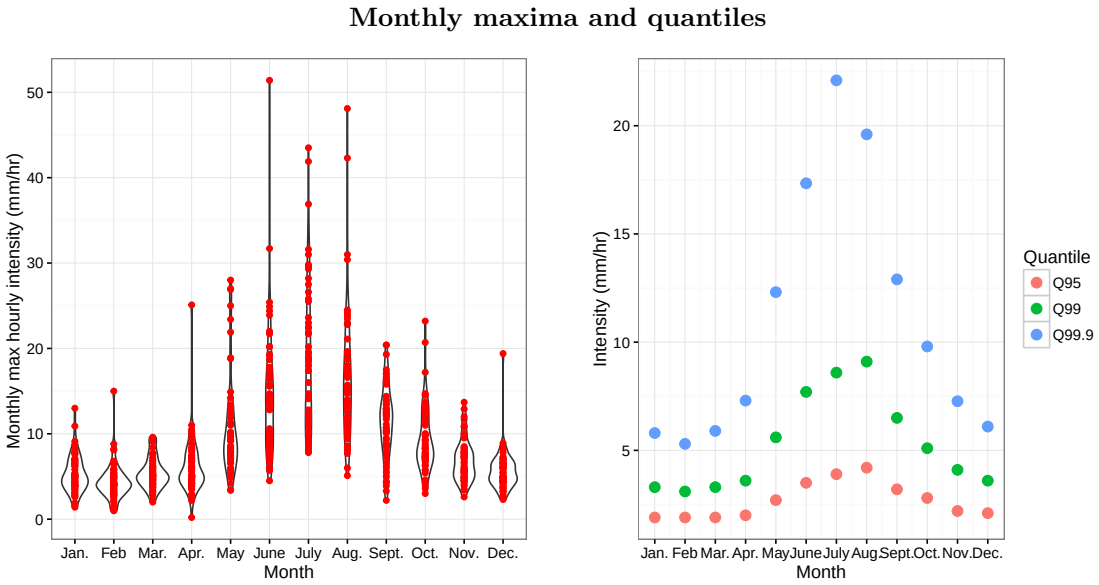

(a) Violin monthly maxima

(b) Quantiles

Figure 4.7: On the left side violin plots constructed from the monthly maximum hourly intensities (red dots). On the right side the 95%, 99%, 99.9%-quantiles in precipitation intensity of wet hours only for each month.

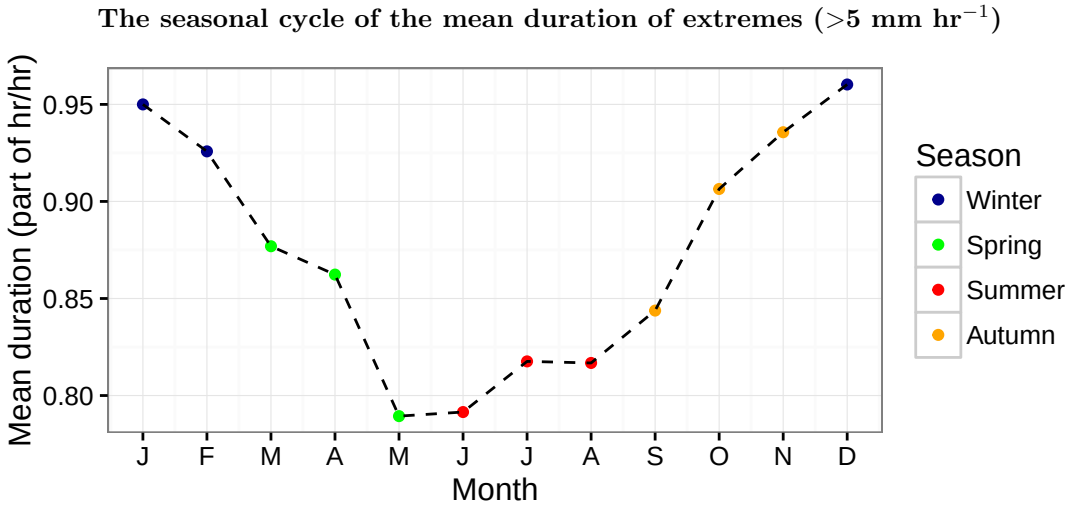

Figure 4.8: The mean monthly duration of precipitation within an hour with an extreme hourly intensity of >5 mm hr^{-1}.

Based on the intensity, frequency and duration characteristics of the different months, the two seasons which differ the most are the winter (consisting of the months December-January) and the summer (June-August). In the following figure (Figure 4.9) we plot the mean number of wet hours per day, the distribution of duration (of precipitation) within an hour and the relation between intensity and duration. For all these plots, we show results of the defined winter and summer season.

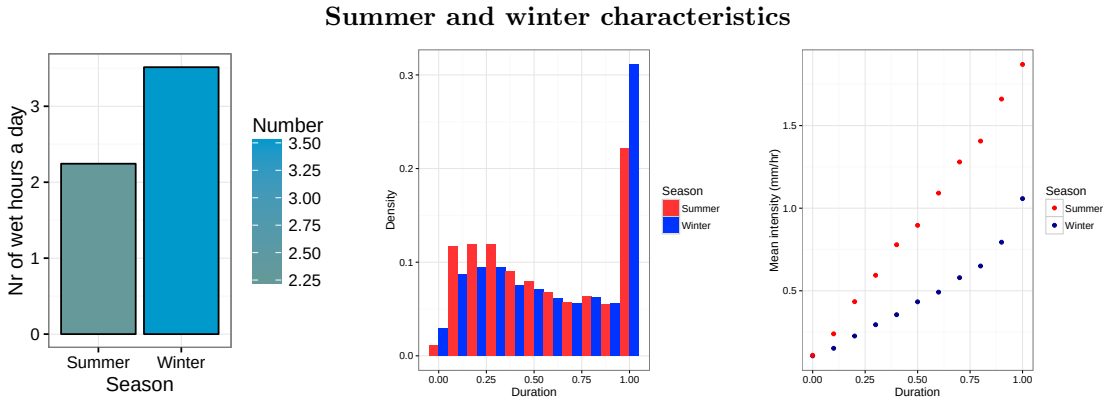

(a) Number of wet hours a day (b) Distribution duration (c) Intensity vs duration

Figure 4.9: The mean number of wet hours a day, the distribution of all durations (of wetness within an hour) and mean intensity of wet hours plotted against duration for summer (red) and winter (blue) data.

Figure 4.9a confirms what we already deduced from Figure 4.6b, namely that in winter time (daily) precipitation is spread out over more hours than in summer time. The mean difference in wet hours a day is ~ 1.3 hours. The overall shape of the summer distribution of mean durations has a peak at an hourly fraction 0.20 and the overall shape of the winter distribution at an hourly fraction of 0.25. Both distributions have a positive skew and an outlying density value for the longest hourly fraction. For approximately 25% of the wet hours it is raining for the entire hour (Figure 4.9b). This occurs $\sim 4.5\%$ more in winter than in summer (4.9b). However, the summer has relatively higher frequencies for events with a duration between 0.1-0.4 hour.

Moreover, we investigated whether for the same duration more summer precipitation accumulates or more winter precipitation in Figure 4.9c. Take into account that we plotted the mean intensity as the hourly precipitation accumulated within an hour. Therefore, the longer the duration, the higher the accumulation amount of precipitation amount can be. Figure 4.9c shows that for the same duration more precipitation accumulates within an hour in summer, compared to winter. What is striking about the winter mean intensity against duration, is the sharp increase in slope for the longest durations. So, in winter time when it rains for the entire hour, it rains more intensively. In conclusion, our results confirm theory in that summer precipitation is more short-lasting and intense than winter precipitation.

4.3 Combined seasonal and spatial variability

At last, we include figures that combine spatial and seasonal differentiation.

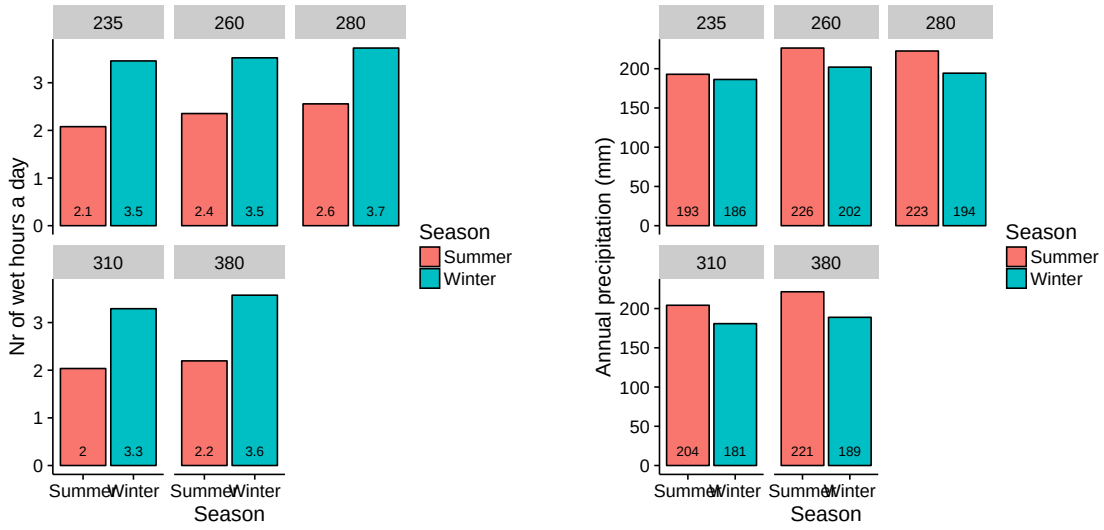

(a) (b)

Figure 4.10: (a) The daily number of wet hours and (b) the amount of annual precipitation (mm) per season and station. De Kooy has station number 235, De Bilt 260, Eelde 280, Vlissingen 310 and Maastricht 380.

What is interesting in Figure 4.10 is that we can clearly observe that every station has a higher daily number of wet hours in winter than in summer, and lower annual amounts of precipitation accumulating in winter than in summer. This difference between summer and winter is larger for the former than the latter. Moreover, the spatial variation in the summer-winter difference is larger for precipitation amounts than for frequencies of wet hours. The summer-winter difference for De Bilt, Eelde and Maastricht in precipitation amount is approximately three times as large as the summer-winter difference for De Kooy. The summer-winter difference in frequency of wet hours is in the range of 1.1-1.4 hour a day for all five stations.

Figure 4.11 gives the violin plots for summer and winter for every station, indicating differences in seasonal extremes. We already concluded that the largest spatial differences exist for the highest intensities and that the highest intensities correspond to summer events. This figure confirms that the differences in the thickness and extent of the violins between the stations are the largest for the summer season. It is worth noting that the spatial difference in extent is mainly due to a couple of outliers. In summary, spatial differences in the Netherlands are not significantly large, except for extremes, and the summer season is the most interesting season when considering extremes.

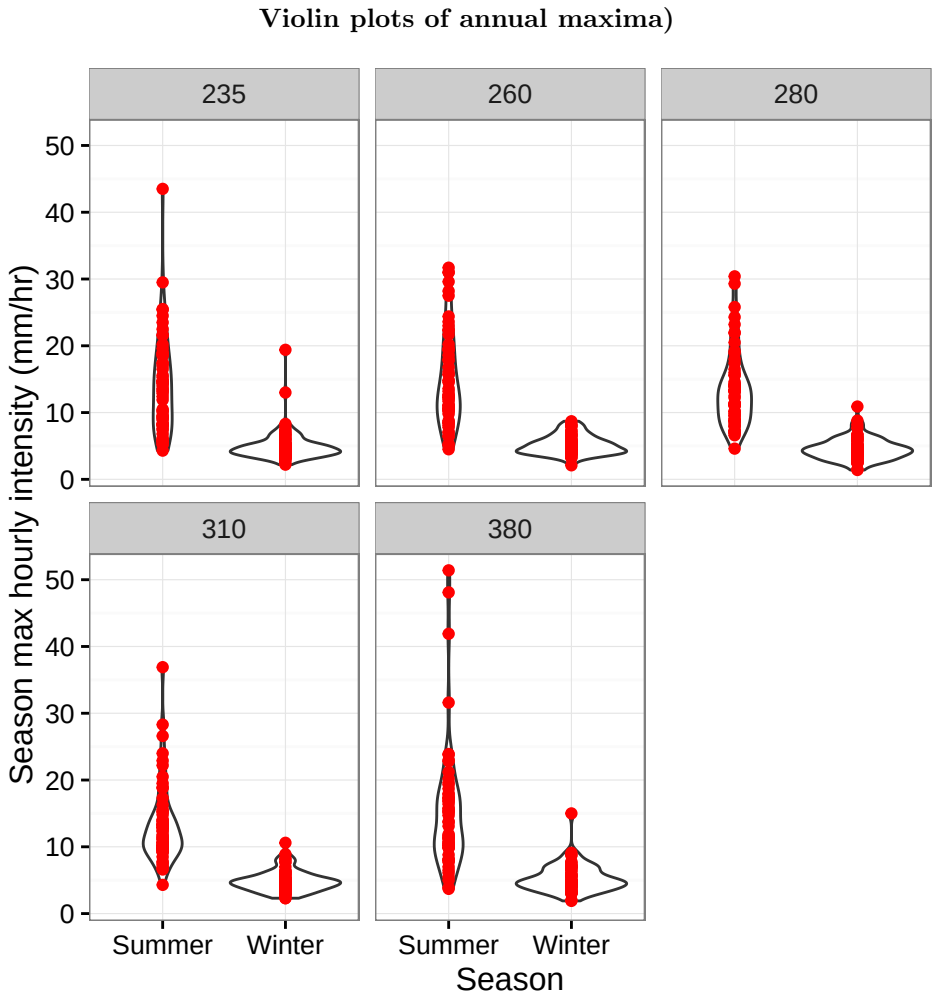

Figure 4.11: The violin plots of the summer and winter annual maxima in hourly intensity per station.

Chapter 5

Trends in extreme precipitation

5.1 Introduction

This chapter focuses on linear trends in hourly precipitation extremes. Whether the hourly intensity (calculated from the hourly precipitation sum as the mean rate of one hour) of extremes increases or decreases linearly in time or remains constant, is investigated for the period 1958 to 2015. Next to intensity, trends in the frequency of wet hours are considered. The latter is counted as the number of wet hours (P $>$ 0.05 mm) for every 2-day period and for every year. Lastly, we also study trends in the 2-day and yearly precipitation sums. Then we can say something about the importance of a trend in frequency or in intensity for the trends in the total precipitation accumulating. Changes in the latter are namely expected to be the result of changes in the former two. Both types of trends are compared to the regression of the mean in time, thereby studying the proportional change. In Chapter 4 we concluded that spatial differences are in general not that high in the Netherlands, however, strong differences exist for extremes. Therefore, it is interesting to consider the trends individual for every station. Moreover, the presence of a signal at multiple stations, enhances the robustness of the trend observed. Furthermore, all three types of data are differentiated on summer and winter season, to deduce the seasonal dependence of trends. Besides, the observed trends are tested on level of significance by a Monte Carlo permutation test. In addition, we quantified the trends by investigating the rates.

5.2 Intensity

5.2.1 All hours

First, we study the regression of the quantiles for every station in Figure 5.1, based on the intensity of every hour in the period 1958 to 2015. As the data consist of dry hours (P $<$ 0.05 mm/hr) for approximately 88% of the time (Chapter 4), the quantile values corresponding to the 50% and 75% fits are always zero, therefore they are excluded from this figure.

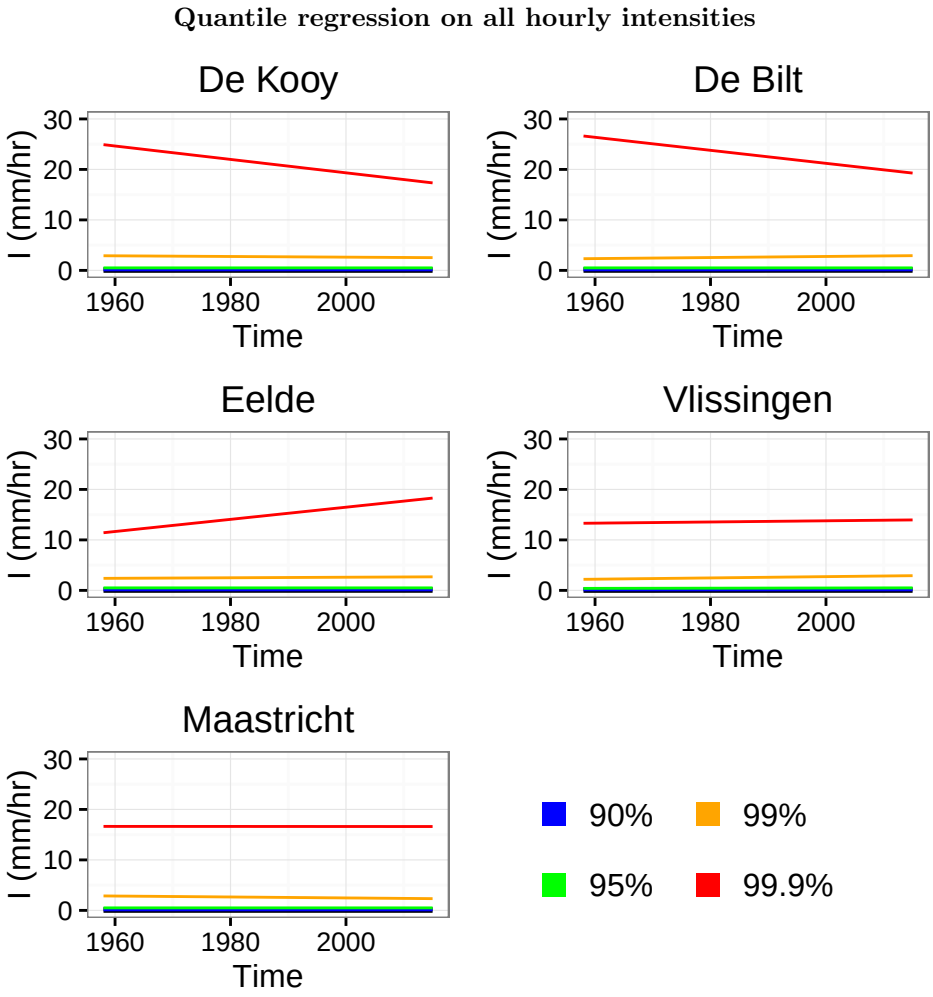

Figure 5.1: Quantile regression fits with $\tau = 90, 95, 99, 99.9$ % on all hourly precipitation intensities (mm/hr), for all stations.

From this figure 5.1 we can not clearly observe trends for the different quantiles, except for the 99.9% fit, corresponding to values higher than 11-27 mm/hr, occurring 0.1% of the time ($\sim$ 9 hours per year). In fact, these 99.9%-quantile trends differ highly between the five stations. As these trends are based on $\sim$ 510 data points in total, it might be that the trends are not significant. We will discuss in more detail the significance of the plotted quantile lines at the end of this paragraph. Next to the amount of data points, trends can be biased. From Section 2.4.2 we know that the assumption of independence of errors may be violated by the autocorrelation nature of time series. The magnitude of the trend is influenced by serial correlation, when present in the data set (Yue et al., 2002). Therefore, we now investigate whether there is any significant autocorrelation and partial autocorrelation present in the hourly intensity values.

Figure 5.2 shows the autocorrelation and partial autocorrelation plot for the hourly data set of De Bilt. For the other stations we did not include the same figures, because for both functions there are no large differences between the stations.

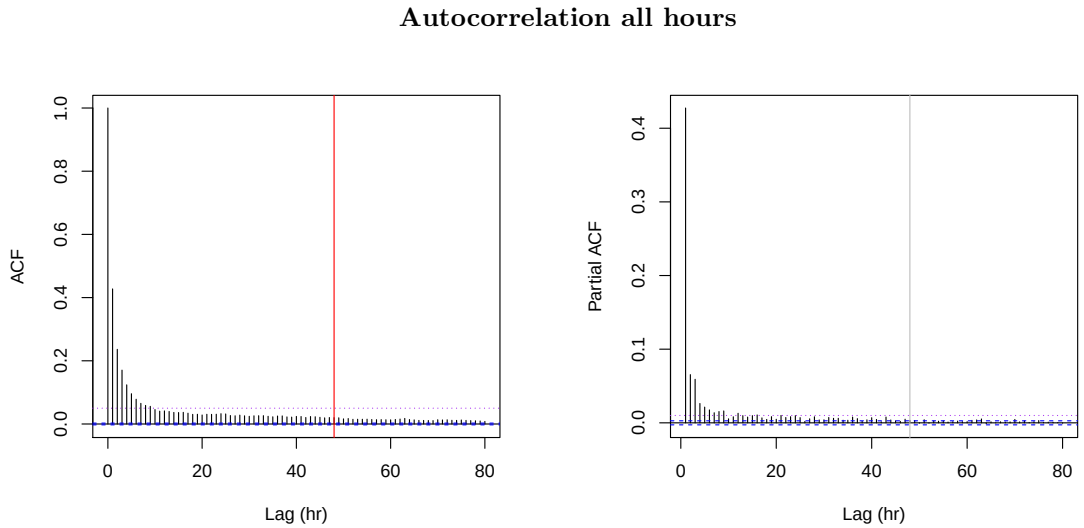

(a) De Bilt (b) De Bilt

Figure 5.2: Autocorrelation and partial autocorrelation function (ACF and PACF) for all hour precipitation data of station De Bilt. The dotted purple lines gives levels of 0.05 ACF and 0.01 PACF, and the red lines indicate a lag of 48 hours.

For lags of 1 to 48 hours the autocorrelation and partial autocorrelation values are significant (> 0.05). Moreover, a winter depression will not last longer than 2 days (and summer rain events are mainly on the scale of several hours). Therefore, we will now apply quantile regression on the maximum value for periods of 2 days to remove significant serial correlation.

5.2.2 2-day maxima

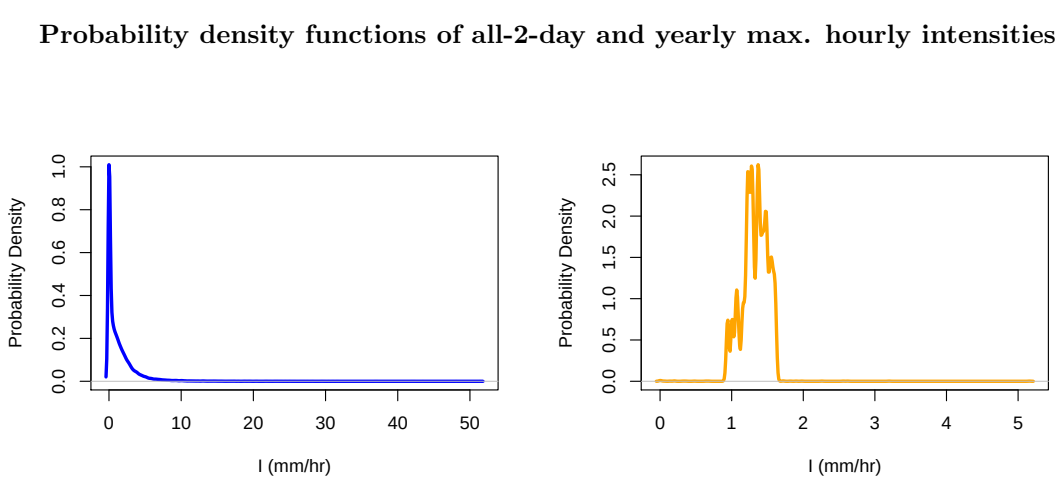

(a) All (b) Yearly mean

Figure 5.3: Probability density functions of (a) all-2-day max. and (b) yearly mean 2-day max. hourly intensities (mm/hr). All stations are combined.

As the probability density function of the 2-day intensity maxima has no Gaussian shape (see Figure 5.3), it is not right to use linear least-squares regression from a statistical point of view (as

explained in Chapter 2). However, the probability density function of yearly mean 2-day maxima has a more normal distribution. Thus, we only use ordinary least squares regression on the yearly mean 2-day maxima (Figure 5.4). Figure 5.4 also demonstrates the quantile regression fits on 2-day maxima in intensity. Note that all 2-day periods (not only wet 2-day periods) are included in this trend analysis. In contrast to Figure 5.1, where only regression of the 99.9% quantile lines was visible, in this plot also the 99% quantile line seems to regress linearly. This arises from the new time scale, because the 99.9%-quantile line is not the same as in the previous figure s only the maxima of 2 days are considered.

In Figure 5.4 the 99%- and 99.9%-quantiles are computed from the (quantile regression) minimization function to values higher than 9-10 mm/hr and 16-20 mm/hr respectively. We can already deduce from this figure that spatial differences exist in the magnitude and sign of the trend and that these differences are higher for the 99.9%-quantile than for the 99%-quantile. The 99.9% quantile lines for 2-day maxima in intensities measured at De Kooy and Eelde decrease linearly in time with rates of 0.1 and 0.05 mm/hr/yr respectively, while the same quantile lines increase for De Bilt and Maastricht (at rates of 0.13 and 0.07 mm/hr/yr) and remains almost constant for Vlissingen ($\sim$ 0.02 mm/hr/yr). No visible trends are observed for the yearly mean intensity and the 75%, 90%, 95%-quantiles.

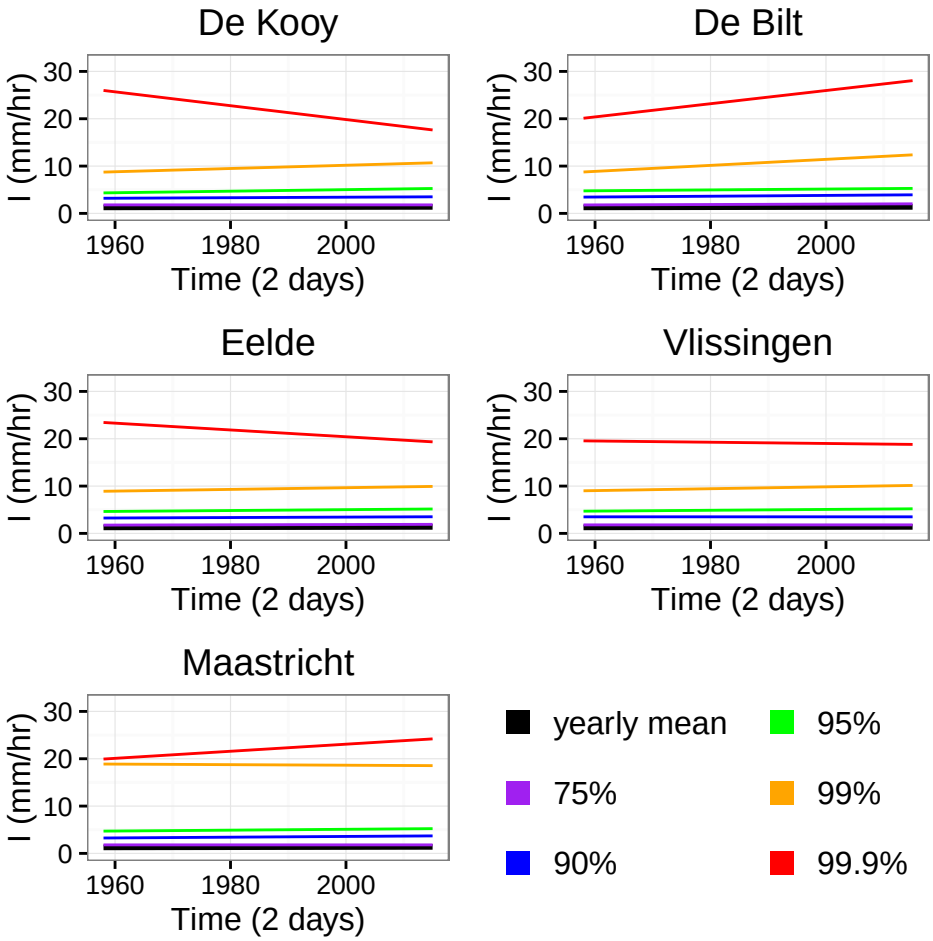

Figure 5.4: For all stations quantile regression fits with $\tau = 75, 90, 95, 99, 99.9$ % on 2-day maxima in hourly precipitation intensities (I) in mm/hr, given by colored lines. The black lines are the ordinary least squares regression on the yearly means of 2-day intensity maxima.

Only for De Bilt Figure 5.4 suggests that the 99%- and 99.9%-quantiles increase considerable in time. Whether the 99 and 99.9%-quantile trends for De Bilt are significant is investigated by a 9999 Monte Carlo permutation test of the ordinary least squares regression coefficient. The corresponding probability density functions of the permuted slopes are shown in Figure 5.5.

For De Bilt, both the 99%-quantile, and the 99.9%-quantile are not significant (P=0.8734). This might be due to the limitation in the number of values higher than the 99%- and 99.9%-quantile ($\sim$ 106 and 11 data points). If the 99.9% is not significant for all stations, this might explain the opposing signals.

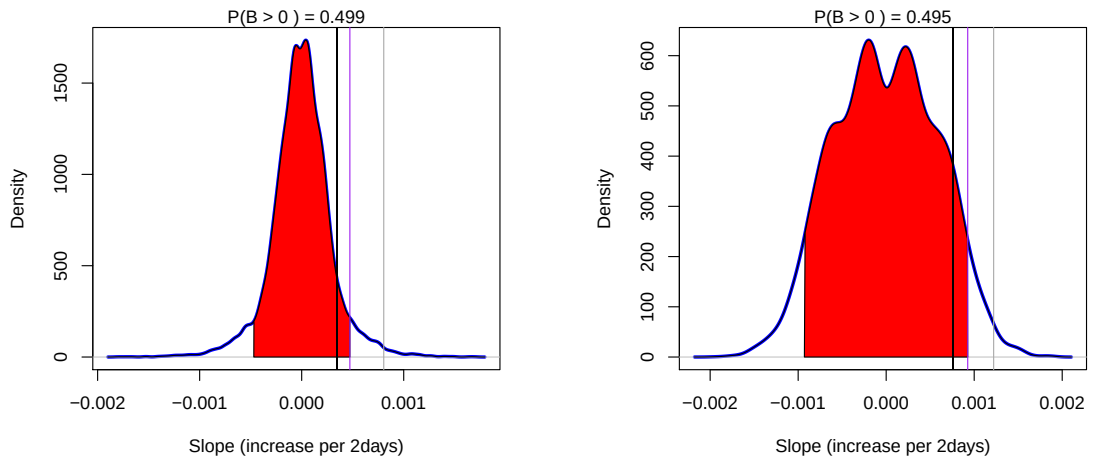

(a) 99% fit

(b) 99.9% fit

Figure 5.5: Probability density functions for 9999 Monte Carlo permuted slopes based on $\tau = (a)99$, and (b) 99.9%-fitted values of 2-day maxima in hourly precipitation intensities (mm/hr) for De Bilt. The purple (gray) lines give the upper-tail slope at the 95% (99%) confidence level. The black lines indicate the observed regression coefficients.

Next, to verify whether the (99% and) 99.9% quantile lines are indeed insignificant for the other stations, we will also study the p-values for the quantile fits of the other stations. In fact, the significance of all quantile lines and ordinary least square lines is determined for all stations and displayed in Table 5.1. A green cell indicates a significant positive trend ($p \geq 0.95$). A cell in this table is colored red when the quantile line is significantly not-increasing, so it is constant or decreasing. ($p \leq 0.05$).

Table 5.1: Significance table for all fits on 2-day max. hourly intensity data

Location		Quantiles of fit						OLS
Station	STN	50%	75%	90%	95%	Q99%	99.9%	Yearly mean
De Kooy	235	0.15	0.06	0.96	1.00	0.84	0.07	0.9435
De Bilt	260	0.05	0.99	1.00	0.95	0.91	0.90	0.9435
Eelde	280	0.01	0.96	0.93	0.92	0.73	0.26	0.9329
Vlissingen	310	0.91	0.07	0.30	0.96	0.82	0.47	0.9235
Maastricht	380	0.25	0.11	0.98	0.95	0.45	0.67	0.7176

All 99.9% quantile regression fits are indeed insignificant (Table 5.1). The surprising opposing regression lines for this quantile can thus not be detected as true trends, but may be influenced by the limited amount of data points. All the 99%-quantile fits are also insignificant. Multiple quantile regression lines are significantly positive for the 2-day intensity maxima; 6 on the 95% confidence level and 3 on the 99% confidence level. What is striking about the other p-values for De Bilt, is that it has three quantiles which increase significantly at the 99% or 95% confidence level, while the 50%-quantile is significantly not-increasing. For all stations large differences exist in the p-values for the different quantiles. It should be recognized that zero significant increasing trends are detected for the 50%-quantile fit and the ordinary least squares fits on the yearly means, whereas a maximum of four significant trends is detected for the 95%-quantile fit. Note that the p values of the ordinary least squares fits are based on only 58 years. A general disproportional

increase of relatively high intensities compared to relatively moderate intensities can be recognized in the amount of significant increasing trends per quantile.

In AR5 of the Intergovernmental Panel on Climate Change ((IPCC, 2013)) a shifting probability density function (PDF) for intensity towards higher values as a result of temperature increase is proposed. However, does our observation of dissimilarity in the presence and magnitude of significant trends in the quantile fits for a station contradict to the theory of a shifting probability density function (PDF) for intensity with temperature? Considering the method of quantile regression this does not need to be the case. In quantile regression there are no quantiles calculated for each time period, which would correspond to the PDF at that time. Quantile regression is namely a minimization function on the entire data set (Chapter 2). Therefore, the fitted lines are not a result of a clear step-wise shifts in time of the entire PDF and corresponding quantiles. This means that comparing the behavior of the different quantile lines for one station is not meaningful, but comparing a certain quantile between different stations is. Dissimilarity in trends with respect to the quantiles is also observed in a study of Malik, Bookhagen, and Mucha (2016), which uses quantile regression as well.

Figure 5.6 demonstrates the change in PDF by plotting the PDF of the 5-year period 1958-1962 next to the 5-year period 2011-2015. This figure confirms that there are not true changes for different parts of the intensity spectrum. However, compared to the older period, the newer period shows a decrease in lower intensities and an increase in higher intensities. Nonetheless, clear horizontal movement of the PDF is not visible.

In addition, the study of Malik, Bookhagen, and Mucha (2016) detected spatial inhomogeneity in trends for India. Despite the fact that the Netherlands is a relatively small country compared to India, spatial differences are present in the magnitude and amount of significant trends.

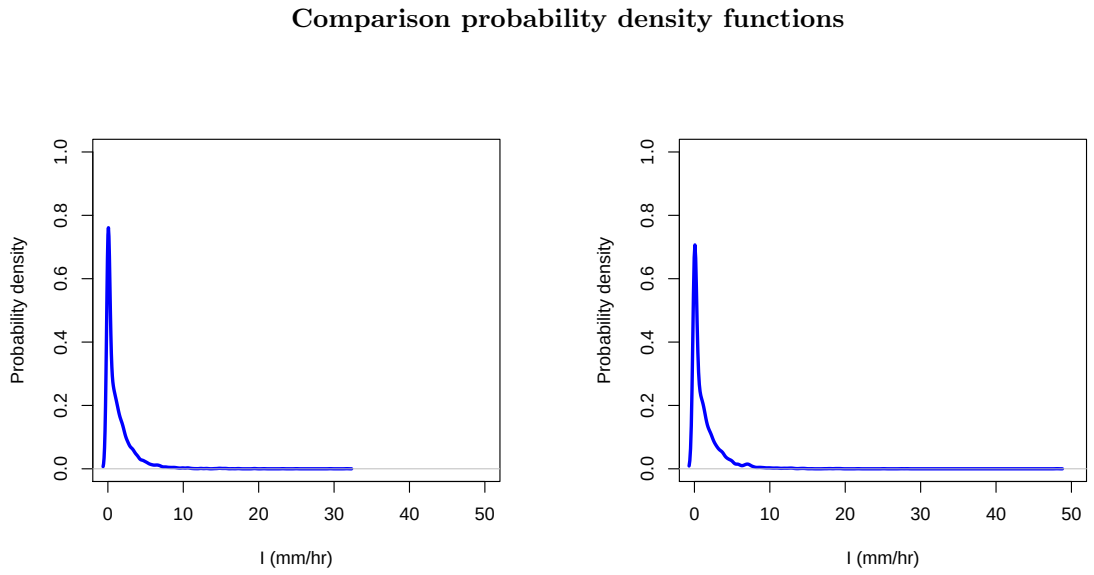

(a) 1958-1970

(b) 2003-2015

Figure 5.6: Probability density functions of all 2-day maxima in intensities for the period 1958-1970 (a) and for the period 2003-2015 (b).

In Chapter 6 we hope to find an explanation for spatial differences in intensity. Although the trends are characterized by spatial inhomogeneity and dissimilarity with respect to the quantiles,

it should be stressed that almost all significant trends detected are positive. For the two non-increasing 50%-quantile lines, we still have to determine whether these are significant constant or decreasing lines. In general, we can conclude that through a time period of 58 years the precipitation intensity of extreme events increases.

Not only the presence and sign of a trend is important, but also the magnitude of the trend. Table 5.2 displays the rates of increase in intensity (mm/hr) per year for all significant trends.

Table 5.2: Rates of significant trends of "moderate"-"high" extreme intensities

Location		Rates (2-day max mm/hr per year)			
Station	STN	50%	75%	90%	95%
De Kooy	235	-	-	$5.4e^{-3}$	$1.6e^{-2}$
De Bilt	260	$2.3e^{-14}$	$4.2e^{-3}$	$8.5e^{-3}$	$9.0e^{-3}$
Eelde	280	$-5.5e^{-16}$	$2.8e^{-3}$	-	-
Vlissingen	310	-	-	-	$8.9e^{-3}$
Maastricht	380	-	-	$7.8e^{-3}$	$9.1e^{-3}$

As all the trends for the 99%- and 99.9%-quantile fits are insignificant, their rates are excluded from Table 5.2. Take into mind, that although no significant trends are found for the highest quantiles, trends can still exist. A larger data set might give significant trends for the highest quantiles, which are then assumably positive, as all the other detected trends are positive (except for the 50%-quantile of De Bilt and Eelde).The computation of the rates of all significant rates, does not only gives us the magnitude, but also verifies whether a trend is indeed positive, constant or negative. Table 5.2 shows that the two non-increasing trends are so close to zero that they are negligible, and can be considered constant in time.

The four highest rates in 2-day intensity maxima, on the order of 0.01 mm/hr/yr, are those of the highest quantile (95%) for all stations except Eelde. For the entire period of 58 years this translates to an increase of the intensity of extreme hourly precipitation (for the 5-10% highest 2-day maxima) of 0.5-1 mm/hr. In magnitude this change equals the difference in mean intensity between summer and winter (Chapter 4). All the other significant increasing trends have rates on the order of 0.001-0.01 mm/hr/yr. In general, the higher the quantile per station, the higher the magnitude of the detected trend. The yearly mean of the maxima increases on the order of 0.001 mm/hr/yr.

This disproportional increase of the intensity of "high" extremes (P>90% or 95%) compared to the mean and "low" extremes(P>50% or 75%), is consistent with the observations of the IPCC (stated in Chapter 1). Our findings can thus be explained by the theory that low and moderate intensities correspond more to large-scale precipitation, which is more constrained by the energy budget of the atmosphere, while the extreme precipitation (and related intensity) has a non-linear dependency on moisture availability. To investigate what explains the spatial differences in the detection of significant trends and why intensity maxima in general increase in time, we will dive deeper into the causes behind these trends in Chapter 6.

In Table 5.3 we provided the relative rates of all significant trends of "low"-"high" extreme intensities. The rates of trends in "low" extremes (50%-quantiles) are negligible, but the rates of trends in "moderate"-"high" extremes vary are approximately 0.2-0.4%/yr, which demonstrates that the disproportionality is less robust. The rates of 95%-quantiles of De Bilt and Maastricht are lower than expected.

Table 5.3: Relative rates of significant trends of "moderate"-"high" extreme intensities

Location		Rates (% per year)			
Station	STN	50%	75%	90%	95%
De Kooy	235	-	-	0.17	0.38
De Bilt	260	$3.9e^{-12}$	0.23	0.25	0.19
Eelde	280	-9.2^{-14}	0.16	-	-
Vlissingen	310	-	-	-	0.19
Maastricht	380	-	-	0.24	0.19

5.2.3 Summer vs winter

In this paragraph we will distinguish between summer and winter trends in 2-day maxima, as the type of precipitation (characterized by specific intensity) is season dependent (Chapter 4). For the summer extremes, we could probably take shorter (independent) periods for sampling maxima based on the autocorrelation and partial autocorrelation, because of their local, short-lasting character. This would increase the amount of samples and this might improve the significance of any trends present. However, as we want to compare the trends between summer and winter season, we do not want to have 2 different approaches of data selection, as this could induce seasonal differences without physical basis. Figure 5.7 shows the quantile trends in 2-day maxima of both seasons. The 99.9%-quantiles are left out of this figure, as this would correspond to only 2.87 data points respectively (0.1% of the 2-day maxima within 3 winter or summer months for 58 years).

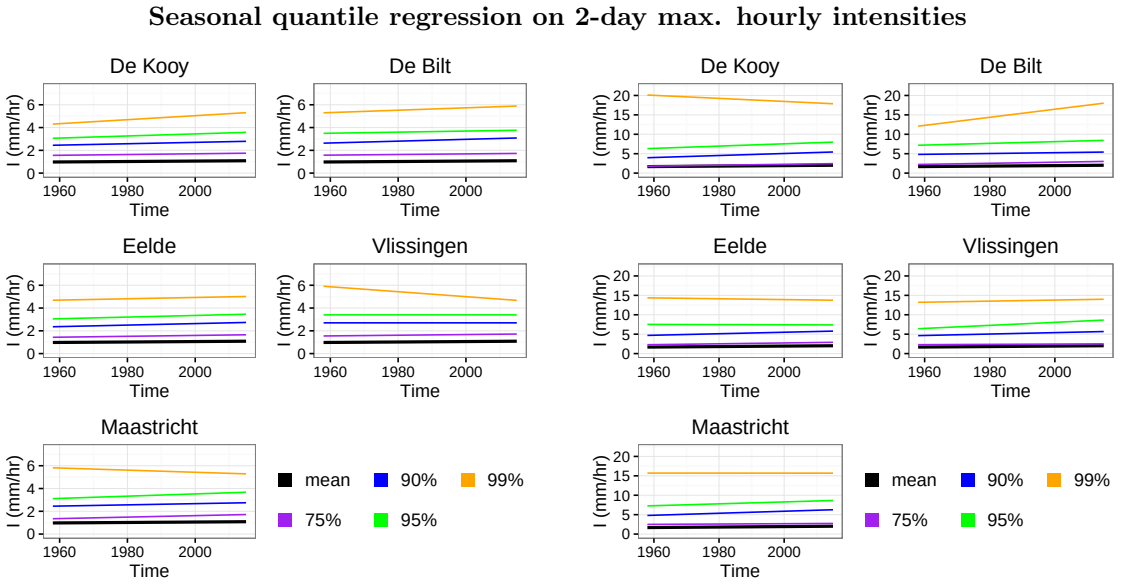

(a) Winter

(b) Summer

Figure 5.7: Quantile regression fits with τ = 75, 90, 95 and 99% on 2-day winter (left) and summer (right) maxima in hourly precipitation intensities (mm/hr), for all stations. The black line represents the ordinary least squares regression of the yearly means.

What is striking, is the difference between summer and winter in magnitude of the extremes. Where the highest quantile for winter data represents values higher than 5-6 mm/hr, the highest quantile for summer data corresponds to extreme intensities higher than 12-20 mm/hr. Both the magnitude, and the spatial differences (in sign and magnitude) for this quantile is bigger for the summer season, than for the winter season, which corresponds to our conclusions from Chapter 4.

Precipitation events are generally more intense in summer. Besides, we find that spatial differences are also relatively high for more intense precipitation, which could be explained from the probability density functions shown in Chapter 4. Namely the more intense the hourly precipitation is, the lower the chance of occurrence, so the higher the effect of outliers. Whether these fits for the high quantiles with large spatial differences are significant, will be tested in the next part. The fits for the lower quantiles seem all to be constant or increasing in time for summer intensities, as well as for winter intensities. Furthermore, the winter 99%-quantile lines are positive for De Kooy, De Bilt and Eelde and negative for Vlissingen and Maastricht. For summer, this quantile line is negative for De Kooy, positive for De Bilt, and near constant for Eelde, Vlissingen and Maastricht.

Comparing the summer and winter trends for the 99%-quantile to the observed trends of all 2-day maxima in Figure 5.4, those of De Kooy and Eelde are recognized as summer trends. Nonetheless, we expect trends in the upper part of the probability density function of all 2-day intensity maxima to be based on summer data, as those have the highest values. This also holds for De Bilt, but not for Maastricht of which the positive trend for all 2-day intensity maxima is not detected as a summer (or winter) trend. Nevertheless, when considering only summer data we have a different probability density function than we have for all 2-day data. Therefore, the 99%-quantile for 2-day (all hour) data probably corresponds better to the 95%-quantile for 2-day summer data. This more or less holds for Maastricht, De Kooy, De Bilt and Vlissingen, but not for Eelde. Next to studying the plotted regression lines, the significance of all quantile lines is tested and the corresponding p-values are showed in Table 5.4.

Table 5.4: Significance table for all fits and specified to summer and winter intensity data

Location		Quantiles of fit			
		Summer			
Station	STN	50%	75%	90%	95%
De Kooy	235	0.90	0.99	0.99	0.94
De Bilt	260	0.28	0.99	0.84	0.86
Eelde	280	0.78	0.99	0.95	0.49
Vlissingen	310	0.86	0.71	0.96	0.97
Maastricht	380	0.53	0.73	0.98	0.86
		Winter			
De Kooy	235	0.21	0.91	0.97	0.98
De Bilt	260	0.95	0.86	0.97	0.78
Eelde	280	0.26	0.96	0.99	0.88
Vlissingen	310	0.97	0.87	0.29	0.37
Maastricht	380	0.12	0.99	0.92	0.97

No significant trends are detected for the fitted ordinary least squares and 99%- and 99.9%-quantiles, so they are excluded from Table 5.4. For both seasons multiple significant positive trends are demonstrated for intensities corresponding to the 50%-95%-quantiles (Table 5.4). Even for the 50%-quantile no significant non-increasing trends are found. For all stations approximately two significant trends in 2-day maxima per station and season are detected. For the winter season there are larger spatial dissimilarity in the type of quantile trends (ranging from 50%-95%) than for the summer season (concentrated on 75%-90%). In Chapter 6 we hope to discover why the intensity maxima increase for both seasons and what explains the dissimilarity in quantiles.

Significant summer trends have positive rates ranging between 0.01-0.04 mm/hr in 2-day maxima per year and winter trends have positive rates ranging between 0.003-0.01 mm/hr in 2-day maximum per year. Comparing absolute summer and winter rates, we can conclude that summer trends resemble better the trends in the highest all-2-day maxima, which confirms our observation of higher summer intensities compared to winter intensities (Figure 5.7). Over a period of 58 years

the highest 5-10% 2-day intensity maxima have increased with 1.1-2.3 mm/hr for summer data only, and with 0.35-0.6 mm/hr for winter data only. Both seasons show a disproportionality in the growth, with larger rates corresponding to higher quantiles of intensities. The largest summer rates are those corresponding to the 90%-quantile of De Kooy and the 95%-quantile of Vlissingen. The largest winter rates correspond to the 95%-quantiles of De Kooy and Maastricht.

When considering the relative rates of significant trends in "high" intensities, rates of 0.1-0.6%/yr are found for summer, which are stronger than the winter rates (0.1-0.3%/yr) in "high" intensities. For the lowest quantiles only significant and strong winter trends are found. What is more striking, is that for winter we observe reversed disproportionality. The highest relative rates, on the order of 0.5-0.7%yr, namely correspond to the lowest (50%) significant quantile trends.

5.2.4 Summary

To summarize, we found significant increasing trends in the intensity of the 25-5% highest 2-day maxima (0.2-0.4%/yr). In 58 years the highest maxima have increased with 0.5-1 mm/hr. This can be compared to a change of at least the total difference in mean intensity between summer and winter. Besides, similar as to other studies we observed that the "high" extremes increase in a disproportional way, compared to the mean, "low" and "moderate" extremes. Moreover, positive trends were present in both winter as summer data for respectively the 50-5% and 25-5% highest 2-day season maxima. However, the trends in "high" extremes are likely to be summer trends. The summer 2-day intensity maxima are one order stronger (in absolute way) than the winter trends, but keep into mind that summer intensity maxima are generally one order higher than winter intensity maxima. Considering relative trends, summer trends in intensity are stronger (0.1-0.6%/yr) for the "moderate"-"high" extremes than winter trends (0.1-0.3%/yr), while only significant winter trends are found for "low" extremes (0.5-0.7%yr). For all trends we observe a spatial dissimilarity in the significance and rate of a trend regarding the type of quantile considered.

5.3 Frequency

Next to changes in intensity of extreme precipitation events, is it also relevant to study whether precipitation events occur more, equally or less often in time. In this section, analysis of frequency of wet hours is reported. First, the number of wet hours per 2 days is investigated in Figure 5.8. Next to trends in intensity, we can then draw conclusions on trends in wetness for the same temporal resolution. Second, the same is repeated for the number of wet hours a year, which is a more intuitive approach to look at the changes of wetness in time. Furthermore, we have investigated whether trends in summer and winter wetness differ for the two approaches (but more thoroughly for yearly resolution).

5.3.1 2-day frequency

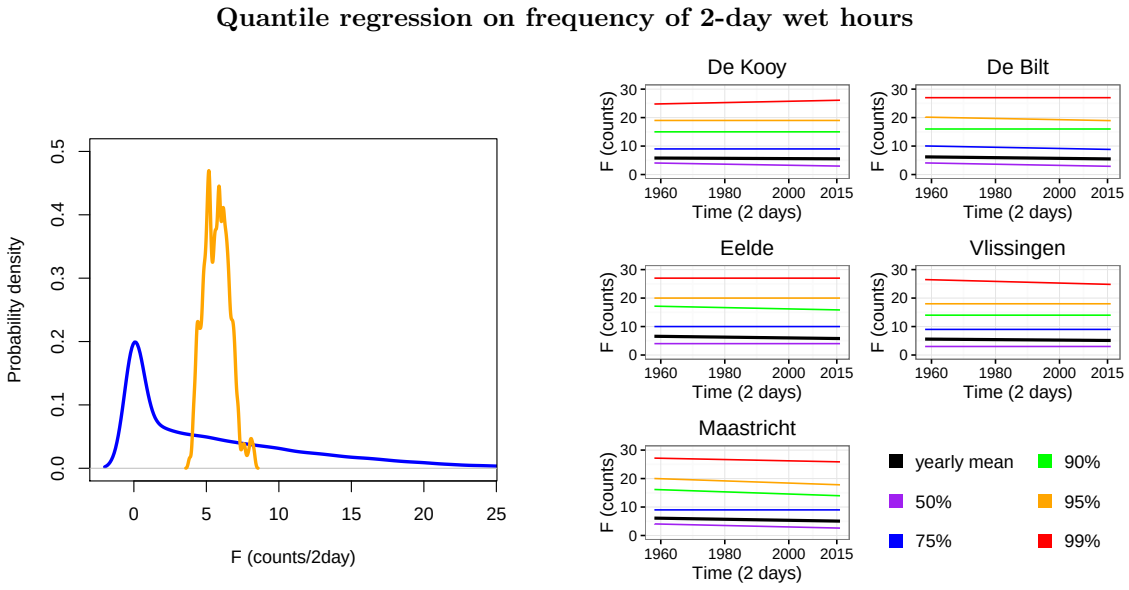

(a) Probability density functions

(b) Quantile regression

Figure 5.8: (a) Probability density functions of all and yearly mean frequencies of hours in which precipitation occurs per 2 days. In (b) quantile regression fits with $\tau = 25, 50, 75$ % on all 2-day frequencies and ordinary least squares regression (black line) on the yearly mean frequency of wet hours per 2 days for all stations. The coefficients of the ordinary least squares regression lines are given in the right corner.

The probability density function of the 2-day frequencies of wet hours (Figure 5.8a) looks more lognormal, than normal, therefore quantile regression is preferred above the ordinary least squares regression. As the yearly mean 2-day frequencies of wet hours are approximately normal distributed, we plotted the ordinary least squares regression of these means. In Figure 5.8b the 25%-quantile is excluded, because the 25% driest 2 days have no wet hours at all. In this figure small negative trends or constant regression lines are visible for the 50%-99%-quantile, except for the 99%-quantile of De Kooy. Spatial differences can be recognized in the strength of the negative signal. Where most of the quantile line of De Bilt and Maastricht have a slight negative slope, most of the quantile lines of De Kooy, Eelde and Vlissingen have no slope. However, all the ordinary least squares regression of the yearly mean 2-day frequencies of wet hours are negative.

To investigate whether a quantile trend is significant, a 9999 Monte Carlo permutation is applied. Of every fitted quantile regression line the corresponding p-value is listed in Table 5.5. From this table we can be deduce that most of the quantile regression lines are significantly non-increasing (which is indicated by the red marking), except for the 99%- and 99.9%-quantiles. In fact, the 99.9%-quantile for 2-day frequency data of Vlissingen is significant. Maastricht and Eelde both have 4 significant non-decreasing trends. Some trends are even below the 1% confidence level, thus very significantly non-decreasing. To verify whether these trends are significantly increasing, we reverse the p-test by counting the p value as all permuted slopes lower than the observed slope. Here, we colored the cells with a significant decreasing trend red and with a significant non-decreasing trend green.

In Table 5.6 we can deduce which trends are significantly decreasing (colored red). Some of the trends which were marked red in Table 5.5 are green in this table. As the p-values from these

Table 5.5: Significance table for all fits on 2-day frequencies of wet hours

Location		Quantiles of fit					
Station	STN	50%	75%	90%	95%	Q99%	99.9%
De Kooy	235	0.07	0.0002	0.01	0.03	0.79	0.27
De Bilt	260	0.002	0.01	0.02	0.09	0.28	0.28
Eelde	280	0.0001	0.001	0.01	0.01	0.31	0.73
Vlissingen	310	0.002	0.01	0.07	0.07	0.11	0.02
Maastricht	380	0.0001	0.0001	0.001	0.004	0.19	0.30

Table 5.6: Significance table for all fits on 2-day frequencies of wet hours (reversed p test)

Location		Quantiles of fit					
Station	STN	50%	75%	90%	95%	Q99%	99.9%
De Kooy	235	0.93	0.004	0.01	0.03	0.21	0.73
De Bilt	260	1.00	0.99	0.02	0.90	0.73	0.72
Eelde	280	0.0001	0.001	0.99	0.01	0.30	0.26
Vlissingen	310	0.002	0.01	0.08	0.07	0.89	0.98
Maastricht	380	1.00	0.0004	1.00	1.00	0.82	0.70

cells indicate that the fitted quantile values are significantly non-increasing and non-decreasing, they must be constant. We checked this for the p-values of these specific cells by plotting the probability density function of all permuted slopes. Those which are indeed zero are excluded from our computation of the rates of significant trends. Only negative rates remain, which are shown in Table 5.7. Several trends remain which are significantly negative; two for the lower quantiles of De Bilt, one for a relatively high quantile of Eelde and of Vlissingen and three for Maastricht. Moreover, most of these trends are significant at the 99% confidence level, which is different from the detected trend in 2-day intensity maxima (those were mostly significant at 95% confidence level).

Table 5.7: Relative rates of significant frequency trends

Location		Rates (%/yr)					
Station	STN	50%	75%	90%	95%	99%	99.9%
De Kooy	235	-	-	-	-	-	-
De Bilt	260	-0.50	-0.21	-	-	-	-
Eelde	280	-	-	-0.13	-	-	-
Vlissingen	310	-	-	-	-	-	-0.32
Maastricht	380	-0.62	-	-0.23	-0.19	-	-

All significant trends in counts of wet hours are verified as being negative by Table 5.7. The relative decreasing rates for the wettest (50-0.1%) 2 days are on the order of 0.1 % per year, while the trends in the mean 2-day wetness decreases with 0.08-0.29%/yr. The strongest negative trend (50% of Maastricht) has a negative rate of approximately 36% in 58 years. For frequency data we do not find the same disproportionality as for intensity data. The mean and the relatively drier 2-days (i.e. lower quantile fits) decrease faster in wetness than the wetter 2-days.

Considering the signal for whole the Netherlands, this corresponds to a reduction of 10.7% in wetness over 58 years. In absolute terms, this means that we have about 100 wet hours per year less, which is equal to the effect of moving from the northern part of the Netherlands (De Bilt or Eelde) to the southern part (Vlissingen or Maastricht) regarding the the spatial difference in wetness (Section 4.1). Mind that coastal regions also have all lower frequency of wet hours in

general.

Overall, a negative signal in frequency is found with large dissimilarity in the significance of trends regarding quantile and station.

5.3.2 Summer vs winter

When frequency data is differentiated on summer and winter season, we only find significant negative summer trends for the 25-5% wettest (as in most wet hours) 2-days with rates of -0.25 to -0.33 %/yr. This equals an absolute decrease in 58 years of approximately 2 wet hours/day for the wettest summer days (i.e. days with a mean of 11 wet hours a day). These trends corresponds to the 75%, 90%, and 95%-quantiles of Eelde and the 90%-quantile of Maastricht. The two significant negative trends for all-2-day maxima of De Bilt and Vlissingen are likely either a spring or autumn trend, or just not detectable as significant because of the fourfolth reduction in data compared to all-2-day data. Further, we were interested whether stronger signals can be found, when we study the amount of wet hours a year. In Section 5.3.3 analysis of yearly frequencies of wet hours is performed.

5.3.3 Yearly frequency

In this section we investigate trends of wetness by counting the number of wet hours a year, a winter and a summer. First, we study the probability density function of wet hours a year to determine which kind of regression approach is suitable.

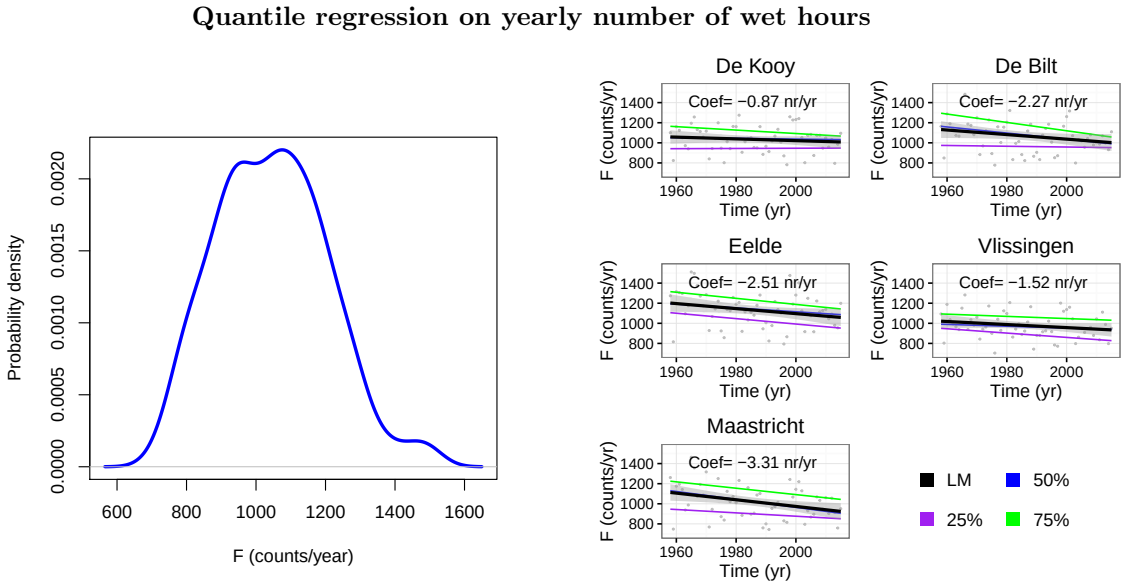

(a) Probability density function

(b) Quantile regression

Figure 5.9: (a) Probability density function of the number of wet hours a year. In (b) ordinary least squares regression (black line) and quantile regression fits with $\tau = 25, 50, 75$ % on the number of wet hours a year for all stations.

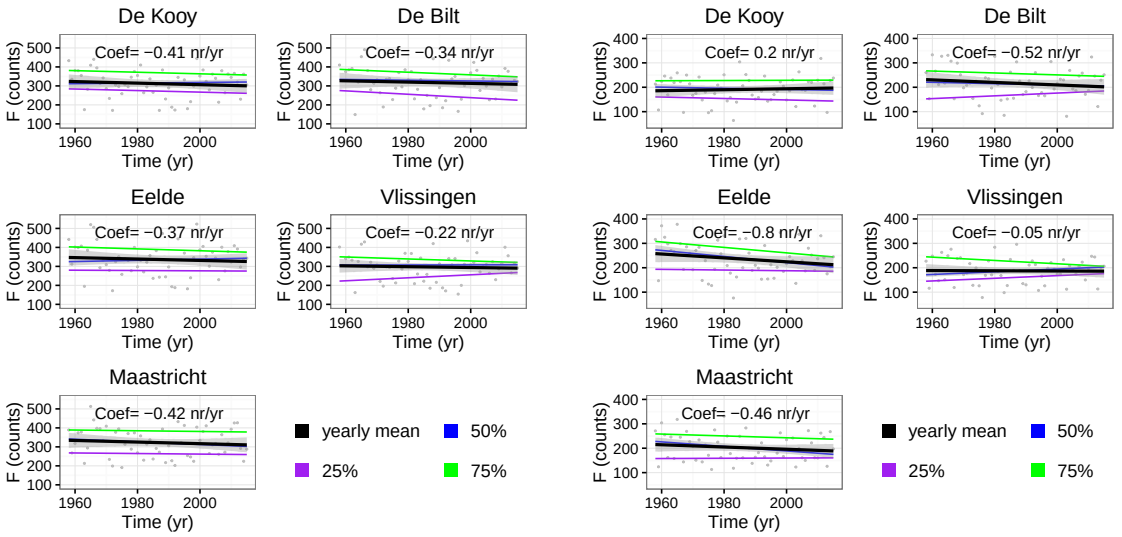

(a) Winter

(b) Summer

Figure 5.10: Ordinary least squares regression (black lines) and quantile regression fits with $\tau =$ 25, 50, 75 % on the number of wet hours a year, for (a) only winter and (b) only summer data, for all stations.

The probability density function of the number of wet hours a year approaches a Gaussian distribution, therefore ordinary least squares regression is valid for this data. All ordinary least squares regression fits demonstrate a negative trend in the amount of wet hours a year. The magnitude of these trends differ largely between the five stations. The negative trend for Maastricht is the strongest (coefficient of -3.31 counts/yr), which is twice as much as the one for Vlissingen (-1.52 counts/yr), and three times as much as the one for De Kooy (-0.87 counts/yr). Moreover, the quantile regression lines are all negative, but per station and per quantile there are differences in the steepness.

To investigate whether these trends are also season dependent, we plotted the same kind of figure for winter and summer (Figure 5.10). All the only ordinary least squares regression trends are positive, except for the summer trend of De Kooy. The coefficient of the annual trend in the number of wet hours is the lowest for De Kooy (Figure 5.9b), which is probably due to the partial compensation of the negative winter trend (Figure 5.10a) by the positive summer trend (Figure 5.10b). However, a negative trend in spring and/or autumn is also required to give us a rate of 0.87 nr/yr for ordinary least squares regression on yearly resolution for De Kooy. Spatial differences are well visible in the magnitude of the trends, which differs more for summer trends (maximum variability of 1 count/yr), compared to winter trends (maximum variability of 0.2 count/yr)(Figure 5.10). This difference in spatial variability between summer and winter is well explainable. As summer (winter) precipitation events have generally a local (large) scale, changes in the amount of wet hours will be influenced relatively more by local (widespread) processes in summer (winter). Overall, a robust signal is present of decreasing yearly, winter and summer frequencies of wet hours, so that underlying cause(s) are expected to play a role for all seasons.

Quantile regression lines are also considered in this figure, allowing us to say something about the changes in extreme wet summer and winters. Most of the quantile fits show negative trends in the amount of wet hours a year, except for the 25%-quantile fit of Vlissingen (winter and summer) and De Bilt (summer). This suggest that the signal of decreasing frequency is stronger for wetter years, than for drier years. Thus, disproportionality is also recognized in the decreasing trends in counts of wet hours a year. Although less obvious as for intensity data, the quantile regression lines

for frequency data differ among the five stations as well. The p-values, expressing the significance of any decreasing trend, are listed in Table 5.8.

Table 5.8: Significance table for all quantile regression fits on frequency data with yearly resolution

Location		Quantiles of fit					
		All year					
Station	STN	50%	75%	90%	95%	Q99%	99.9%
De Kooy	235	0.66	0.87	0.36	0.59	0.84	0.84
De Bilt	260	0.97	1.00	0.99	0.59	0.60	0.60
Eelde	280	0.93	0.98	0.89	0.67	0.77	0.78
Vlissingen	310	0.79	0.61	0.83	0.94	0.73	0.72
Maastricht	380	0.99	0.96	1.00	0.89	0.90	0.90
		Summer					
De Kooy	235	0.55	0.41	0.33	0.15	0.35	0.35
De Bilt	260	0.68	0.76	0.95	0.95	0.78	0.78
Eelde	280	0.93	0.89	0.47	0.75	0.79	0.80
Vlissingen	310	0.18	0.91	0.78	0.67	0.15	0.15
Maastricht	380	0.83	0.76	0.92	0.77	0.94	0.94
		Winter					
De Kooy	235	0.49	0.74	0.94	0.85	0.40	0.40
De Bilt	260	0.62	0.85	0.85	0.80	0.41	0.41
Eelde	280	0.28	0.77	0.91	0.92	0.41	0.41
Vlissingen	310	0.44	0.80	0.58	0.76	0.40	0.40
Maastricht	380	0.81	0.56	0.31	0.67	0.61	0.60

De Bilt and Maastricht have the most (three) significant decreasing trends, whereas De Kooy and Vlissingen have no significant (decreasing) trends. For summer only two significant negative trends are found,and for winter none. Large spatial differences exist for the amount of significant trends found for data on yearly resolution. Although, the negative signal is clearly present in the slope of the quantile regression lines, the small sample size (58 years) is likely limiting the detection of significant trends.

Furthermore, the ordinary least squares regression fits are tested on significance with help of the 9999 Monte Carlo permutation test. Table 5.9 presents the p values for all stations and differentiated on all year, summer and winter yearly frequencies of wet hours. We can deduce from this table that only the ordinary least squares regression fits based on all-year frequencies are significant, namely for De Bilt, Eelde and Maastricht, and none based on summer or winter frequencies. It is highly likely that the detection of trends based on data of yearly resolution, especially when only summer or winter data is considered, is limited by its sample size (only 58 yearly values). Nevertheless, a lot of p values are nearly significant and these values plus the plotted regression lines all indicate decreases in the frequency of wet hours, similar to the detected trends for data on a 2-day resolution.

5.3.4 Summary

In short, in this section we found multiple indications of decreasing trends in the number of wet hours for all station. Next to visible negative slopes in the quantile and linear ordinary least squares regression, several negative trends in frequency of wet hours were detected being significant (even on the 99% confidence level) for frequency data on a 2-day and on a yearly resolution. The negative trends for the wettest 2 days range between 0.1-0.6 %/yr. The mean wetness decreases at a rate of 0.08-0.29 %/yr (depending on the station). For the whole Netherlands the total

Table 5.9: The p-values of ordinary least squares regression fits, based on yearly frequencies for all stations and differentiated on all year, summer and winter data

	STN	All year	Summer	Winter
1	235	0.80	0.31	0.78
2	260	0.96	0.85	0.70
3	280	0.97	0.93	0.71
4	310	0.93	0.54	0.65
5	380	1.00	0.86	0.76

change in 58 years correspond to 100 wet hours less on average a year, which equals in magnitude the total spatial difference in mean wetness between northern and southern situated stations. So, this 58-year change is the same as moving from (more frequently raining) northern part of the Netherlands to the (less frequently raining) southern part.
However, the negative signal in frequency of wet hours is less robust than the positive signal in intensity maxima, as for the former larger spatial differences in the number of significant trends exist than for the latter. Besides, we detect a reverse disproportionality. In other words, the mean and the drier 2 days show a stronger decrease in the counts of wet hours than the wetter days.

Unlike the analysis of intensities we do not use maxima data in frequencies, as we consider 2-day counts of all wet hours. The lack of significant trends in frequency based on data of a yearly resolution for the quantile regression approach, as well as for the ordinary least squares regression approach, is likely due to the limited sample size.

We do not find significant winter trends, but only significant summer trends for the 25-5% wettest (as in most wet hours) 2-days with negative rates of -0.25 to -0.33 %/yr. This equals an absolute decrease in 58 years of approximately 2 wet hours/day for the wettest summer days (i.e. days with a mean of 11 wet hours a day).

5.4 Amount of precipitation

In this chapter we found significant increasing trends in the extreme hourly intensity, while no trend was detected for the mean hourly intensity. Moreover, we observed evident indications of decreasing frequency of wet hours. In view of these trends, it is interesting to investigate whether there are also changes in the total amount of precipitation through the same period. This would allow us to determine whether the two opposite trends, in 2-day intensity maxima and frequency of wet hours, cancel each other or whether one trend is more dominantly influencing the total amount of precipitation than the other. Whereas the 2-day precipitation sums are distributed non-normal, the yearly mean of 2-day precipitation sums and the yearly precipitation sums are distributed normal (Figure 5.11. So ordinary least squares regression is only applicable for the latter two.

5.4.1 2-day and yearly precipitation sums

In Figure 5.12 the quantile regression for both the 2-day, and the yearly precipitation sums is shown. The 25%-quantile is excluded from Figure 5.12a, as the fitted values are zero for this quantile on 2-day resolution.

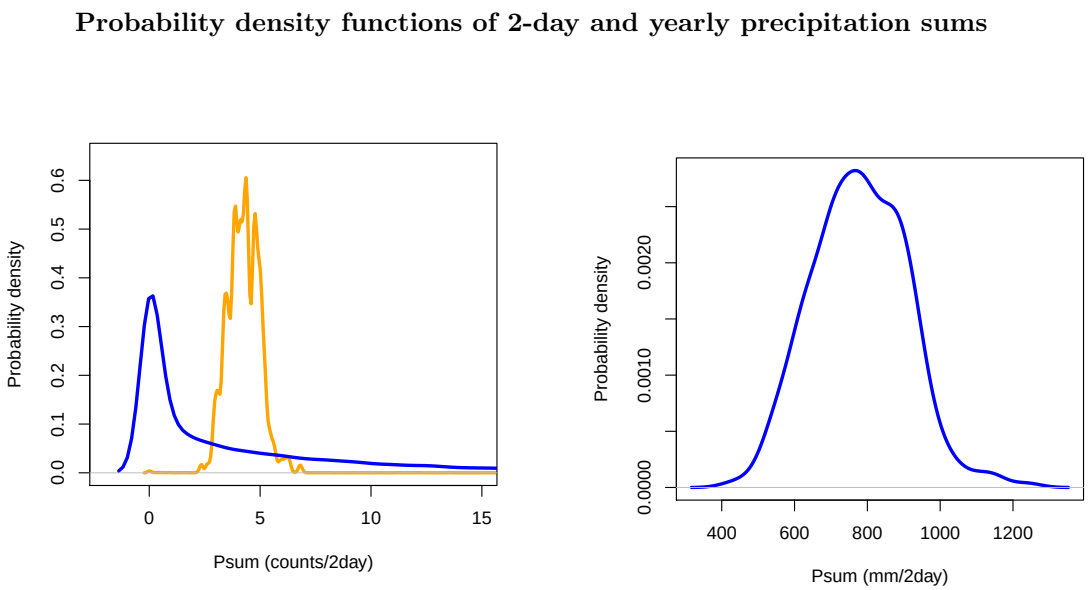

(a) All 2-day (blue) and yearly mean Psum (orange)

(b) Yearly Psum

Figure 5.11: Probability density functions of all 2-day (a) and yearly (b) precipitation sums of wet hour a year (a).

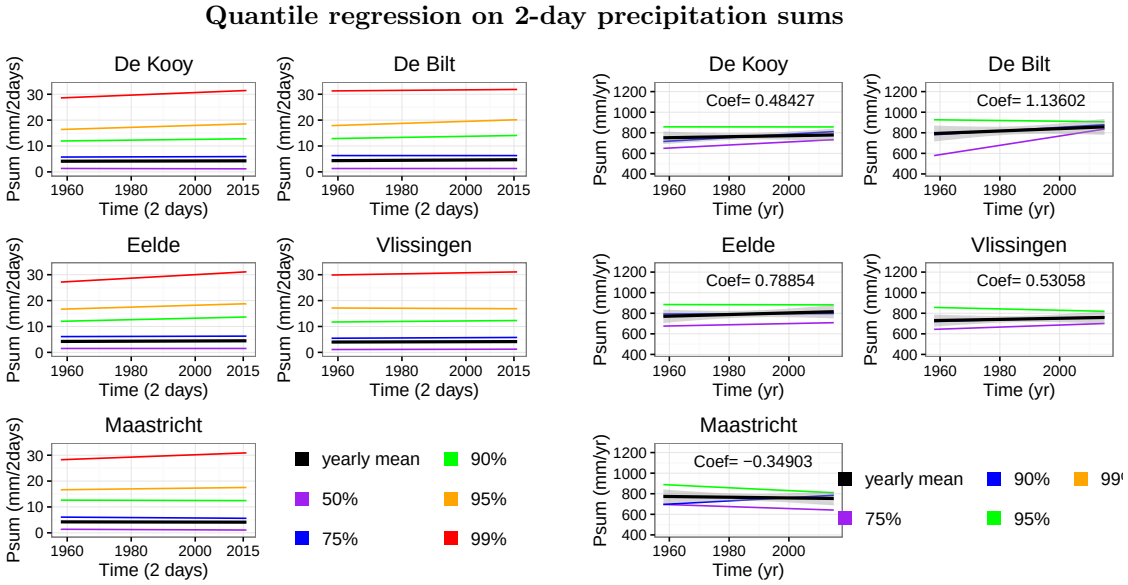

(a) 2 days

(b) Yearly

Figure 5.12: Quantile regression fits of 2-day (a) and yearly (b) precipitation sums for all stations.

For the stations De Kooy, De Bilt and Eelde the quantile lines of the 2-day precipitation sums increase for the 90%- and 95%-quantiles, whereas the quantile lines of the same quantile are constant for Vlissingen and Maastricht (Figure 5.12a). The 99%-quantile line increases for all stations, but spatial differences are visible regarding the slope (with largest slopes for De Kooy and Eelde). Changes in the lower quantiles (50%- and 75%-quantiles) and in the yearly means of 2-day precipitation sums are hard to detect. For the yearly data increasing ordinary least squares regression

lines are visible, except for Maastricht (Figure 5.12b). The ordinary least squares regression coefficient for De Bilt is about twice as high as the coefficient for De Kooy and Vlissingen. In De Bilt the 75%-quantile seems to increase the most, suggesting that the ordinary least squares regression trend is mostly due to an increase in moderately high precipitation sums (between the 75%- and 90% quantile). For Maastricht, the 90%-quantile increases, whereas all the other quantile lines decreases. This would mean that precipitation sums between the 90%- and 95%-quantile increases significantly. The dissimilarity in quantiles is not fully understood, but might be the result of the way quantile regression works (similar as described in Section 5.2.2).

More interesting is the deviation for Maastricht in the sign of the trend. In Sections 5.3.1 and 5.3.3 we saw that the negative trends in 2-day and yearly frequency of wet hours are strongest for Maastricht, while from Section 5.2.2 we know that the 2-day intensity maxima (see Section 5.2.2) does not increase more or less for Maastricht compared to the other stations. Changes in precipitation sums are expected to be the combined result of changes in intensity and frequency (Chapter 4). When the yearly trend in in intensity maxima for Maastricht is also approximately constant, this deviation in trend for the precipitation sum is expected. Whereas the negative trend in frequency of wet hours dominates the trend in precipitations sums of Maastricht, the positive trend in intensity of the more extreme events is apparently dominating the trend in the precipitation sums of the other stations.

The strongest increasing trend regarding ordinary least squares regression in precipitation sums is the one for De Bilt, which can be easily understood. We namely observed the most significant positive trends in maxima intensity for De Bilt. Besides, maybe the highest quantiles also have a positive trend. The latter could be true if the corresponding trends can only not be detected as significant due to the limited sample size. Although, 2-day trends of decreasing frequencies of wet hours are found for De Bilt, these only apply on the relatively drier 2-days (50%- and 75%-quantiles) and with less strong absolute rates. However, the yearly trend of frequency of wet hours is moderately high for De Bilt, but not detected as being significant at the 95% confidence level.

What is more striking, is that the (moderate) positive yearly trends in precipitation sums for the two coastal stations, Vlissingen and De Kooy, are quite similar in both the ordinary least squares regression slope, and the slopes of the quantiles lines. (add explanation or express ignorance, but yearly LR of intensity needed).

The significance of the observed 2-day and yearly quantile regression lines is investigated with a 9999 Monte Carlo permutation test, in which we have tested whether the slopes are significantly higher than zero. Table 5.10 gives the p-values resultant from this test.

In Table 5.11 we observe significant trends for the 2-day precipitation sums. The p-values point out significant positive trends for the 95%-quantiles of De Kooy and De Bilt, for the 90%-, and 95%-quantiles of Eelde, and for the 99%-quantile of Vlissingen and Maastricht. All these trends are significant at the 95% confidence level, except for the 90%-quantile of Eelde, which is significant at the 99% confidence level. What is striking is that the trends detected for the 95%-quantile correspond to the more northern situated stations (De Kooy, De Bilt and Eelde) and those for the 99%-quantile for the more southern situated stations (Vlissingen and Maastricht). This could be a temperature related difference, as mean temperature is higher for the northern part of the Netherlands, than of the southern part of the Netherlands. Moreover, we saw in Chapter 4 that higher intensities correspond to the summer months, in which the temperature is obviously higher compared to the winter months. In Chapter 6 we will investigate the precipitation intensity-temperature relationship in more detail.

Furthermore, we find significant positive trends for the ordinary least squares fit on the yearly means of all stations, except Maastricht for which we find a significant negative trend. For the

Table 5.10: Significance table for all fits on 2-day sums of precipitation

Location		Quantiles of fit						OLS fit
Station	STN	50%	75%	90%	95%	Q99%	99.9%	Yearly means
2-day sums								
De Kooy	235	0.21	0.70	0.86	0.97	0.16	0.24	1.00
De Bilt	260	0.26	0.37	0.93	0.97	0.10	0.90	1.00
Eelde	280	0.46	0.64	1.00	0.98	0.93	0.77	1.00
Vlissingen	310	0.73	0.81	0.82	0.39	0.97	0.83	1.00
Maastricht	380	0.06	0.13	0.36	0.78	0.98	0.92	0.0001
Yearly sums								
De Kooy	235	0.90	0.49	0.26	0.47	0.40	0.39	0.6937
De Bilt	260	0.93	0.41	0.32	0.36	0.65	0.65	0.8318
Eelde	280	0.58	0.41	0.72	0.80	0.80	0.80	0.7874
Vlissingen	310	0.78	0.45	0.32	0.31	0.25	0.24	0.6937
Maastricht	380	0.83	0.34	0.07	0.20	0.19	0.19	0.6937

yearly precipitation sums, we do not find any significant trends. This might be due to a too small sample size.

Table 5.11: Relative rates of significant trends in precipitation sums

Location		Rates (mm/2 days/yr)						
Station	STN	50%	75%	90%	95%	99%	99.9%	OLS
De Kooy	235	-	-	-	0.23	-	-	0.31
De Bilt	260	-	-	-	0.22	-	-	0.059
Eelde	280	-	-	0.24	0.22	-	-	0.096
Vlissingen	310	-	-	-	-	0.069	-	0.13
Maastricht	380	-	-	-	-	0.16	-	-0.29

Table 5.11 provides the relative rates of the trends in 2-day precipitation sums, which range between 0.05-0.25%/yr. This can be translated to an increase of approximately 1 mm/day in 58 years for the days (90-99% quantile) with highest accumulation amounts. The ordinary least squares fits demonstrates a negative change of -0.29%/year for Maastricht (over 58 years a reduction of 16.8%) and for the other stations positive changes between 0.06-0.31 %/year (over 58 years increases of 3.5-18%).

The absolute regression coefficients are on the order of 0.01 mm/2 days/yr (more specifically 1.2-2.7 mm/2days in 58 years). This holds only for the precipitation sums higher than the 90%-, 95%- or 99%-quantiles, with spatial differences in the type of quantile for which a trend is significant. The highest absolute rate (0.046 mm/2 days/year) corresponds to the 99%-quantile of precipitation sums for Maastricht, while the lowest rate (0.021 mm/2 days/year) relates to the same quantile, but then for Vlissingen. The spatial differences in absolute rates are not that high, as they are all of the same order. Admittedly, the detected trends apply on approximately the same quantile, so that they are better comparable than the rates for intensity maxima or frequency of wet hours.

Considering both the signs of the trends in intensity and frequency, and the related disproportionality of the trends, we can explain why only trends for the highest precipitation sums are significant. The positive trend for the highest intensity maxima is ten times stronger than the trend for the yearly mean of the intensity maxima. On the contrary, the negative trend for the yearly mean frequency of wet hours is stronger than the wetter days. On the one hand, the trends

in the highest precipitation sums are significantly positive, as they are more dominated by the trends in intensity extremes than by trends in frequency of wet hours. On the other hand, the trends in the lower or mean precipitation sums are constant to non-significantly positive, as the trends in frequency and intensity are approximately in balance.

5.4.2 Summer vs winter

In order to investigate whether the increases in 2-day precipitation sums are in fact more summer than winter trends, vice versa or both, we did the same analysis on summer and winter 2-day precipitation sums. In Figure 5.13a we plotted the significant summer trends and in Figure 5.13b the significant winter trends. Note that the y-axis of are differently scaled per station in the summer. For the winter the fitted quantile values of the significant trends differ less, therefore the same scale (but lower than for summer) is used.

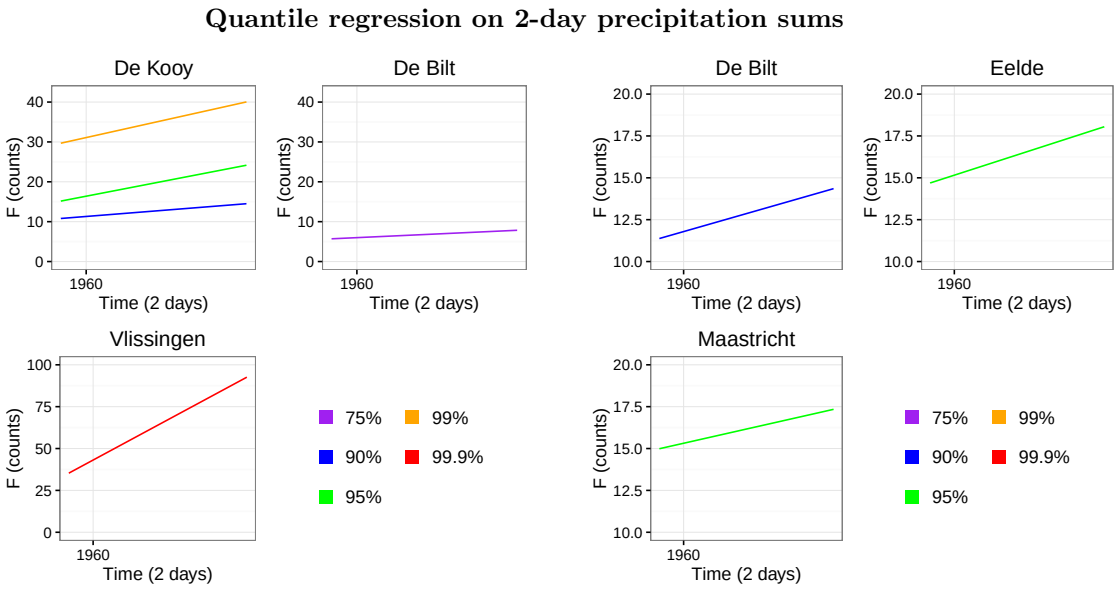

(a) Summer

(b) Winter

Figure 5.13: Quantile regression fits of significant summer (a) and winter trends (b) in 2-day precipitation sums.

First of all, Figure 5.13 demonstrates that the few significant trends on seasonal level found are positive. The relative rates of summer trends range between 0.60-2.8 %/yr for the 25-0.1% highest precipitation sums (with the highest for the 99.9% of Vlissingen). Four out of five of least squares trends of the summer mean in 2-day precipitation sum are positive, with rates between -0.43 to 0.78%/yr. Only Maastricht shows a negative signal in the mean. The rates show that large spatial differences are present. The summer mean precipitation accumulating per year in De Kooy has increased with 330 mm in 58 years, while for Maastricht this has decreased with 282 mm in 58 years. So, we observe an approximately 300 mm shift in yearly mean accumulated from the most southern non-coastal station to the most northern coastal station.

The winter quantile regression rates vary between 0.27 to 0.45 %/yr (in 58 years this is an increase of 1.2-1.5 mm/day) for the highest 10-5% 2-day sums, while the rates of the (OLS) yearly mean are all negative from -0.19 to -0.56 %/yr (in 58 years a decrease of -0.3 to -0.9 mm/day).

So, we observe positive trends in the highest and mean summer precipitation sums and highest winter precipitation sums, but negative trends in the mean winter precipitation sums. The positive trends in the highest summer precipitation sums are stronger than trends in the mean summer of highest winter precipitation sums.

De Kooy has the largest number of significant trends, which are all summer trends (for the 75%-,90%- and 95% quantiles). De Bilt has one significant summer and one significant winter trend. On the one hand Vlissingen only has one significant summer trend, on the other hand Eelde and Maastricht only have significant winter trends . What is also interesting, is that three of the significant all-2-day trends, corresponding to the 95%-quantile of De Bilt, the 95%-quantile of Eelde, and the 99%-quantile of Maastricht, are recognized as winter trends in Figure 5.13. The significant all-2-day trends of the 95%-quantile of De Kooy and the 99%-quantile of Vlissingen can be observed as summer trends.

What is striking, is that the summer trends in precipitation sums are only present for coastal stations, while winter trends in precipitation sums are only present for non-coastal stations (with the position of De Bilt in between the two types, regarding its distance to the coast). If this not due to coincidence, it might be due to a different mechanism behind the positive summer and winter trends. Besides, we already observed that ordinary least squares regression of the precipitation sums for De Kooy and Vlissingen are quite similar, but mind that this accounts for precipitation sums on yearly resolution. Moreover, we detected only for non-coastal stations (i.e. Eelde and Maastricht) significant negative trends in summer frequencies of the wettest 2 days (Section 5.3.2). This corresponds well with the fact that we do not detect significant positive trends in summer precipitation sums for non-coastal stations In Chapter 6 we hope to learn more about the reason for changes in precipitation sums and the related spatial differences.

5.4.3 Summary

Overall, we detected multiple significant positive trends in precipitation sums for the 90-99%-quantile and in the OLS fits of the yearly means. For each station 1 significant quantile trend is found, except for the station of Eelde (for which 2 trends are found). The detected trends correspond to the 95%-quantile for the more northern situated stations (De Kooy, De Bilt and Eelde) and to the 99%-quantile for the more southern situated stations (Vlissingen and Maastricht). This difference in quantile, which means a difference in the degree of extremeness of the intensity, could be related to temperature. The precipitation intensity-temperature relationship will be studied in Chapter 6. Although, we only consider maxima intensities in contrast to all-hour frequencies of wet hours, the trends in precipitation sums seems to be dominated more by the positive trends in intensity maxima compared to the negative trends in frequency of wet hours. In the last 58 years the 5% highest 2-day precipitation sums have increased with 1.2-2.7 mm.

When only studying summer and winter trends, we found that trends in all-2-day precipitation sums of coastal stations are in fact summer trends, while those of non-coastal stations are winter trends. Moreover, the trends in the highest and mean summer precipitation sums and highest winter precipitation sums are positive, while the trends in the mean winter precipitation sums are negative. Besides, the positive trends in the highest summer precipitation sums are stronger (0.60-2.8 %/yr) than trends in the mean summer (-0.43 to 0.78%/yr) of highest winter precipitation sums (0.27 to 0.45 %/yr). Negative trends are found for the yearly mean winter precipitation sums.

Chapter 6

Causes of changes in hourly precipitation extremes

6.1 Introduction

In this chapter we attempt to find an explanation for the observed intensification of hourly precipitation extremes, and the decrease in the occurrence of wet hours. In order to find a mechanism we apply a fourfold analysis. Firstly, we identify key variables by describing their relationship to (extreme) precipitation, as found from theory. Secondly, correlation matrices of these variables are plotted to provide a first-hand overview of the strength of any possible relationships. Thirdly, we regress the key variables in time, in order to investigate whether we find changes in time that might explain the observed changes for precipitation. We bundle the data for all five stations to improve the detection of relationships, except for CAPE data of which we only have data from one station, number 260 De Bilt. Moreover, we compare the magnitude and sign of these trends with the observed trends found in Chapter 5. Lastly, we plot the distribution of the variable in question and the quantile regression lines for intensity over the remaining variable(s) for two different time periods. By comparing the two periods for both plots we can validate whether the distribution of the variable or its relation with precipitation extremes changes in time. In this part we differentiate between summer and winter season to understand the seasonal dependency of the causes of increasing intensity of heavy hourly precipitation and decreasing precipitation time.

6.2 Detection of key variables

6.2.1 Theory

In this section we describe the relation of multiple variables to (extreme) precipitation. These are temperature, relative humidity, dewpoint temperature, convective available potential energy, wind strength, cloud condensation nuclei, topography, and weather code.

Temperature

Since 1950 many of the observed changes in temperature are unprecedented on a time scale of decades to millennia. For the period 1880-2012 the IPCC (2013) stated that the linear trend in temperature shows a warming of 0.85°C. For more recent data (1951-1989) the relative increase is higher, with a rate of 0.92°C/century.

Temperature at the surface, as well as the gradient of the temperature with height, influences precipitation intensity and occurrence in many ways. It plays a role into the entire chain, from the source of moisture, cloud formation and precipitation production up to and including the falling process (Sumner, 1988).

First, in order to produce precipitation, atmospheric moisture needs to be available. In general, the higher the temperature, the more evaporation can take place, and the more moisture is supplied to the atmosphere. Note that the surface temperature cools, as evaporation consumes latent heat.

Second, the ability of air to hold water vapor increases with temperature according to the Clausius-Clapeyron equation. However, air does not absorb water vapor, so this is correctly phrased as: a higher temperature results in a higher equilibrium vapor pressure (Wallace and Hobbs, 2006, p.80,81). The effect of this relation is that when temperature increases in a changing climate, saturation will occur less often (e.g. the saturation level is harder to reach)(Wallace and Hobbs, 2006, p.80,81), but under extreme conditions more moisture can fall down as precipitation from an air column (Pall and Stone, 2007; Lenderink and Van Meijgaard, 2010; Hardwick Jones and Sharma, 2010; Lenderink and Van Oldenborgh, 2011). Further elaboration on air's ability to hold moisture linked to (extreme) precipitation will follow in Section 6.2.1.

Third, from Chapter 3 we know that cloud droplet formation depends on the equilibrium vapor pressure, so indirectly on the internal temperature of the cloud. In short, both the amount of available atmospheric moisture, and cloud formation depends on the temperature.

Fourth, a strong temperature gradient with warm air at the surface and cold air aloft leads to buoyant and vertical unstable air. The strength of updrafts is determined by the strength of instability of the air. A measure of the vertical instability is the Convective Available Potential Energy (CAPE). As we have data of CAPE, we will further discuss its relation to temperature in the following paragraph. Lastly, processes within a cloud regarding droplet growth depend on the internal temperature and temperature differences (Chapter 3).

To summarize, an increase in temperature might cause an increase in extreme precipitation and a decrease in the amount of wet hours, via changes in the atmospheric temperature gradient, dewpoint temperature and CAPE.

Relative humidity and Dewpoint temperature

The specific humidity is the ratio between the mass of the water vapor in the sample and the total mass of the sample. It gives the actual amount of water vapor in an air sample (Sumner, 1988). The specific humidity gives an indication about the level of saturation for a certain temperature and pressure.

An increase in water vapor of a saturated air parcel without changing temperature or pressure will result in oversaturation. Most of the time air must be at least saturated for condensation to occur, leading to cloud or fog formation (Sumner, 1988). The moment that the water vapor pressure (e) rises till the point it equals the saturation vapor pressure ($e = e_s$), an equilibrium exist between the rate of condensation and evaporation and air is said to be saturated with respect to a plane surface of pure water at temperature T, and the pressure e_s (Markowski and Richardson, 2010, pp. 12-13), (Wallace and Hobbs, 2006, pp. 80-81). The expression of e_s in T is called the Clausius-Clapeyron equation,

$$\frac{de_s}{dT} = \frac{L_v e_s}{R_v T^2}, \tag{6.1}$$

in which L_v is the specific latent heat of vaporization and R_v the gas constant for water vapor

($R_v = 461.51 Jkg^{-1}K^{-1}$) (Bolton, 1980).

This relation is shown in the following figure.

Water vapor and change in water vapor in relation to temperature

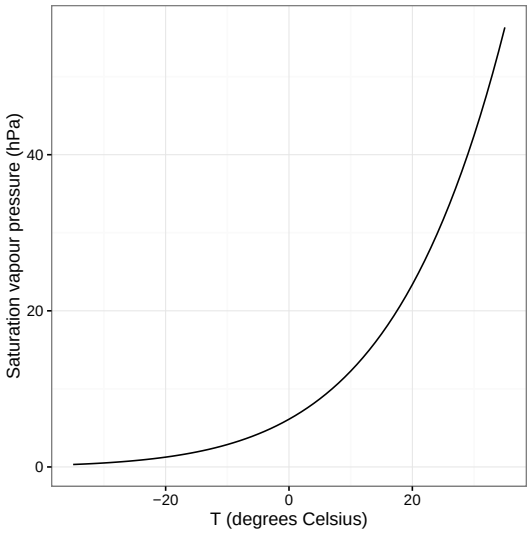

Figure 6.1: Saturation vapor pressure, e_s

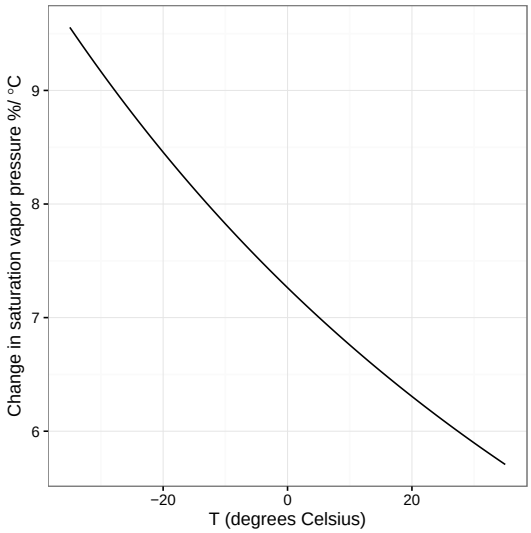

Figure 6.2: Change in e_s per δT

We can deduce from Figure 6.1 that the saturation vapor pressure increases rapidly with temperature. This means that more water vapor can be present in warmer air without reaching saturation. Therefore, the Clausius-Clapeyron equation predicts that under the constraint of constant relative humidity (Ingram, 2002), an increasing temperature leads to an exponential increase in specific humidity (Trenberth, 1999; Allen and Ingram, 2002; Pall and Stone, 2007; Pierrehumbert and Roca, 2007). And the heaviest rainfall events are likely to occur when all available moisture in a volume of air precipitates effectively. Therefore, we might expect the highest quantiles of the rainfall probability density function to increase in ratio with the Clausius Clapeyron equation (Pall and Stone, 2007).

To investigate the change of the saturation vapor pressure with increasing temperature we took the derivative of the Clausius-Clapeyron equation to temperature. Figure 6.2 demonstrates that a certain increase in temperature has a larger impact on the saturation vapor pressure for colder temperatures than for warmer temperatures. For T $< 0°$C e_s increases with more than 7%, while for temperatures higher than 20° Celsius it is less than 6%. For this reason we would expect that any trends in extremes caused by global warming-induced changes in moisture-holding capacity are stronger visible for winter than for summer.

Dewpoint temperature is a widely used measure for the amount of moisture in the air (Lawrence, 2005). The dewpoint temperature (Td) is the temperature to which air at initial temperature and pressure must be cooled isobarically to become saturated, and can be expressed in terms of the vapor pressure $e_s(Td) = e(t)$ (Lawrence, 2005). An expression of the dewpoint temperature in terms of relative humidity is,

$$T_d = \frac{T}{1 - \frac{Tln(\frac{RH}{100})}{L_v R_v}} \tag{6.2}$$

When relative humidity is assumed to be constant in time (Pall and Stone, 2007) and the temperature rises, the numerator will increase, the term $\frac{Tln(\frac{RH}{100})}{L_v R_v}$ will increase, so that the denumerator $(1-$ term $\uparrow)$ will decrease. As the change in Td is the product of an increase in the numerator and a decrease in the denumerator, Td will increase. So indeed the atmospheric moisture, indicated by Td, will rise under constraint of constant relative humidity and rising temperature.

Convective Available Potential Energy

As explained in the theoretical background section (Chapter 3) initial cooling of moist air is a prerequisite in the formation of clouds. This occurs often in the process of vertical uplift, such that rising air cools adiabatically with height. Rising of air occurs as a result of density differences.

If we exclude mixing of air with its environment, we can consider the thought experiment of a rising air parcel. The air parcel will rise as long as the temperature of the surrounding air is lower than its own. Buoyancy is then given by: $a = (T_p - T_0)g/T_0$. With a, the buoyancy, T_p, the internal temperature of the air parcel, T_0, the external temperature and g, the acceleration due to gravity (Sumner, 1988, pp. 55-56). Thus, for convection to occur an air parcel must have enough potential energy, which is indicated by the Convective Available Potential Energy (CAPE). CAPE represents namely the vertically integrated positive buoyancy of a parcel experiencing adiabatic ascent,

$$CAPE = g \int_{z_L CL}^{z_L NB} B dz \tag{6.3}$$

in which g is the acceleration due to gravity (m s^{-2}), z_{LCL} the lifted condensation level, z_{LNB} the level of no buoyancy and B the buoyancy force. This can also be expressed, similar to Chapter 2, as:

$$CAPE = g \int_{z_1}^{z_2} \frac{T - \bar{T}}{\bar{T}} dz \tag{6.4}$$

with T, the temperature of the air parcel, and $\bar{T}$, the temperature of the environment. The units for CAPE are J/kg.

The LCL is the height till which an air parcel follows a dry adiabat when lifted upwards. Further lifting leads to condensation of the air parcel, which will then follow the wet adiabat (Lin, 2007). In other words, condensation releases latent heat, which warms the air parcel, so that an air parcel will continue to rise further due to its enhanced buoyancy with respect to its environment. The LCL thus depends on the moisture content of air. The LNB is the height at which the buoyancy of the air parcel equals the buoyancy of the surrounding air, so that the air parcel has lost its potential energy to rise further. As CAPE represents the potential energy of an air parcel, it can be read from a thermodynamic diagram, as proportional to the area between the LFC and LNB enclosed by the environmental temperature curve and the wet adiabat of the air parcel. A necessity for convection is that the air parcel is forced to the LCL, for which the amount of supplied energy is called the convective inhibition (CIN) (Lin, 2007). In summary, CAPE can be seen as a measure for potentially buoyancy-driven vertical motion.

In pre-thunder conditions CAPE values can range from a few hundreds up to thousands of $\frac{J}{kg}$, with maxima on the order of 5000-7000 J kg^{-1} (Krennert, 2016). The Storm Prediction Center of the National Oceanic and Atmospheric Administration (NOAA) divides CAPE values in four classes: "weak instability" (CAPE less than 1000 J kg^{-1}), "moderate instability" (CAPE between 1000-2500 J kg^{-1}), "strong instability" (CAPE from 2500-4000 J kg^{-1}) and "extreme instability" (CAPE greater than 4000 J kg^{-1})((*EXPLANATION OF SPC SEVERE WEATHER PARAMETERS*)). Studying CAPE is considered as an indicator of the probability of occurrence and the intensity of deep, moist convection (Krennert, 2016).

Assuming zero horizontal advection the maximum vertical velocity of an air parcel is reached when all the potential energy is released into kinetic energy Lin (2007), i.e.

$$W_{max} = \sqrt{2}CAPE \tag{6.5}$$

The definition of CAPE does not include the existence of liquid water loading, entrainment, the vertical motions in the air or aerodynamic effects, which all decrease the value of CAPE. Therefore, in the real world CAPE is usually an overestimation of the vertical instability and of updraft strength (Krennert, 2016; Thompson, 2016). The updrafts of supercells can nonetheless be much stronger than indicated by CAPE, due to vertical shear effects (McCaul Jr and Weisman, 2001; Service, 2001).

As already explained in 6.2.1 an increase in the present and/or strength of the updrafts, which is characterized by the degree of CAPE, can lead to enhanced moisture influx. This leads to more intense or longer showers depending on the conditions of precipitation production. In Chapter 3 we stated that precipitation associated with convection is relatively intense. In brief, higher CAPE corresponding to higher probability of occurrence and stronger convection might cause higher intensity of precipitation and/or higher amount of wet hours.

Wind shear and strength

The strength of wind speed is determined by the horizontal temperature-related pressure gradient (Bonan, 2015) and CAPE-associated convergence of air (Ahrens, 2012). Smits and Können (2005) concluded that for the period 1962-2002 the wind speed for the Netherlands has decreased.

Severe local storms are associated with wind shear, pronounced shifts in wind speeds and/or direction with height (Browning, 1964; Wingo and Cecil, 2010). The four types of storms distinguished on the way of development are: supercell, multicell, a collection of numerous individual precipitation cells as for example squall-line storms and mesoscale convective complexes (Sumner, 1988, p. 156). Some of these storms can develop into larger storms delivering an hour or two of very intense precipitation at a point. A storm can obtain a self-perpetuating character due to pronounced wind shear, as this permits the continual introduction of fresh and moist air into the system at the lower-level developing edge and the venting of used air aloft, while the downdraft remains separated from the updraft (Sumner, 1988, p. 156). Wind shear is therefore related to the lifetime of a storm (up to several hours).

Unfortunately we do not have observations of wind speed at higher levels for our time period of 58 years, so we can analyse changes of the wind shear in time for a certain station. Instead we can study the horizontal wind speed at 10 m, and use this an indicator of wind shear. Higher wind speeds also lead to faster propagation of fronts and local showers over a station. Therefore, we would expect a higher intensity. However, we could also argue the other way around, weak wind speeds or fast turning of the wind around a location can result in a longer duration of an intensive precipitation system over a station. In a back-building or occlusion event, high hourly precipitation sums can accumulate (Schumacher and Johnson, 2005; Łupikasza, 2016).

In other words, changes in wind speed could influence the intensity of precipitation in two ways; (i) via the organisation of a storm under restriction of strong wind shear, and (ii) via the way of propagation of precipitation systems over a station.

Other important variables

Three variables which are further important to explain changes in precipitation extremes, but not used in this research for different reasons, are (i) the distribution, type and size of cloud conden-

sation nuclei (CCNs), (ii) the topography and (iii) the weather type. We will briefly describe their relationships, so we may suggest possible explanations of the spatial differences found in Chapter 4. Moreover, we can keep them in mind in the case we cannot explain changes in (extreme) precipitation by the changes in the aforementioned variables only.

First, the presence of CCNs is vital to cloud formation, and the concentration of CCNs may have an impact on the probability of occurrence or intensity of precipitation. Many of the CCNs are aerosols, very small particles or liquid droplets that are suspended in the air for a long time and that form nuclei on which condensation can occur. Their size is on the order 0.1 to 1 micron and they originate from industrial pollution or natural sources as sea salt spraying or dimethyl sulfide emission from oceans (Sumner, 1988). The bigger the size of an CCN, the lower the saturation vapor pressure above its surface, and the higher the preference for condensation compared to evaporation. Bonding forces are namely stronger for CCNs that are less curved (Chapter 3). Whether aerosols are hygroscopic also determines how easily condensation can take place.

The concentration of aerosols over oceans and the coast is small in this comparatively clean air environment, but their size is often large, so that precipitation-sized droplets may easily form. In contrary, the air over continental areas contains more nuclei from terrestrial sources, which differ more in size. This results in a larger minimum cloud thickness for shower development, as moisture is spread among more and smaller aerosols.

We do not posses data about CCNs distribution and properties. Therefore, in our study of the causes of changes in precipitation we can not take into account the effect of changes in CCNs. Overall, the distribution, size and type of CCN is important for cloud formation, and indirectly for precipitation production.

Second, topography plays an important role in the distribution and intensity of precipitation. At temperate latitudes warm sectors in frontal depressions or mesoscale systems can be moderately intensive, when uplifted by relief (Sumner, 1988). Although the enhanced magnitude and extent of precipitation due to relief is governed by the height and longitudinal extent of the relief barrier, low hills of only tens of meters in height can lead to notable increases in precipitation (Bergeron, 1968; Sumner, 1988). Even for the Netherlands, where gradients are relatively small, notable precipitation increases are detected by Ter Maat et al. (2013) for the area of the Veluwe. Despite the fact that the topography in the Veluwe has an maximum elevation of only just over 100 m and moderate steepness. The differences in monthly domain-averaged precipitation sums between the Veluwe and its surroundings, are 17% in winter and 10% in summer. Next to the Veluwe, the southern part of the country also has a higher elevation with a maximum of approximately 325 m.

In our study the station at Maastricht has the highest elevation (114 m see Chapter 2). This might explain that the highest precipitation intensities were measured at this station. However, we do not have enough stations with spatial differences in topography, to analyse the effect of topography on the intensity and occurrence of precipitation. Moreover, as topographic gradients are not expected to change significantly in time, this is not an appropriate variable to study trends in hourly precipitation extremes. In short, even small-elevation differences in the Netherlands can lead to significant spatial differences in hourly precipitation extremes. On the one hand, we are interested in trends, and thus, these can not be explained by topographic gradients, which are constant for the time scale we look at. On the other hand, we can reason why we observed the highest extreme intensities at Maastricht (Chapter 4).

Third, human-made visual observations indicated by "present weather" (WW) codes are available in our data . With help of this code, which is approved by the World Meteorological Organization, 100 different weather types are distinguished by two-digit numbers (0-99)(see Dai (2001) for a complete list). Heavy precipitation is related to certain conditions in the cloud and at the surface. Two weather types, differentiated on WW, often occurring simultaneously with intense

precipitation are (i) hail, and (ii) thunderstorms.

(i) The majority of severe local storms associated with self-perpetuating convectional systems, are characterized by significant hail production (Sumner, 1988). For the production of hail deep and strong convection is required. Convectional precipitation, which is often intense in nature, is mostly produced by the Bergeron-Findeisen process. This stems from the fact that very intense precipitation (sometimes in form of hail or ice pellets) is resultant from the considerable vertical development of the clouds (such that the cloud height exceeds the 0°C isotherm).

(ii) Lightning occurs in vigorous convective clouds, in which ice particles and hail are thought be key players in charge generation. The majority of the lightning discharge originates from thunderstorms extending above the freezing level. However, for all-water clouds there are also well-documented UK observations of lightning events (Atkinson, 1989; Lee, 1986; Mason, 1972; Office, 1997).

Although we have hourly measurements of weather codes, we do not use them in this study, because in the course of time visual measurements of weather codes are automatized, and these are computed from different variables among which intensity (Rulfová and Kyselỳ, 2013). Differentiation between variables on basis of the automatic WW measurements would not have a physical meaning when attempting to explain differences in intensity.

Summary theory

To summarize, an increase in temperature leads potentially to more atmosphere moisture via evaporation, but with a negative feedback on the temperature, and a higher ability of the air to hold moisture. The latter is expressed in the dewpoint temperature and goes hand in hand with an expected decrease in the amount of wet hours and a concentration of precipitation in the more intense wet hours. The influx of moisture may also by enhanced by stronger updrafts, of which CAPE is a measure, via larger atmospheric temperature gradients. The strength of wind speed, which is temperature and CAPE related, influences precipitation intensity via the organisation of storms under condition of strong wind shear and the way precipitation systems propagate over a station. Stronger wind speeds correspond to higher extreme precipitation, except for situations in which back-building convection or occlusion occurs. Although, precipitation production depends on the concentration and size of CCNs, the internal temperature in a cloud, and the topography, no research is dedicated to these variables due to restriction in the vertical and horizontal extent of our data.

6.2.2 Identification of relationships

Introduction

In this part we try to identify relationships explaining the trends found in hourly precipitation in Chapter 5. First, we start with a study of correlations and the type of relationship (e.g. linear or non-linear) for the variables described as important to precipitation intensity in Section 6.2.1. Next, we compare trends in the key variable(s) to the observed trends in hourly intensity. Lastly, we study temporal changes in the seasonal distribution of the key variable(s) and in their relationships with precipitation intensity. Note that in this chapter we include duration data, in which duration is defined as the hourly fraction of time that precipitation occurs, to find the true precipitation intensity (PI). This allows us to distinguish between hours with the same precipitation sum, of which one is very intense and short-lasting, and the other less intense and long-lasting. Here, P is the hourly precipitation sum.

Correlation matrices

To have an easy and clear overview of the strength of relationships between multiple variables, we plotted heatmaps of the Pearson correlation coefficients. The Pearson correlation coefficient is a widely used statistic giving a measure of the strength of linear relationships (Zou, Tuncali, and Silverman, 2003). A heatmap shows the strength of all relationships between the following 7 variables: PI, I, DR (duration of precipitation within an hour), T, Td, FH (10m-wind strength, averaged as last 10 minutes of an hour), RH (relative humidity) and CAPE. For all variables, except for CAPE, we combined the measurements of the five stations, in order to clarify the relationships. We considered only wet hours, as we are interested in the relationship between the occurrence or intensity of wet hours and not in the occurrence of dry hours.

For CAPE only measurements of station De Bilt are available (Chapter 2). Next to a different spatial resolution, CAPE measurements also have a different time length (1993-2015) and temporal resolution. Therefore, we plotted the relationships with CAPE in a separate heatmap (Figure 6.4d), which of which the correlation coefficients are computed from all days on which CAPE is measured at least once. We added variable N, the number of CAPE measurements a day. Observed CAPE values have high daily variability, but CAPE is measured 1-6 times a day, so that this daily variability is not always captured. Next to the fact that large CAPE can result in intense precipitation, CAPE also decreases due to cold precipitation (negative feedback). This is described in Chapter 3 as the interception of updrafts (which need vertical instability) by cold downdrafts. For these reasons we compared daily CAPE maxima in two different ways with precipitation; (i) to the cumulative daily precipitation sum, and (ii) to the daily or 2-day maxima in precipitation sum and intensity. From Section 6.2.1 we expect positive relationships between the variables T, Td, FH and CAPE with P and I. Next to comparison of all wet hour values, we also looked at the correlation coefficients for the wet 2-day maxima.

Figure 6.3 provides an overview of the Pearson correlation coefficients for all variables, except CAPE, for all wet hours. The two highest coefficients are between T and TD (0.97) and P and I (0.75). The strong relationship between T and TD (dewpoint temperature) is straight forward; following the definition of dew point temperature itself: the dewpoint temperature is the temperature till which air has to be cooled to become saturated. For moist air (RH> 50%) the following rule of thumbs holds: the dewpoint temperature decreases with ±1°C for every 5% decrease in relative humidity. As the data considered in this chapter only contains the wet hours, most of them will fulfill the assumption of a moist air and therefore a strong linear correlation is present. This corresponds to Pearson correlation coefficient of almost 1.

The hourly precipitation sum (P) is the product of the hourly duration, DR, and intensity, PI. The relationship between PI and I is stronger (0.75) than the relationship between PI and DR (0.35). The third highest coefficient is the one between DR and RH (0.38). The higher the relative humidity, the higher the percentage of saturation at a certain temperature. Apparently this

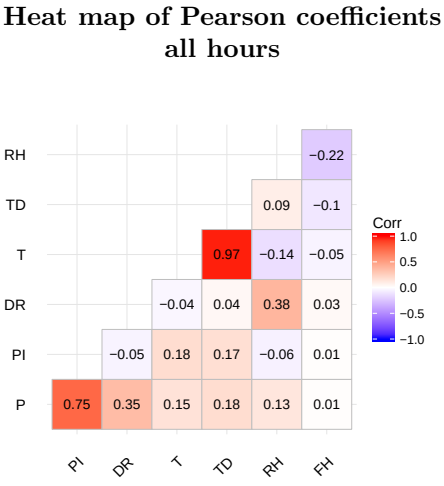

Figure 6.3: Heatmap consisting of Pearson correlation coefficients for the relations between precipitation intensity (PI) and sum (P), duration (DR), temperature (T), relative humidity (RH), wind strength (FH) for all wet hours. Coloring from blue to red gives the sign and strength of the relationship as is shown in the legend.

percentage says more about the duration of precipitation
within an hour than about the magnitude of the precipitation sum (or precipitation intensity PI). Higher RH is partially related to longer durations of precipitation within an hour, which could mean that with higher saturation it generally takes longer before precipitation stops due to undersaturation. However, there are of course also events where RH is high and the precipitation intensive, this explains why the coefficient is not super high.

What is more striking from Figure 6.3 is the relatively high negative correlation between RH and FH. So the lower the wind speed, the high the relative humidity. The reason for this relation is uncertain, but it could be that low wind speeds at the time and place of a large precipitation system results in stationarity of moist air.

Four other positive correlation coefficients, which are a bit higher than the rest, are those between (i) PI and T, (ii) PI and Td, (iii) I and T, and (iv) I and Td. From Section 6.2.1 we know that temperature can influence precipitation amount (P) and intensity (PI) via enhanced evaporation and updrafts and higher ability of air to hold moisture. As evaporation is important at the place and time of moisture influx, it could be that this relation holds a remote and lagged relationship. Hence, the relation does not have to be strong (coefficient of 0.15) when comparing temperature and precipitation measured at the same time and only on the location of precipitation accumulation. However, more and counteracting relationships can play a role. The relationship between P or I and T via enhanced updrafts should also be present in the relationship between CAPE and P or I. For De Bilt we plotted the CAPE 2-day maxima in relationship to other 2-day maxima and the cumulative 2-day precipitation sum (see Figure **??**).

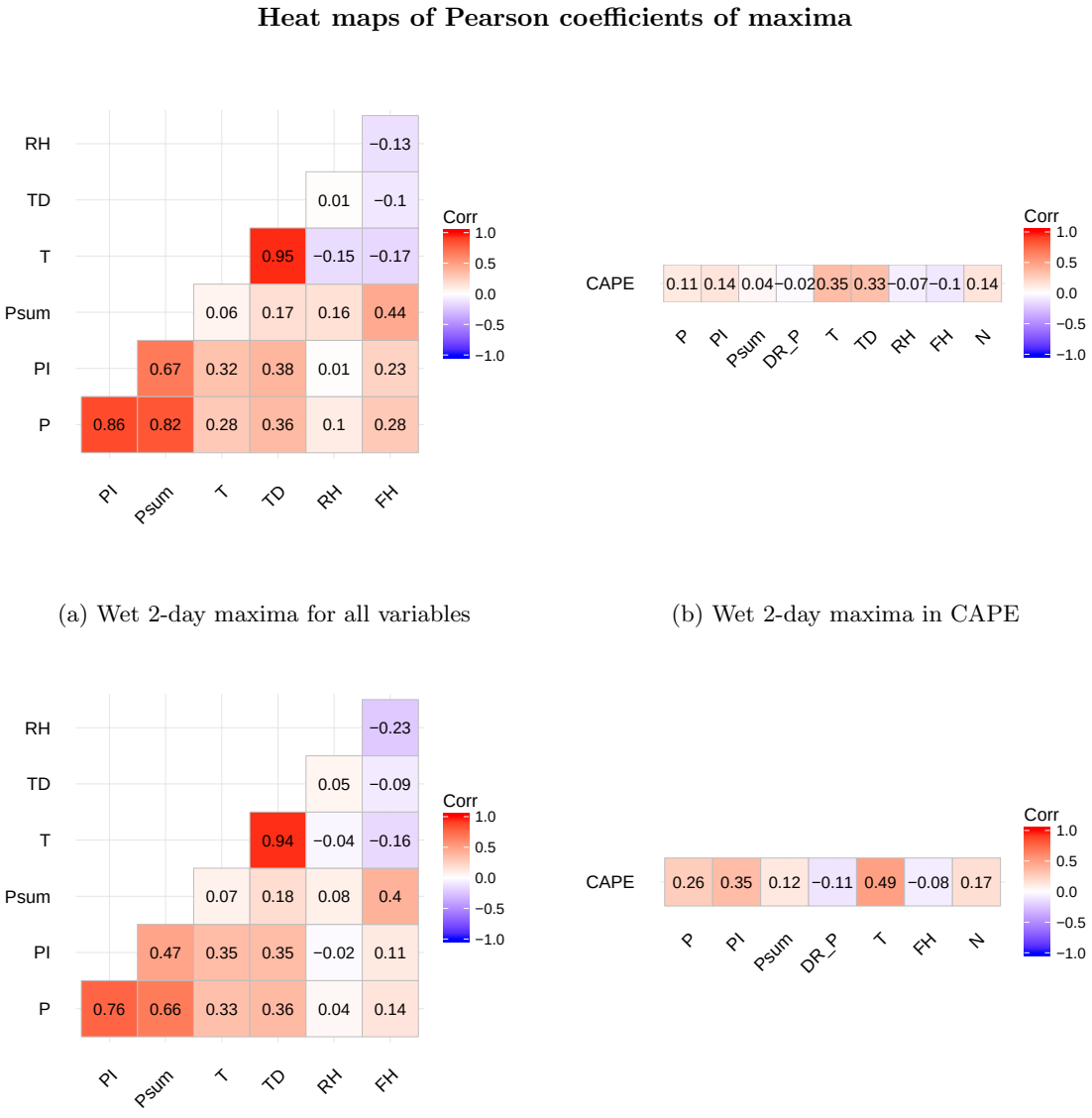

(a) Wet 2-day maxima for all variables

(b) Wet 2-day maxima in CAPE

(c) Wet daily maxima for all variables, except CAPE

(d) CAPE a wet day

Figure 6.4: Heatmap consisting of maxima in Pearson correlation coefficients of the variables: hourly mean precipitation intensity (P), precipitation intensity (PI), precipitation sum (Psum), duration at the time of maximum precipitation (DR_P) wind strength (FH), relative humidity (RH), temperature(T) and dewpoint temperature(TD). The heatmaps are computed from: (a) 2-day maxima of all variables (averaged over all stations), except CAPE, (b) 2-day CAPE maxima in relation to other variables for de Bilt, (c) daily maxima of all variables except CAPE, and (d) daily CAPE maxima in relation to other variables for de Bilt. N (N) is the 2-day (daily) count of CAPE measurements. Only Psum is not a maxima, but the daily or 2-day precipitation sum. Coloring from blue to red gives the sign and strength of the relationship as is shown in the legend.

The relationship between maxima in CAPE and T is indeed relatively strong for a time scale of 2 days and for the Bilt, as can be deduced from the relatively high correlation coefficient (0.35) in Figure 6.4b. The highest correlation between 2-day CAPE and precipitation variables (Figure 6.4b), is the one between the 2-day maxima in CAPE and precipitation intensity (0.14). N shows

the effect of the number of CAPE measurements a 2 days on the magnitude of the CAPE 2-day maxima, which is just as strong as the relation between CAPEmax2d and PImax2d, but weaker than the relation between 2-day CAPE and temperature or dewpoint temperature.

As we studied the maxima in mean hourly precipitation intensity (P) for independent 2-day periods in Chapter 5, we included the correlation coefficients for 2-day maxima in P (and in true precipitation intensity, PI, and the 2-day precipitation sum, Psum) in relation to the 2-day maxima in T, Td, FH, and RH (Figure 6.4a). Eventually we want to explain the observed trends found in Chapter 5. Therefore, it is relevant to investigate the correlation coefficients for the same temporal resolution. Besides, this approach zooms in more on the precipitation extremes, as 2-day maxima are considered. Keep into mind that the maxima of the different variables do not have to be measured at the same moment in time. On the one hand, this can enhance correlations in a biased way, if the hours are widely spaced in time. On the other hand, lower correlation coefficients are found when we look at correlation between 2-day maxima in P and the variables T, TD, and FH, measured at the time of the maximum in P. Negative feedback is then assumed to play a role, as for example cooling of the air due to precipitation. Analysis of the lags between the different maxima, showed that the maxima mainly occur at the same time up to 3 hours lags. Besides, the extremes in precipitation are often of the convective type, which is restricted to the hours that insolation is strongest.

We observe the same relationships which are relative high as in Figures 6.3 and 6.4d, which are stronger in Figures **??**. This shows that the relationships are stronger for the extremes. Figure 6.4a shows correlation coefficients of 0.28 and 0.36 for the relations between the 2-day maxima in hourly precipitation sums (P) and 2-day maxima in T and Td. Hence,the theory in which precipitation intensity relates to the ability of air to hold moisture, matches with the relatively high correlation coefficient (0.38) between 2-day maxima in PI and TD, with the latter as measure of moisture.

Even higher coefficients (0.32-0.38) are found when the 2-day maxima in precipitation intensities are considered instead of P (Figure 6.4a). The correlation coefficients between precipitation 2-day maxima and CAPE are lower, 0.11-0.14.

In fact, the largest changes in magnitude of the correlation coefficients, when switching from all-hour to 2-day maxima, are detected for wind speed (FH of 0.01-0.03 to 0.44). Especially the correlation between the 2-day maxima in FH and the 2-day precipitation sum is high (0.44). 2-day precipitation sum correspond more to long-lasting precipitation events than maxima in hourly precipitation sum and intensity. Besides, long-(short)-lasting events are generally characterized by events of a larger (more local) scale. Therefore, 2-day precipitation sums might depend on the synoptic settings. When these settings correspond to a large pressure gradient, high wind speeds are also present. In short, the correlation between 2-day precipitation sums and 2-day maxima in wind speeds could be explained by the synoptic setting. Except for CAPE, daily maxima give no higher correlation coefficients than 2-day maxima.

Till now we used Pearson coefficients, which indicate the strength of linear relationships between variables (Chapter 2). However, what if some or most of the variables depend in a non-linear way on each other? In order to investigate the type of relationship (i.e. linear or non-linear) we plotted the point clouds of all possible relations for wet 2-day maxima in T, TD, CAPE, FH and P (Figure 6.5).

Figure 6.5 confirms the linear relationship between (maxima in) T and Td, which we already suggested in this section. Multiple point clouds indicate semi-exponential and exponential relationships. With semi-exponential we mean that both a linear shape, and an exponential shape can be recognized in the point cloud. This is the case for 2-day maxima in P in relation tot 2-day maxima in T or Td. On contrast, the 2-day maxima in CAPE relate to all other variables clearly in an exponential way. The 2-day maxima in FH relate to P and CAPE maxima in a more exponential way, while the relations with 2-day maxima in T and Td do not have a distinctive form. Nonetheless, it is apparent that linearity can not be assumed for most of the relationships. Besides, another assumption for Pearson correlation coefficients is normal-distributed variables (Chapter 2). In Chapter 5 we already observed non-normal probability density functions for all hours and 2-day maxima in P. In contrast to the Pearson correlation, the Spearman rank correlation does not assume normal-distributed data or linearity of relationships (Chapter 2).

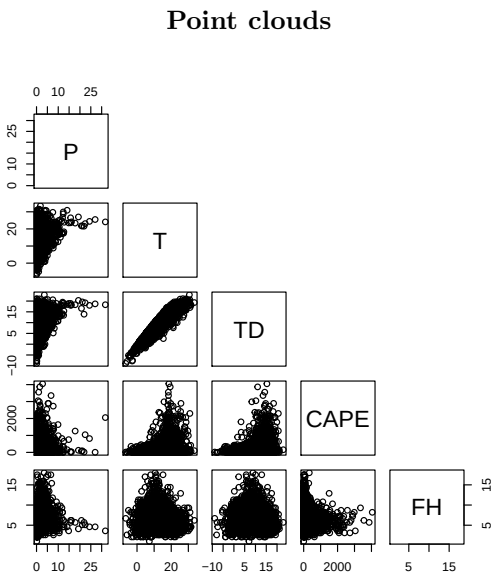

Figure 6.5: Points clouds showing the the wet 2-day maxima of the following variables: hourly mean precipitation intensity (P), temperature(T), dewpoint temperature(TD), convective available potential energy (CAPE), and wind strength (FH), measured in De Bilt. Note that the x- and y-axes differ in scale.

Figure 6.6 shows two heatmaps of Spearman rank correlation coefficients, one for all wet 2-day maxima of all variables, except CAPE, and one for the variables in relation to CAPE for De Bilt only. As shifting to a daily maxima did not result in improvement for the previous Figure, we do not include daily figures for this approach.

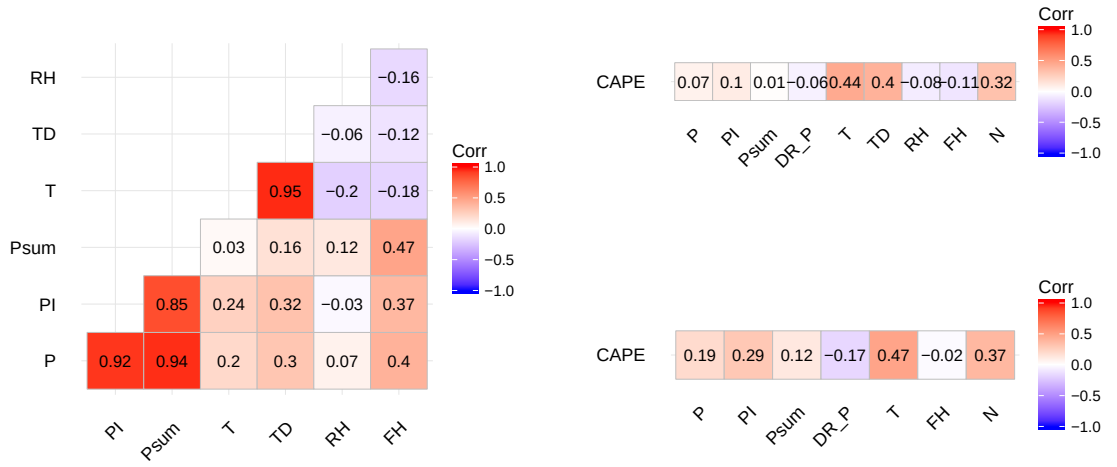

(a) Wet 2-day maxima for all variables, except CAPE

(b) Wet 2-day (top) and daily (bottom) maxima in CAPE

Figure 6.6: Heatmap consisting of Spearman correlation coefficients of the maxima of the variables hourly precipitation sum (P), precipitation intensity (PI), temperature(T), dewpoint temperature(TD), relative humidity (RH), and wind strength (FH), and of the 2-day precipitation sum (Psum). The heatmaps are computed from: (a) 2-day maxima of all variables (averaged over all stations), except CAPE, (b) 2-day CAPE maxima and daily CAPE maxima in relation to other variables for de Bilt. N is the 2-day count of CAPE measurements. Coloring from blue to red gives the sign and strength of the relationship as is shown in the legend.

The Spearman correlation coefficients are all lower than the Pearson correlation coefficients for wet 2-day maxima, except for those corresponding to the possible relations with FH 2-day maxima, the relations between the different precipitation maxima (P, PI and Psum) and the linear relation between T and TD 2-day maxima (Figure 6.6). The wind speed is both for 2-day precipitation sums, and for 2-day maxima in P and PI the strongest explanatory factor (coefficients of 0.37-0.47). It can be explained that the Spearman correlation coefficients are not higher in general than the Pearson correlations, although the relationships mainly seem to be non-linear. Especially the 2-day maxima in CAPE correlate relatively weakly with precipitation maxima (0.07 and 0.1 with P and PI), However, the Spearman approach is more correct from a statistical point of view. As we expect Spearman correlation coefficients to be stronger for daily CAPE maxima, we plotted these also in Figure 6.6b. The correlations are indeed higher for the daily resolution compared to the 2-day resolution, even 2.5-3 times. Nevertheless, we want to explain changes in 2-day precipitation maxima, so we can only conclude that the influence of the 2-day CAPE maxima is likely to be not that high regarding the strength of the relationship.

To summarize, we find relatively high correlation coefficients for the factors T, Td, CAPE and FH of which we know from theory to have a major influence on precipitation changes. These correlations are stronger for the extremes in these variables than for all-hour values. Different forms of relationships (linear, exponential, combination of both) are recognized by point clouds. Most of the relations are not purely linear, so that Spearman rank correlation coefficient is a better correlation statistic than the Pearson correlation coefficient. Following 2-day maxima FH, the order of strength regarding the Spearman rank correlation with 2-day maxima in P (of which significant trends are found in Chapter 5) is: TD (cor=0.3), T (cor=0.2), and lastly CAPE (cor=0.07).

6.3 Trends in key variables

In this section we investigate whether the key variables, wind strength, CAPE, temperature and dewpoint temperature, regress in time. First, we plot the probability density functions in order to choose the appropriate method(s) of trend analysis for each variable. Ordinary least squares is applied on normal distributed data and quantile regression on both normal and non-normal distributed data. Second, we plot the fitted quantile and ordinary least squares lines. In order to detect the common trend for these variables, we have averaged the 2-day maxima over the 5 stations. We do not differentiate on summer and winter trend in the trend analysis. However, in Section 6.4 we will consider seasonal dependency next to time dependency of the different relationships. Note that trend analysis on 2-day CAPE maxima is applied for the time period for which CAPE data is available (1993-2015) and is not averaged over stations, as only CAPE data from de Bilt is available. We do not study in depth the historical changes in instrumentation and measuring sites for the key variables as we did for precipitation, due to the time restriction of this research. Third, we apply a significance test on the trends.

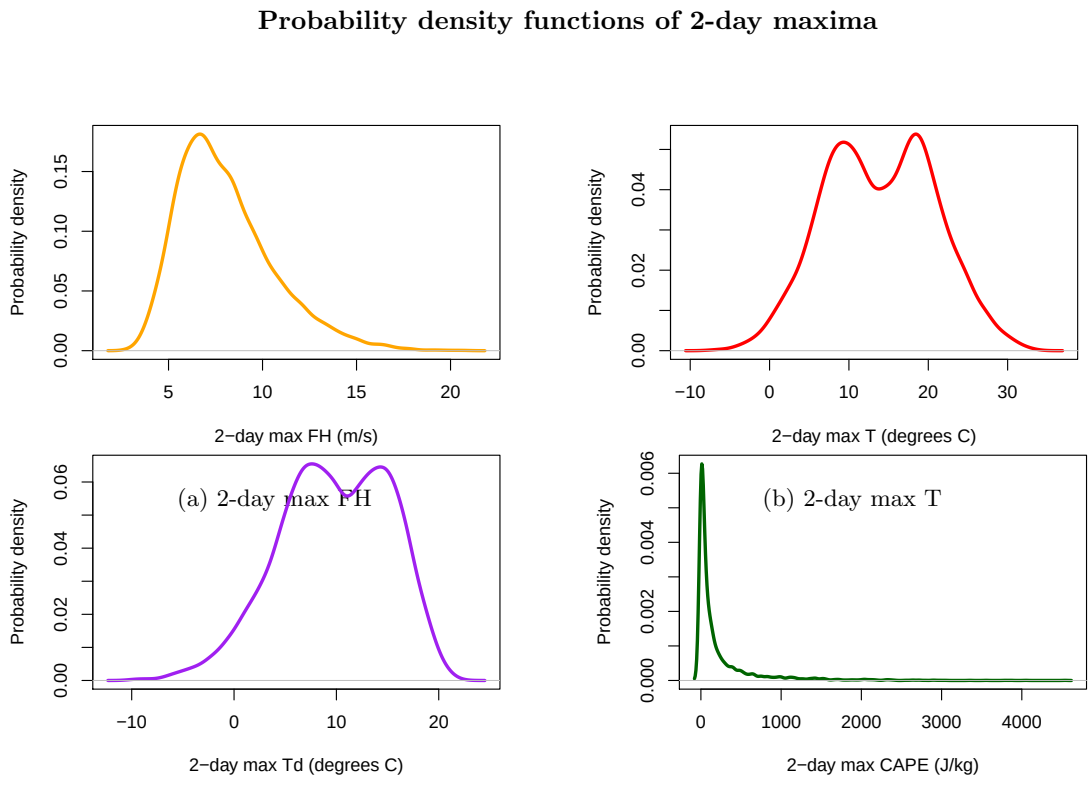

Figure 6.7: Probability density functions of 2-day maxima in (a) wind strength, FH, (b) temperature, T, (c) dewpoint temperature, Td, averaged over all 5 stations, and (d) 2-day maxima in convective available potential energy, CAPE, for only De Bilt. The probability density function of FH is computed from 2-day FH maxima between 1993-2015, to deal with the difference in rounding due to automatization around the year 1993. The other probability density functions are computed from data between 1958-2015. Note that the x- and y-axes differ in scale per variable.

All the probability density functions shown in Figure 6.7 are computed from the 2-day maxima between 1958-2015, except for the probability density function of the FH maxima. Before the automatization of wind speed measurements (in 1993) data was not rounded to 1 m/s. As two types of data (rounded and non-rounded) give a strange appearance of the probability density function, we decided to only plot the 2-day FH maxima measured from 1993 onward. However, the form of this probability density function is not different from the probability density function consisting of all FH maxima.

The 2-day maxima in FH, T and TD are distributed approximately in a normal way, compared to the 2-day maxima in CAPE which are distributed in a non-normal way (Figure 6.7). For this difference in probability density functions, we only apply least squares on the 2-day maxima of FH, T and TD. Note that the probability density function of wind speed is not entirely symmetric. For 2-day CAPE maxima we apply ordinary least squares regression on the yearly means 2-day maxima, which are normal-distributed. For all data we study the quantile regression fits on the 2-day maxima. As precipitation extremes are stronger correlated to the extremes in the explanatory factors, the trends in the higher quantiles are the most interesting. The results of the trend analysis for the 4 variables are listed here.

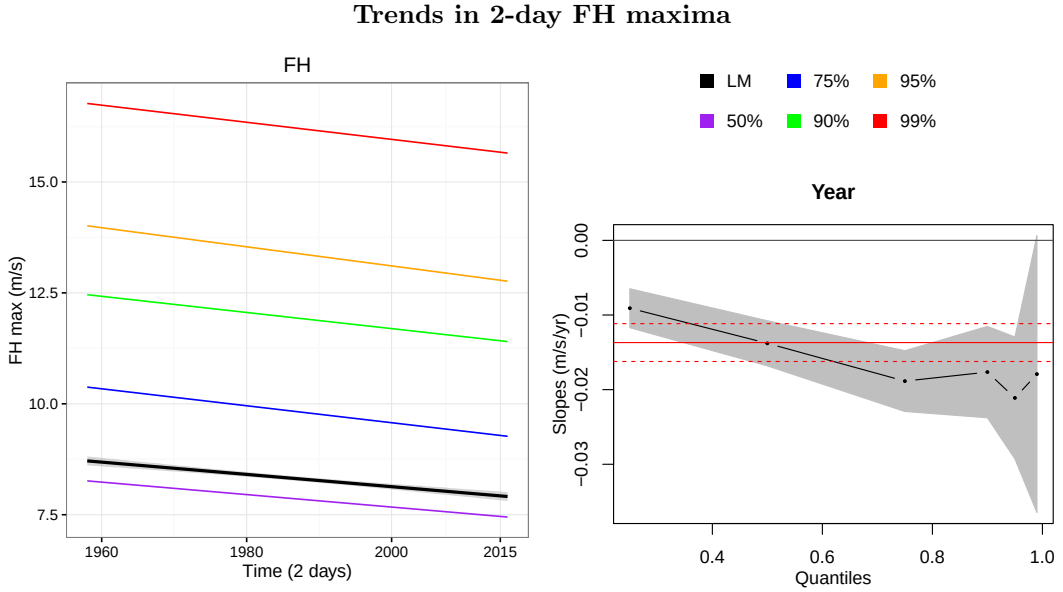

(a) Quantile regression

(b) Legend and yearly rates

Figure 6.8: (a) Quantile regression lines with $\tau = 75, 90, 95, 99, 99.9$ % of 2-day maxima in wind speed averaged over all stations, and (b) the corresponding legend and yearly rates in FH in m/s/yr. The black line in (a) provides the ordinary least squares fit of the 2-day FH maxima. In (b) each black dot is the slope coefficient for the quantile indicated on the x-axis and the gray band represents the corresponding confidence interval.

First, Figure 6.8 presents quantile and ordinary least squares (OLS) fits for 2-day maxima in wind speeds and the corresponding rates. A negative signal is detected for the 2-day maxima in FH. For the period 1958-2015 the OLS fit on the maxima has the exact same negative slope coefficient, -0.014 m/s/yr, as the 50%-quantile regression line (Figure 6.8b). Additionally, we again find higher slopes for the higher quantiles and the strongest trend for the 95%-quantile (-0.02 m/s/yr). It is worth noting that Figure 6.8b shows that the 99% quantile regression fit has a relatively wide confidence interval, so there is high uncertainty for this fit.

Although the decreasing of the wind speed for the Netherlands is consistent with the study of (Smits and Können, 2005), the reason for the negative signal not investigated in this thesis. It might have to do with changes in the position of the jet stream. A decrease in FH is not expected to explain the increase in P, as we know from theory that high wind strength (as component of strong wind shear) favors extreme precipitation via storm development and faster propagation of frontal systems over a certain site (Section 6.2.1). However, wind shear can also exist when we have weak surface winds and strong upper-level winds. Besides, back-building or occlusion events are associated with weak winds and can involve high hourly amounts of accumulated precipitation at a specific location (as described in Section 6.2.1). On the contrary, the correlation of the precipitation maxima was highest with maxima in FH.

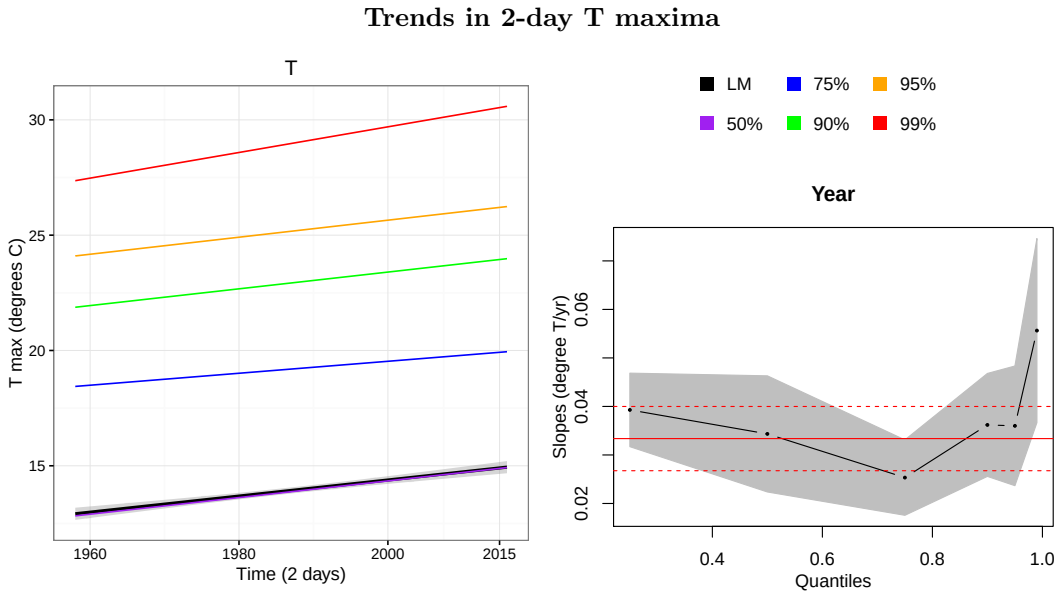

(a) Quantile regression

(b) Legend and yearly rates

Figure 6.9: (a) Quantile regression lines with $\tau = 75, 90, 95, 99, 99.9$ % of 2-day maxima in temperature averaged over all stations, and (b) the corresponding legend and yearly rates in T in °C/yr. The black line in (a) provides the ordinary least squares fit of the 2-day T maxima. In (b) each black dot is the slope coefficient for the quantile indicated on the x-axis and the gray band represents the corresponding confidence interval.

Second, we studied the trends in temperature for the same period, of which the results are shown in Figure 6.9. In contrast to FH, positive quantile and ordinary least squares (OLS) trends are found for the 2-day maxima in T (Figure 6.9a). What is more striking, is that for the quantile lines the general rule, namely that for the higher the quantile we have a stronger trend, is not applicable here. Figure 6.9b demonstrates that the weakest slope is detected for the 75%-quantile (0.025 °C/yr). Nonetheless, the strongest slope is detected for the highest (99%) quantile (increase in 2-day maxima of 0.06 °C/yr), . Besides, not only the 90%- and 95%-quantile lines have a stronger slope than the OLS line, but also the 25%- and 50%-quantile lines.

The OLS of the 2-day or yearly means T maxima gives an increase of approximately 3.5 °C/century, which is almost four times as high as the global rate in temperature for this time period (6.2.1). Note that we only consider temperature extremes (i.e. 2-day maxima) measured in the Netherlands, and we know from Chapter 1 that local extremes can increase faster than the global average. The relative rates vary between 0.23-0.30 %/year. Rates are higher for the northern coastal region compared to the southern inland region of the Netherlands.

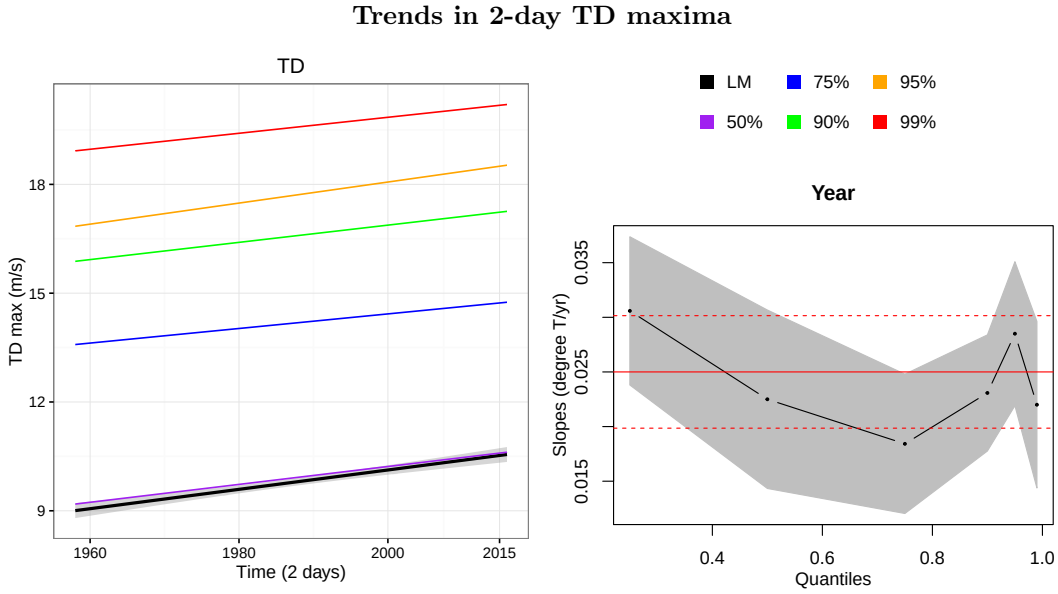

(a) Quantile regression

(b) Legend and yearly rates

Figure 6.10: (a) Quantile regression lines with $\tau = 75, 90, 95, 99, 99.9$ % of 2-day maxima in dewpoint temperature averaged over all stations, and (b) the corresponding legend and yearly rates in TD in °C/yr. The black line in (a) provides the ordinary least squares fit of the TD maxima. In (b) each black dot is the slope coefficient for the quantile indicated on the x-axis and the gray band represents the corresponding confidence interval.

Third, we applied trend analysis on the 2-day maxima in TD (see Figure 6.10). From Figure 6.10a we can deduce that 2-day maxima increase in time for the period 1958-2015. The ordinary least squares line has a slope coefficient of 0.025 °C/yr, which is larger than most of the other fits. Only two quantiles have stronger slopes, the 25%-quantile and the 95% quantile. Remarkably the slope of the 25%-quantile is the highest, namely 0.031 °C/yr. However, the confidence interval is relatively wide for the lower quantiles. Nevertheless, the lower boundary of the confidence interval is always above 0.012, so these trends are significantly positive.

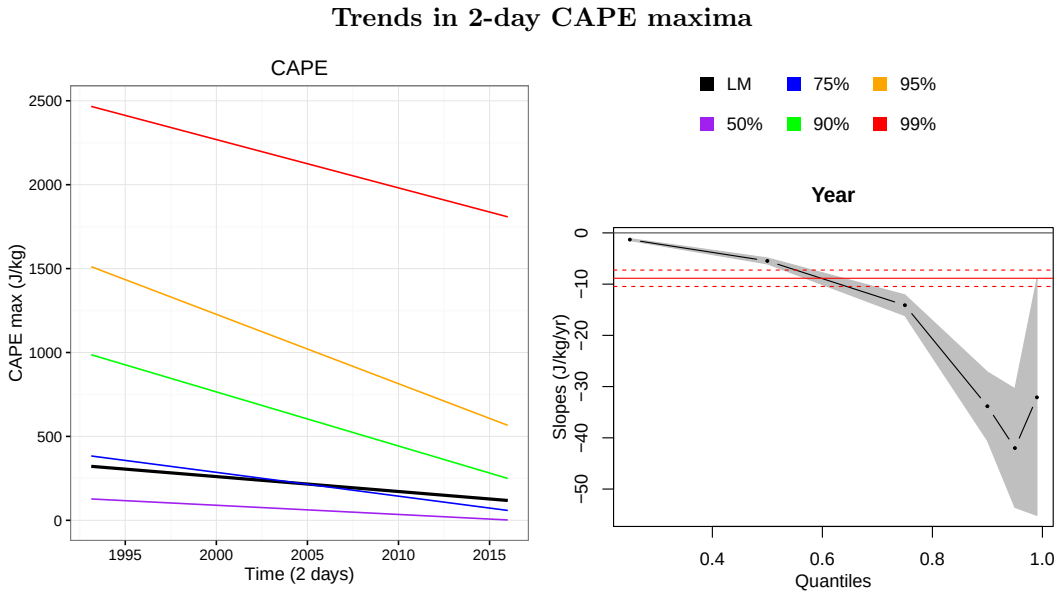

(a) Quantile regression

(b) Legend and yearly rates

Figure 6.11: (a) Quantile regression lines with $\tau = 75, 90, 95, 99, 99.9$ % of 2-day maxima in convective available potential energy averaged over all stations, (b) the corresponding legend and yearly rates in CAPE in J/kg/yr. The black line in (a) provides the ordinary least squares fit of the 2-day CAPE maxima. In (b) each black dot is the slope coefficient for the quantile indicated on the x-axis and the gray band represents the corresponding confidence interval.

Finally, we repeat the quantile regression fitting for 2-day CAPE values measured between 1993 and 2015 for station De Bilt. From Figure 6.11a we can deduce that CAPE values in De Bilt have decreased for this period. The ordinary least squares of the yearly mean in 2-day maxima has a negative slope of approximately -10 J/kg/yr (Figure 6.11b), which is stronger negative than the lower (25%- and 50%-) quantiles, but weaker negative than the higher (75%-,90%-,95%,99%) quantiles. The strongest trend is found for the 5% highest 2-day CAPE maxima with a decreasing rate of 42 J/kg/yr. The highest quantile lines (90-99%-quantiles) are summer trends, as the winter CAPE values do not exceed 500 J/kg, this is shown in the next section (Section 6.4).

Furthermore, we can observe that the higher the quantile, the larger the confidence interval. The reason for this is that a lower samples size belongs to a higher quantile, which enhances the uncertainty in the regression fit. At the end of this section we will investigate the significance of all the different quantile regression lines for all variables.

Nonetheless, we want to emphasize that the observed negative trends in CAPE are not able to explain the observed positive trends in precipitation intensity. From theory we know that high CAPE values express the potential of strong updrafts, which are required for convective systems with intensive summer precipitation. On the contrary, we only consider trends in CAPE for the period 1993-2015 here, which can not be fully compared to trends in precipitation maxima for the period 1958-2015. Furthermore, the decreasing resolution of CAPE measurements could also influence a negative signal. All in all, we can not draw conclusions about the validity of the observed negative trend and the likelihood of this trend to be the cause of the trend in P.

In order to investigate the significance of all trends, we conduct a 9999 Monte Carlo permutation test. For wind speed (FH) and CAPE we tested whether the observed slope is significantly lower than all randomly permuted slopes in order to detect a negative trend, while for temperature (T) and dewpoint temperature (Td) we tested it vice versa in order to detect a significant positive

trend.

Table 6.1 gives an overview of the significance of the trends. A red (green) marking of a cell indicates a decreasing (increasing) trend significant at the 95% confidence level (CL). All the linear and quantile regression trends are significant, except for the 99%-quantile of 2-day maxima in FH (p=0.94), of which we already discussed the large uncertainty by its confidence interval.

Table 6.1: The p values of the quantile regression trends with Q25-Q99 corresponding to the τ=25-99%-quantile.

Variable	Q25	Q50	Q75	Q90	Q95	Q99	LM
FH	1.00	1.00	1.00	1.00	1.00	0.94	1.00
T	1.00	1.00	1.00	1.00	1.00	1.00	1.00
TD	1.00	1.00	1.00	1.00	1.00	1.00	1.00
CAPE	1.00	1.00	1.00	1.00	1.00	0.98	1.00

In short, in this section we detected significant (99% CL) negative trends in wind speed and CAPE and significant (99% CL) positive trends in temperature and dewpoint temperature for the ordinary least squares regression fits and almost all quantiles fits. For wind speed the type of relation (positive or negative) with precipitation intensity is ambiguous and for CAPE a negative trend is not expected to explain the trend in P. However, whether this trend is truly negative for the period 1958-2015 is doubtful regarding the data which is limited in time length and contains a decrease in resolution in time. The changes in temperature and dewpoint temperature remain as potential causes of the trends in intensification of precipitation.

6.4 Seasonal and temporal differences in relations

Introduction

In this section we zoom in on seasonal and temporal differences in relationships between maxima in the key factors (T, Td, FH, and CAPE) by comparing summer and winter season and a begin (1958-1986) and an end period (1987-2015). For every variable we plot the relations between the maxima in hourly precipitation sums and other variables as point clouds differentiating on summer and winter. We also present the summer and winter frequency distributions of the variables. Furthermore, we plot binned summer and winter quantile regression to express changes in precipitation maxima as a function of changes in the other maxima. In case of temperature and dewpoint temperature we compare the quantile regression lines to a Clausius Clapeyron scaling. For each of the three figures per relationship we compare between the first and second time period, in order to answer the question whether the changes in precipitation are caused by the changes in statistics of the key variable in question or by a changes in the relationship with that key variable. As binning and differentiating on period and season lowers the resolution greatly, we chose to use the daily maxima instead of the 2-day maxima. This section is ordered per variable.

Temperature

In figure 6.12A the precipitation maxima (of wet days only) increase with maxima in temperature in a non-linear way. Clear differences are visible between winter and summer. The winter precipitation are generally lower and the points slope more gently with respect to temperature maxima. Both the summer and the winter data resembles a triangle shape, with a monotonic increase till approximately 25°C summer temperature and 10°C winter temperature and a decrease after these maxima.

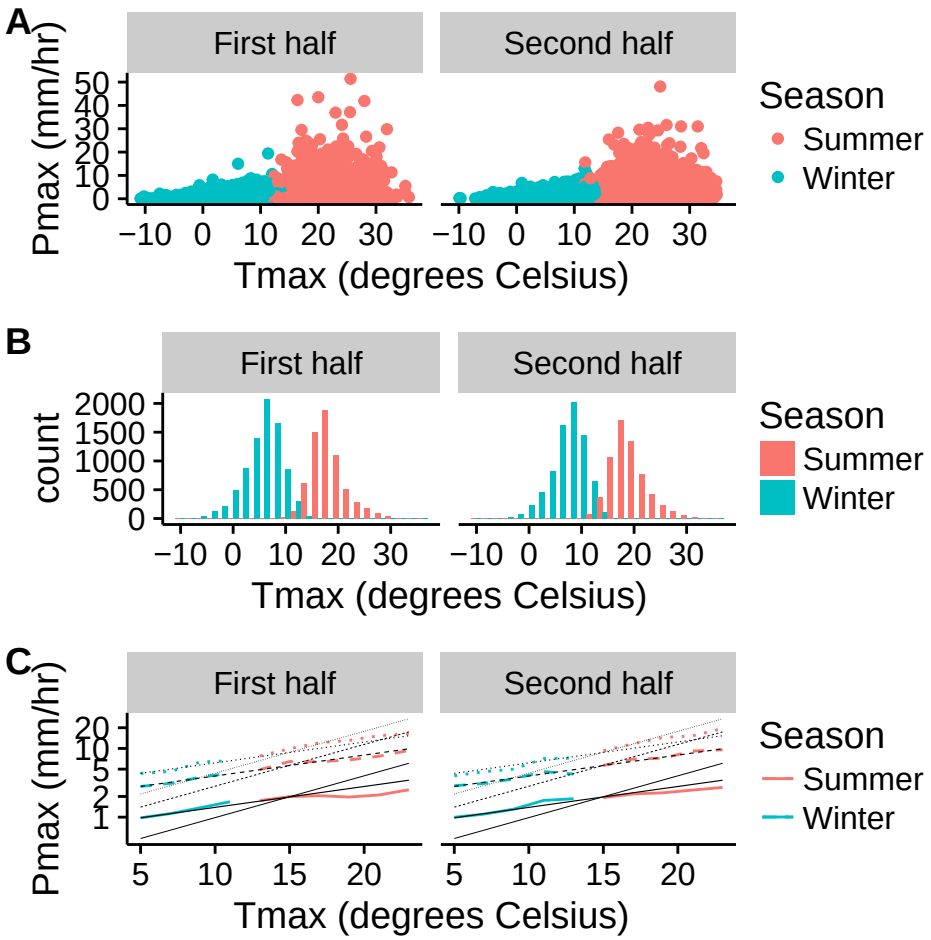

Figure 6.12: (A) The daily maxima in precipitation of wet days are plotted against maxima in temperature. B shows the distribution of temperature maxima, and C demonstrates the regression of the mean (solid colored line), the 95% (dashed colored line) and 99% (dotted colored line)-quantiles in precipitation over temperature. Temperature is binned with steps of 2°C. The black lines present the normal (black line) and double (thinner black line) Clausius-Clapeyron scaling for the mean and quantiles with the same line style (i.e. solid, dashed and dotted). Summer and winter differences are indicated by the blue (winter) and pink (summer) color. On the left side the information is provided for the first period (1958-1986), and on the right side the same is provided for the second period (1987-2015).

For both periods the seasonal characteristics and overall shape are visible, but there are also differences between the point clouds. On the one hand, the first period has more outliers (> 32 mm/hr for summer data, > 12 mm/hr for winter data), on the other hand the second period has

more (and higher) summer intensities at temperatures > 30 °C and winter intensities at temperatures > 10 °C.

To investigate the influence of the temperature distributions on the shape of the point clouds, we plotted the summer and winter distributions of temperature for each period (Figure 6.12B). In Figure 6.12B for each bin of 2 degrees Celsius the number of wet hours per season per period is counted. Summer and winter distributions for both periods have similar Gaussian shapes with a temperature difference of 12°C between the peaks. More wet hours exist in winter than in summer, explaining the magnitude difference between the winter and summer distribution.

For the first period the peak in number of winter data per bin is at 6-8 °C, while the summer peak is around 16-18 degrees Celsius. For the second period the winter peak is shifted to a higher bin (to 8-10 °C). Although, the summer peak is not shifted towards a higher bin, the bars after the peak are relatively higher for the second period compared to the first period.

As the temperature distributions have a Gaussian shape, the chance on an extreme in intensity are highest for the middle bins with the highest numbers of data per bin. However, the point clouds do not only have a triangle shape, but they are also tilted towards a positive relationship between P and T. Besides, the maxima in summer and winter precipitation intensity in Figure 6.12A are for higher temperatures than expected from the distributions.

In order to remove any influence of how the temperature is distributed on its relation with precipitation intensity, we computed the mean summer and winter precipitation maxima for each temperature bin with more than 200 samples. In Figure 6.12C the solid lines connect these means. Moreover, the 95% and 99% quantile lines are plotted as dashed and dotted lines to visualize the temperature relation with "high" extremes in precipitation. Mind the logarithmic scale of the y-axis. The mean and quantile lines are compared to the Clausius-Clapeyron (CC) scaling, to find out whether this precipitation-temperature relationship can be deduced directly from the CC equation, or whether other dynamics are involved.

From Figure 6.12C can be deduced that the mean and quantile lines quite nicely follow the Clausius-Clapeyron equation (of which the scaling is given by the black lines with the same style in linetypes). With a thin black lines a super CC-scaling (twice what is expected from the CC equation) is indicated. Only for some parts, such as the 95% and 99% quantile lines for temperatures higher than 15 degrees, a super CC-scaling is found. What is striking is that this also holds for the winter mean and quantile lines for temperatures lower than 2 degrees for the first period. It might be still influenced by the amount of data in a bin. Significant differences between summer and winter P-T relationships are not found.

When comparing the two periods little differences are present for the upper parts of the winter and summer mean and quantile lines. The winter lines regress further (in a flat way) with respect to temperature for the second half compared to the first half. This is explained by the shift in the temperature distribution to higher winter values. The upper parts of the summer mean is less deviating from the CC-scaling and the upper parts of the quantile lines are relatively more aligned with the super CC-scaling. Nevertheless, changes in the distribution are more clearly visible for this time period comparison than changes in the P-T relationships.

Dewpoint temperature

In this section we investigated changes in the point clouds, distributions and binned mean and quantile lines for dewpoint temperature (Td) between the two seasons and time periods (Figure 6.13). For increasing dewpoint temperature we observe the same monotonic increase of precipitation intensity as for temperature. Besides, more outliers are present in the first half of the

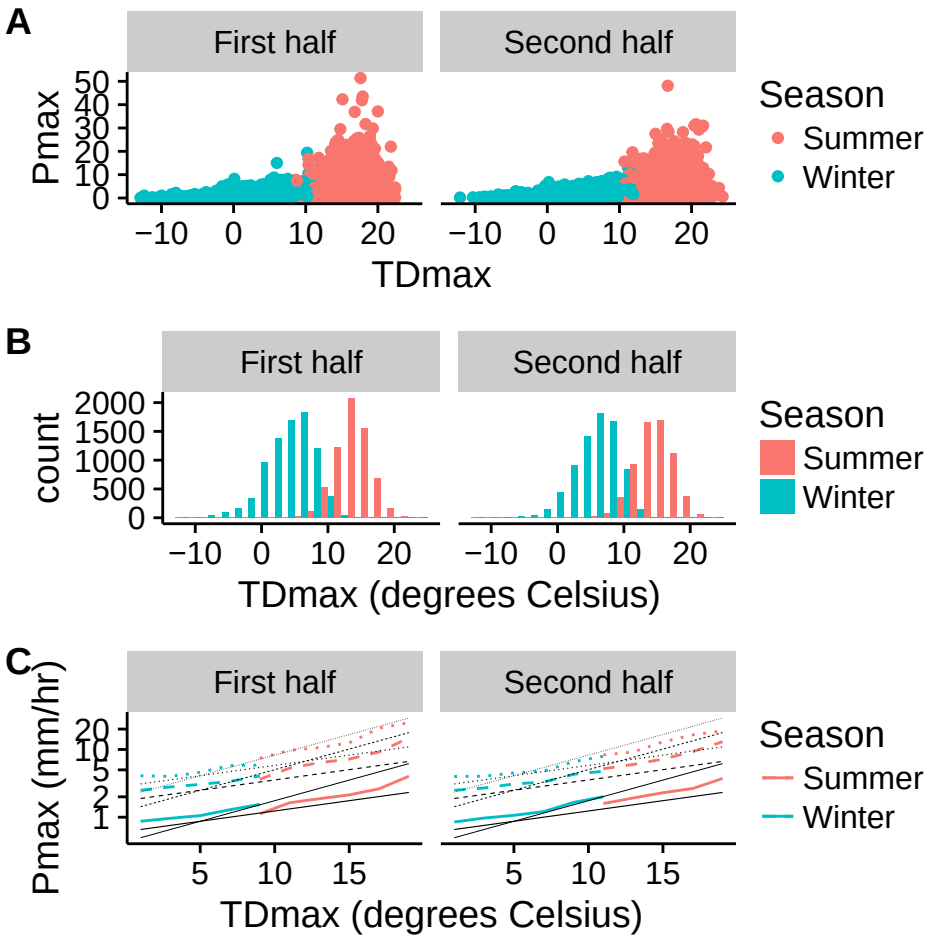

Figure 6.13: (A) The daily maxima in precipitation of wet days are plotted against maxima in dewpoint temperature. B shows the distribution of dewpoint temperature maxima, and C demonstrates the regression of the mean (solid colored line), the 95% (dashed colored line) and 99% (dotted colored line)-quantiles in precipitation over temperature. Dewpoint temperature is binned with steps of 2°C. The black lines present the normal (black line) and double (thinner black line) Clausius-Clapeyron scaling for the mean and quantiles with the same line style (i.e. solid, dashed and dotted). Summer and winter differences are indicated by the blue (winter) and pink (summer) color. On the left side the information is provided for the first period (1958-1986), and on the right side the same is provided for the second period (1987-2015).

time period, while a shift is visible from relatively high counts of low winter and summer intensities in the first half to relatively high counts of high winter and summer intensities in the second half. As we know from Section 6.2.2 that temperature and dewpoint temperature have a strong linear relationship, these similar features for T and Td are not unexpected. However, regarding the binned mean and quantile lines for dewpoint temperature, relatively more parts are scaled to the super CC-scaling, compared to temperature. Nonetheless, regarding the comparison of the two time periods, no notable changes in the relationship between P and Td are detected, while the dewpoint temperature distribution clearly shifts towards higher dew point temperatures.

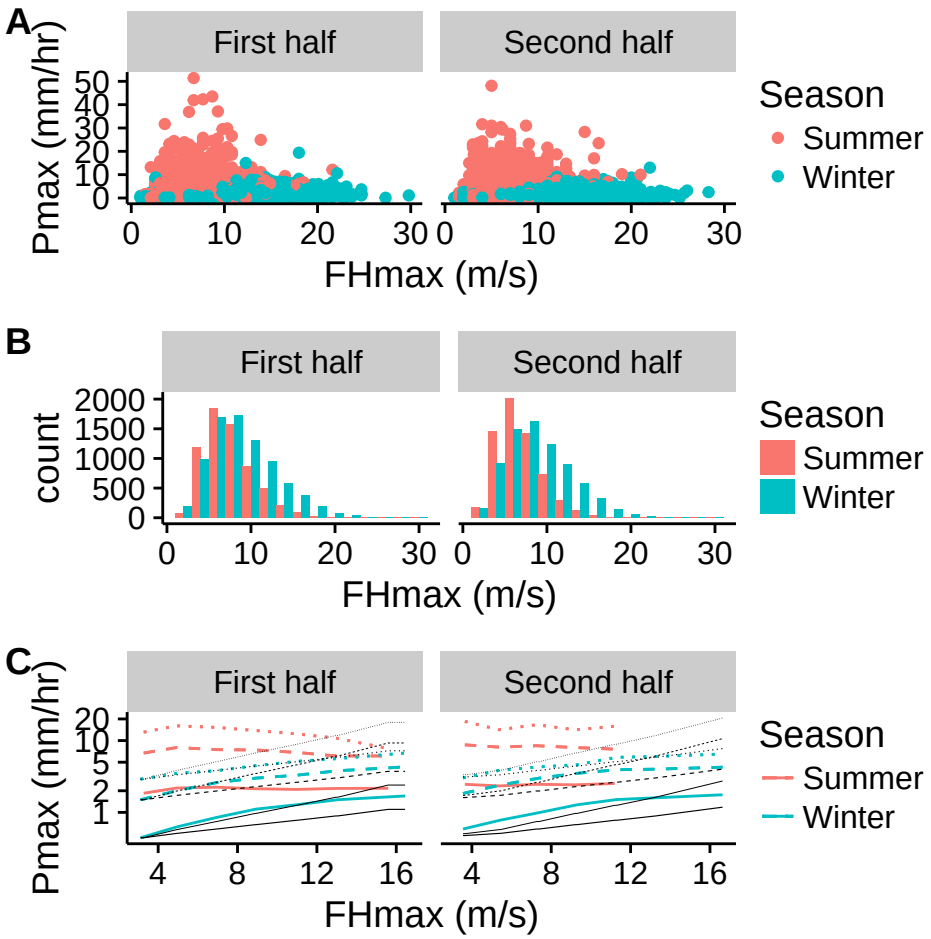

Figure 6.14: (A) The daily maxima in precipitation of wet days are plotted against maxima in wind speed (FH). B shows the distribution of FH maxima, and C demonstrates the regression of the mean (solid colored line), the 95% (dashed colored line) and 99% (dotted colored line)-quantiles in precipitation over FH. FH is binned with steps of 1 m/s. The black lines present the normal (black line) and double (thinner black line) Clausius-Clapeyron scaling for the mean and quantiles with the same line style (i.e. solid, dashed and dotted). Summer and winter differences are indicated by the blue (winter) and pink (summer) color. On the left side the information is provided for the first period (1958-1986), and on the right side the same is provided for the second period (1987-2015).

Wind strength

Furthermore, we investigated whether the summer and winter point clouds, distributions and mean and quantile lines of the maxima in wind speed (FH) change in time. Although, we already know from Section 6.3 that its uncertain whether the general long-term trend in FH maxima can explain the change in P, it is still interesting to analyse the seasonal and temporal differences.

In Figure 6.14 we plotted the result. Clear differences between summer and winter can be seen from Figures 6.14A,B; summer is recognized by relatively high precipitation maxima and low wind speeds, while for winter it is vice versa. This could correspond to a seasonal difference in sign of the relationship between P and FH. In summer weak surface winds favors intense precipitation via back-building of convective systems under condition of sufficient wind shear, while in winter strong

surface winds favors intense precipitation via fast propagation of frontal systems. Additionally the summer distribution has a more asymmetric shape with a more pronounced peak compared to the winter distribution. Considering the time-related change in distributions we do observe small decreases in the frequencies of winter maxima, but we do not for the frequencies of summer maxima.

Figure 6.14C shows the change in the P-FH relationship. Although, the CC- and super CC-scaling do not have a physical meaning here, they are plotted so we can better compare the regression of the mean and quantile lines with the same regression for temperature and dewpoint temperature. What is striking from this figure, is that we indeed observe a sign difference between summer and winter in the P-FH relationship. With negative (first period) to constant (second period) slopes for the summer regression fits of P over FH, and positive slopes for the winter regression fits.

When considering the transition from the first to the second period we observe in 6.14A,B a decrease in the FH maxima, which is seen in (1) a reduction of the maxima in number of outliers in summer precipitation maxima (which was also observed in the T and Td plots), (2) an increase of the frequencies of relatively weak summer wind speeds and (3) a slight lowering of the summer bars corresponding to the higher wind speed maxima. From 6.14C we deduce that there are less summer precipitation maxima for high wind speed maxima (pink lines do not extend further for temperatures $> 11°C$). Moreover, the summer regression provides a less negative P-FH relationship in time. The winter regression lines are for a larger part aligned with the CC scaling in the second period compared to the first period.

Regarding the decrease in summer precipitation outliers in time, we do not expect that when the trend in wind speed is leading to higher P, this is a summer trend. Despite of a negative trend in the overall wind speeds, it could be that an intensification of the winter P-FH relationship explains the positive trend in P. Although, the latter can be related to faster propagation of frontal systems with higher wind speeds, we can not draw conclusions whether changes in FH have caused the intensification of precipitation.

CAPE

Finally, we would like to discuss changes in CAPE maxima and their relationship with precipitation maxima. However, we only have CAPE data from 1993 till 2015. Therefore, time comparison is not possible. Moreover, we only have data for De Bilt, so the resolution is too low to do the same binned plotting for precipitation maxima over CAPE maxima.

In Figure 6.15 we have plot the summer and winter point clouds, providing information about the seasonal P-CAPE relationship, and the distributions of summer and winter CAPE maxima. The values of CAPE maxima are very seasonal dependent, as can been deduced from Figure 6.15. Winter data are confined to low CAPE maxima of < 500 J/kg and low precipitation intensity maxima of < 10 mm/hr, whereas summer data has weak to high CAPE maxima (up to 5000 J/kg). For both seasons a highly asymmetric (lognormal) distribution can be detected, although the summer distribution is wider in shape than the winter distribution.

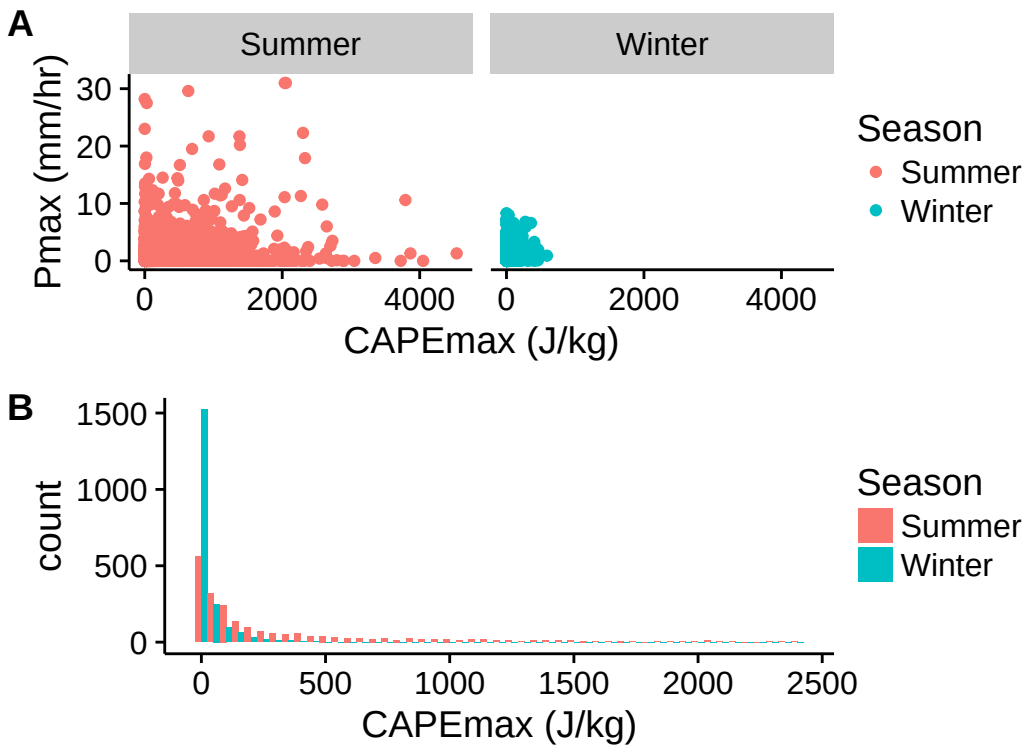

Figure 6.15: (A) The daily maxima in precipitation of wet days are plotted against maxima in CAPE (FH). B shows the distribution of CAPE maxima. Summer and winter differences are indicated by the blue (winter) and pink (summer) color. Note that only information is given about the period 1993-2015.

Summary

To summarize, we found strong seasonal differences in relationships between precipitation and T, Td, FH en CAPE maxima and in the distributions for each variable. In general, in summer we have relatively high daily maxima in temperature (mainly between 12-24°C), dewpoint temperature (most values between 9-20°C), and CAPE values (mainly between 0-2500 J kg^{-1}) and relatively low daily maxima in wind speed (2-12 m/s) compared to winter daily maxima (respectively 0-14°C,-2 - 12°C, 0-500 J/kg, 2-18 m/s).

Positive exponential relationships, comparable with CC (and partially super CC) scaling, are found for binned summer and winter P-T and binned winter P-FH mean and quantile lines. Summer and winter maxima in mean hourly intensity are similarly sensitive for changes in temperature and dewpoint temperature, except for the highest (summer) intensities which are less sensitive to increases in (dewpoint) temperature. Winter maxima in wind speed are more aligned to CC scaling than summer maxima.

When comparing the second half of the time period to the first half, the P-T and P-TD relationships are slightly more aligned to the CC-scaling, while the P-FH quantile lines are less aligned from the CC-scaling. Moreover, the P-T and P-TD are as strong or stronger for the more extreme P maxima (95%- and 99%-quantiles), compared to the mean P maxima. This is vice versa for the P-FH relationship. However, for all three variables the timewise shift in distribution from higher summer and winter T and TD maxima and lower winter FH maxima is more clearly visible than changes in their relationships with P. So, changes are more related to changing statistics than to

changing dynamics.

Due to the ambiguous relation between wind speed and precipitation, we can not draw conclusions on whether the negative signal in FH explains the positive signal in P (Section 6.3). If this would be case, then it might have to do with faster propagation of frontal systems in winter associated with weak surface winds.

In contrast to FH, we expect that the changes in precipitation are likely influenced by changes in the distribution of temperature and dewpoint temperature. A shift to higher temperature and dewpoint temperature is then linked in an exponential way, shown in Figures 6.12,6.13C by the alignment with CC- to super CC- scaling, to higher precipitation intensities. The increase of temperature leads to an increase of the moisture holding capacity (expressed in Td), which leads to an intensification of precipitation extremes. This also holds with the detected negative trend in the frequency of wet hours. Air is less quickly saturated at higher temperatures, consequently there are less (2-day) hours in which saturation is reached.

Chapter 7

Discussion

7.1 Introduction

In this chapter we discuss the results and their implications in four parts. In the first part the objectives, theory and results are summarized and put into context of the current knowledge of the research field. The second and third part list respectively the strengths and weaknesses of this thesis. Further recommendations are provided in the last part.

7.2 Summaries

7.2.1 Summary of objectives

The main objective of the present work is to find out how extreme hourly precipitation in the Netherlands changes in time and what the causes are behind observed changes (Chapter 1). We expected that precipitation extremes are related in a non-linear way to the local moisture holding capacity, while the (global) mean precipitation is constrained by the global energy budget. Moreover, the heaviest events are thought to occur when all the moisture in a volume of air is precipitated out. Furthermore, we hypothesized that temperature, dewpoint temperature, vertical instability and wind shear are important factors for the occurrence and magnitude of extreme precipitation. This research also aimed on verifying the super Clausius-Clapeyron scaling found by Lenderink (2008,2010,2011). As this is argued to be the result of a shift from stratiform precipitation (dominating type in winter) to convective precipitation (dominating type in summer) with temperature, we considered precipitation-(dewpoint)temperature relationships separately for summer and winter. The main theory and findings of this thesis are summarized here and listed in order of the chapters.

7.2.2 Summary of theory

In Chapter 3 we brought to the attention the processes of (extreme) precipitation production and the related cloud types. Factors of importance for precipitation production are the cooling of air rich in moisture and CCNs by an external event and the potential for droplets to grow to a sufficient size. Factors of importance for the production of extreme precipitation, which we can study with help of the station data, are vertical instability (by CAPE and temperature), moisture (by dewpoint temperature) and wind shear (partially by wind speed). Furthermore, the two main types, cumuliform and stratiform clouds, are characterized by precipitation intensity.

7.2.3 Summary of results

In Chapter 4 we attempted to distinguish less intense precipitation (being dominantly of the stratiform type, mainly occurring in winter) from the more intense precipitation (being dominantly of the convective type, mainly occurring in summer) by separately analysing for winter and summer. As expected from theory, our results show that in summer both precipitation duration and precipitation intensity are larger than in winter. We define summer as June, July and August, and winter as December, January and February. Under these definitions the difference in extreme intensity between summer and winter is largest. In Chapter 4 we also investigated spatial differences in (extreme) hourly precipitation, and concluded that these differences are large. In the more northern and inland stations it rains more frequently than in the more southern and coastal stations.

In Chapter 5 we analysed trends in 2-day precipitation intensity, frequency and sum, for each station and for summer and winter. A Monte Carlo test provides a robust significant increase of the 25-5% highest 2-day maxima in precipitation intensity (0.2-0.4%/yr). In 58 years the highest maxima have increased with 0.5 mm/hr, which equals in magnitude the total difference in mean intensity between summer and winter. Besides, for summer and winter season significant positive trends are detected for respectively the 50-5% and 25-5% highest 2-day maxima. The trends in "high" extremes are likely to be summer trends. These summer trends are stronger (0.1-0.6%/yr) for the "moderate"-"high" extremes than winter trends (0.1-0.3%/yr), while only significant winter trends are found for "low" extremes (0.5-0.7%yr). Our study confirms previous findings (IPCC, 2013) that the relative increase of "high" extremes is larger than those of the yearly mean and the "low" and "moderate" extremes. In line with the findings of Malik, Bookhagen, and Mucha (2016), quantile trends and their significance show large spatial differences.

Other than positive trends in hourly precipitation intensity, our findings provide unique evidence of negative trends in frequency of wet hours. For every station significant trends, of which most on the 99% confidence level, were found for 2-day and yearly frequencies. The negative trends for the wettest 2 days vary between 0.1-0.6 %/yr and for the mean wetness between 0.08-0.29 %/yr. For the whole Netherlands the total change in 58 years can be translated to 100 wet hours less on average a year. This change is of same magnitude as the total spatial difference in mean wetness between northern and southern situated stations. So, the same change in wetness could be noticed when moving from the (more frequently raining) northern part of the Netherlands to the (less frequently raining) southern part.

When considering the seasonal differences in the 2-day and yearly trends in intensity, it is striking that only significant trends are found for summer frequencies of wet hours. This negative signal in frequency is, however, less robust than the positive signal in intensity. It is worth noting that in contrast to intensity trends, frequency trends are not computed from maxima data, which could explain the lower robustness. Besides, for frequency data on yearly resolution the lack of significant trends is likely due to the limited sample size. Furthermore, we detect a reverse disproportionality. In other words, the mean and the drier 2 days show a stronger decrease in the counts of wet hours than the wetter days. Note that insignificance of a trend does not imply that a trend does not exist. We also want to emphasize that the robustness in sign of the (non-significant and significant) trends is large for frequency of wet hours.

Moreover, for each station we detected significant positive trend in the yearly mean (OLS) and 10-1% highest (quantile regression) 2-day precipitation sums. The latter have increased with 1.2-2.7 mm in the last 58 years, however, differences exist between northern and southern stations. This could be temperature related, as precipitation intensity is temperature dependent (Chapter 6) and the trend in precipitation sum is dominated by the trend in intensity over the trend in frequency (as found in Chapter 5). Furthermore, another striking difference is that significant summer trends in precipitation sums belong to coastal stations, whereas significant winter trends belong to non-coastal stations. This might be related to seasonal dependent changes in moisture

availability (Chapter 6). Additionally, the trends in the highest and mean summer precipitation sums and highest winter precipitation sums are positive, while the trends in the mean winter precipitation sums are negative. Besides, the positive trends in the highest summer precipitation sums are stronger (0.60-2.8 %/yr) than trends in the mean summer (-0.43 to 0.78%/yr) or highest winter precipitation sums (0.27 to 0.45 %/yr). As the are more and stronger significant positive trends in precipitation, these trends seem to be dominated more by the positive trends in intensity maxima compared to the negative trends in frequency of wet hours. Despite the fact, that we only consider maxima intensities in contrast to all-hour frequencies of wet hours.

The dissimilarity in trends regarding the quantile fits for one station is more likely to be the result of the way quantile regression works than to be the result of a changing climate (Section 5.2.2). The different quantile fits are namely independent from each other, as the fits are calculated as a minimization function on the entire data set. Thereby, the fits can not represent a step-wise shift in time of the probability density distribution.

In Chapter 6 where we investigated the causes behind precipitation changes, we uncovered four important factors for extreme precipitation, (i) temperature, (ii) dewpoint temperature, (iii) CAPE and (iv) wind speed. From theory we deduced how these factors relate to extreme precipitation. (1) Increasing temperature can potentially influence extreme precipitation in three ways, via more atmosphere moisture generated by evaporation, a higher ability of the air to hold moisture, and stronger updrafts. (2) Dewpoint temperature is a measure of the air's humidity, which will increase with temperature under constraint of constant relative humidity according to the Clausius-Clapeyron equation. This is expected to result in less frequent, but more intense precipitation. (3) An increasing atmospheric temperature gradient (i.e. surface air increases more in temperature than higher-level air) goes hand in hand with increasing CAPE, which can lead to more influx of moisture. (4) Strong horizontal wind speed can be related to extreme precipitation via (a) strong wind shear important for convective storms to be self-perpetuating, and (b) via horizontal advection of frontal systems.

Furthermore, for these key variables we presented the relationships with precipitation intensity using a bundled data set (all five stations combined).Considering the maxima of the key variables strong (semi-)exponential relationships are revealed. For maxima of the same resolution (e.g. 2 days) as for the trend analysis, we found Spearman correlation coefficients of 0.4 (wind speed), 0.3 (temperature), 0.2 (dewpoint temperature) and 0.07 (CAPE). Moreover, we investigated whether similar trends can be detected for the four key variables as for trends in precipitation intensity. We found positive trends in temperature and dewpoint temperature significant at the 99% confidence level, which can explain the observed changes in precipitation. However, the significant negative trends detected in wind speed, for the period 1958-2015, and in CAPE, for the period 1993-2015, can not explain an intensification of precipitation.

In the last part of Chapter 6 we studied time related changes for summer and winter distributions of the key variables and in the point clouds and quantile regression fits (plotting precipitation intensity over the key variable). Strong seasonal differences were found in the point clouds and distributions. We observe that in summer we have relatively low daily maxima in wind speed (2-12 m/s), compared to winter daily maxima (2-18 m/s). As summer precipitation intensities are higher than winter precipitation intensities, the trends in FH maxima probably do not necessarily match to trends in the most extreme (summer) precipitation. Besides, the explanation of intensification of precipitation by decreasing wind speeds is not understood from theory. For temperature, dewpoint temperature and CAPE we did observe relatively high maxima for summer compared to winter. The comparison of the first period with the second period clearly shows a shift of the temperature and dewpoint temperature distributions towards higher values. Regarding wind speeds the winter maxima have decreased in frequency, while the summer maxima have not changed in frequency in time. Between precipitation and temperature or dewpoint temperature we find positive exponential relationships comparable with CC- and super CC-scaling for binned winter and

summer quantiles. For both key variables the timewise shift in the distribution to higher summer and winter T and TD maxima and lower winter FH maxima is stronger than changes in their relationships with P. Due to the limited period of CAPE measurements, we have not analysed the same time related changes for this variable. However, the potential of CAPE trends to explain the trends in intensification of precipitation is thought to be small, as the correlation for CAPE maxima with precipitation maxima is the lowest of the four key variables and the sign of the significant trends in CAPE does not match theory in explaining trends in precipitation intensity.

All in all, it is more likely that the detected trends in precipitation intensity are caused by shifting of (dewpoint) temperature distributions towards higher values, than by an intensification of the relationship between precipitation and (dewpoint) temperature. Nonetheless, the latter is also observed for a specific temperature range. For the second half in time the P-T(TD) relationship is namely more in line with a super Clausius-Clapeyron scaling, compared to the first half in time. Complementing to the work of Lenderink (2008,2010,2011) we considered summer and winter relationships separately, which can explain why we did not find the super Clausius-Clapeyron scaling for the entire temperature distribution. This confirms Berg and Haerter (2013a) and Berg and Haerter (2013b) as it is likely that the transition from stratiform precipitation (dominated in winter) to convective precipitation (dominated in summer) with temperature accounts for the super Clausius-Clapeyron scaling between (dewpoint) temperature and precipitation in a significant way.

Moreover, from theory we know that warmer air needs a higher pressure to reach the same saturation than colder air with the same moisture content Chapter 6.2.1,and therefore we expected less (2-day) hours in which saturation is reached in a warmer atmosphere. This is in line with our findings, as we detected negative trends in the frequency of wet hours. Besides, compared to the past more can currently precipitate out of the warmer air column under extreme conditions due to the higher moisture-holding capacity, which supports the observed positive trends in the hourly intensities of heavy precipitation.

7.3 Strengths and relevance

In this part we describe the strengths of this study and how the results attribute to the current knowledge base (add?: of this field). First of all, the instrument type, setting and associated historical changes of precipitation measurements are precisely documented.

Complementing research of Buishand and Brandsma (2013), in which analysis of daily precipitation showed spatial differences, this study provides evidence that precipitation extremes are strongly spatial dependent on the hourly level.

Moreover, this study has uncovered multiple significant trends in precipitation characteristics, which could not have been found from the more commonly used daily precipitation data. The detected positive trends in precipitation intensity and negative trends in frequency of wet hours confirm theory related to the Clausius-Clapeyron equation (Pall and Stone, 2007; Lenderink and Van Meijgaard, 2010; Hardwick Jones and Sharma, 2010; Lenderink and Van Oldenborgh, 2011; IPCC, 2013). As the trend analysis consist of 5 Dutch stations representative for all parts of the Netherlands, the robustness of the observed trends is large. Besides, due to the use of quantile regression we could compare the trends of the different stations for the same part (here the extreme part) of the distribution. Unlike the peak-over-threshold approach, the quantile regression approach provides fits that are independent of spatial differences in probability density functions of precipitation data, so that we can analyze properly the spatial differences in trends.

Additionally, this study allows to verify whether the scaling beyond Clausius-Clapeyron found by Lenderink (2008,2010,2011) may be assigned to mixing of winter and summer dominated processes or to climate change. The importance of studying winter and summer extremes separately is revealed in this thesis and by analyzing summer and winter extremes on hourly resolution more

detail is given on the types of precipitation (local summer precipitation) and how much and why these types changes. More insight into the mechanisms behind the trends is gained by thoroughly investigating multiple potential causes from theory, strength of correlations, trend analysis and timewise comparison of distribution and relationship changes. Several important key variables for changes in precipitation are discovered and classified on type of relationship and strength.

7.4 Limitations

The major limitations of this research are discussed in this section. Station data is used for this thesis, which gives spatially limited information. Due to temporal limitation in hourly data, only one station per part of the country (e.g. northwest, central, southwest, southeast and northeast) is used. Next to the horizontal point of view, station data is also limited regarding the precipitation processes. Mainly processes regarding precipitation accumulation are captured, as we solely have point measurements at the surface. Thus, we do not possess information about the conditions for precipitation production, which restricts our investigation into the causes of trends in precipitation characteristics.

Furthermore, we did not homogenize our data set due to multiple reasons described in Chapter 2, which can give an bias regarding the detection of trends. Note, that this bias is assumed to be negligible, as we did not find jumps in our data related to historical changes (Chapter 2).

The independent (2-day) period we chose can still involve some autocorrelation, although in magnitude and from physical objective this is expected to be relatively small. However, we did not investigate the autocorrelation and partial autocorrelation of 2-day precipitation sums, which might have relatively more autocorrelation as it considers precipitation at a larger temporal scale.

Regarding our method of testing significance, we could doubt whether a random resampling of 9999 times is sufficient to represent well all possible outcomes in slopes. A higher number would, however, require undesirable amounts of computation power. Moreover, we could question for which confidence level, a trend is significant. Is a trend significant at the 95% confidence level trustworthy enough? In this study we do not classify the significance of a trend with respect to the type of confidence level used. However, according to Huth and Dubrovský (2016) it is often forgotten in Climate Science that insignificance of trends does not necessarily hold that those trends are not present. Therefore, we want to stress the importance of considering the general sign in all the trends, next to detecting significant trends for time series with a sufficient sample size.

In the analysis of causes behind the observed trends we did not disentangle the (independent) contribution of every key variable in its relationship with precipitation. Temperature namely influences dewpoint temperature and CAPE. Besides, wind speed is the result of a horizontal temperature-related pressure gradient and CAPE-associated convergence of air. Finally, regarding our investigation of the causes behind the detected trends we could argue about whether we can actually determine causality. However, we do state our explanatory relationships with a likelihood. We did not specify the degree of likelihood, as this is a difficult task.

7.5 Recommendations

In this section recommendations for future research are briefly listed, considering data quality, type of data, way of analysis and interpretation, and the potential of scaling up the research.

First, we recommend an extension of the data quality study. This would involve a more thorough investigation of homogenization techniques for hourly data. Moreover, a clear overview of the instrument types, settings and associated historical changes for all measured variables, similar as has been reported here for precipitation (Chapter 2), would help by analyzing the data quality more intensively.

Second, by integrating this research with satellite and/or radar observations the influence of the large-scale settings (i.e. the presence of a meso-scale mid-tropospheric trough or extratropical cyclone or the presence of large-scale wind shear) on precipitation extremes can be studied. Data corresponding to the exact (horizontal and vertical) location and time of precipitation production would complement the data corresponding to the location of precipitation accumulation regarding processes of precipitation formation. So combining hourly rain gauge data with high-resolution spatial and temporal data can improve our understanding about the observed changes in precipitation characteristics in time. Furthermore, we could then test the effect of the resolution of these type of observations (f.e. radar observations are on the order of one to tens of km's) on the ability to capture local extreme precipitation events. Other opportunities for data with a high spatial resolution are the monitoring of the concentration (and type) of CCNs and including more spatial-dependent variables (e.g. soil and altitude) into the analysis of the causes of the detected trends.

Third, a best fit of predictors could be found with a multiple regression technique that is adjusted for multidisciplinary. The found statistics associated with extreme precipitation could be compared to models to validate whether they are able to model extremes in precipitation. Besides, more extensive analysis of precipitation production processes could help to improve the physics within the models. For example, when models are able to simulate the microphysical processes in clouds better, we would gain understanding regarding the causes behind the observed seasonal and spatial trends.

A fourth recommendation for future research is to investigate the spatial dependency of the precipitation trends in more detail for the latest 10-25 years, by adding more stations, as well as satellite and radar observations.

Fifth, in stead of differentiating trends based on season, we could argue to differentiate trends based on type of precipitation systems (e.g. convective versus stratiform). This would give more detailed information about the mechanism behind the observed trends. Including high resolution, synoptic data would allow for disentangling convective from stratiform precipitation.

Sixth, another possibility to complement on the present work is to classify the significance of a certain trend to the type of confidence level used. This would allow for specification into likelihood classes, similar as is carried out in the assessment reports of the IPCC.

Seventh, it would be very interesting to study whether the observed negative signal in frequency of wet hours corresponds to a general negative trend in the amount of wet events or whether the events have become shorter in time. This could be studied by classifying of the hourly data into wet events, which can be deduced from the hourly duration and the sequencing of wet hours in time. It is likely that the amount of wet events decreases in time, as this would match a Clausius-Clapeyron scaling with higher pressures needed for saturation to occur at higher temperatures, resulting in a decreasing possibility of saturation (and thus of wet events).

Eighth, to enlarge the relevancy of the results, we could also apply trend analysis on impacting events. These events can be selected on basis of thresholds, possibly differentiating between "threshold" classes of extreme events on the type of damage (e.g. sewage overflow, traffic delay and agriculture) associated with the intensity of such an event. For trends in hourly intensities > 10 mm/hr to be detected as significant more data is needed. However, as described in 7.4 the sign and magnitude of this class of trends can give relevant information, without the need for significance (Huth and Dubrovský, 2016). Especially in this case, where a lack a wet hours corresponding to the high threshold is likely to be the cause of the insignificance.

Our ninth recommendation for future research is linked to the analysis of CAPE data. A study into the effect of the resolution decrease in CAPE data (e.g. from a mean of 4 times a day to 1 a day) in the course of time, would give more information about the validity of the detected negative trends in CAPE for the period 1993-2015. Furthermore, analyzing trends in precipitation for the same period as trends in CAPE allows for a more correct way of comparison between the two type of data. Additionally, including data of Convective Inhibition (CIN) and implementing the restriction that CAPE $>$ CIN for CAPE to be larger than 0, would give a better indication of the actual potential of vertical motion.

Last but not least, applying similar trend analysis on hourly precipitation data for other European countries enables validation of the robustness of the detected trends. Besides, spatial differences in trends could be investigated on a larger scale. As increases in the precipitation extremes following the Clausius-Clapeyron relationship are limited by moisture, we expect to find a North-South gradient in the trends for Europe.

Chapter 8

Conclusions

The main conclusions of this study and their implications for current and future research are listed in this chapter. This research has revealed large spatial and seasonal differences for hourly precipitation extremes in the Netherlands. Therefore, we considered trends differentiated on station and season. In general, in the summer season precipitation is more short-lasting and intensive, compared to the winter.

Trend analysis performed on the precipitation data for independent 2-day periods has revealed positive signals for intensity maxima, negative signals for frequency of wet hours and constant to positive signals for precipitation sums. Multiple trends are significant ($p > 0.95$ in a permutation test based on 9999 Monte Carlo resamplings) showing a robust increase of the 25-5% highest intensity maxima (on the order of 0.1-0.6%/yr or in 58 years 0.5-2.3 mm/hr for all to summer-only maxima), a decrease in the mean frequency of wet hours (-0.08 to -0.29%/yr) and in the frequency of wet hours of the 25-5% wettest 2-days (-0.1 to -0.6%/yr or in 58 years -0.5-3 hr/day) and a constant to increasing signal in mean (-0.29 to 0.31%/yr) and highest 10-1% precipitation sums (0.05-0.25%/yr or in 58 years 1.2-2.7 mm/2 days).

Considering the seasonal dependence of precipitation intensity and the comparison between all and season-only trends in maxima, we are led to the conclusion that the trends in the "high" extremes are likely to be summer trends. Despite the robustness in sign of the trends for each precipitation characteristic, spatial differences exist in the magnitude and number of significant trends. This is striking for a small country as the Netherlands.

Our study confirms previous findings (IPCC, 2013) that the "high" extremes increase in a disproportional way (e.g. stronger and more significant trends), compared to the yearly mean and "low" extremes. All the trends show dissimilarity in the significance of quantiles fits per station and per season, which is more likely to be the result of the way quantile regression works (e.g. the quantile fits for one station are independent from each other), than the result of changes in physical processes.

We are led to the conclusion that the detected trends in precipitation trends are likely caused by a shift in the (dewpoint) temperature distributions via an increase of the atmospheric moisture holding capacity. This confirms the Clausius-Clapeyron equation and our expectation that more moisture in a column of air results in more precipitation that rains out in an extreme event (Chapter 1). So, global warming likely induces the positive trend in the intensity of extreme hourly precipitation. In Chapter 6.2.1 we stated that warmer air needs a higher pressure to reach the same saturation than colder air with the same moisture content. This is in line with a negative trend in the frequency of wet hours (e.g. hours in which saturation is reached) for a warming of the atmosphere in time.

This research could be improved and extended in several ways. By integrating the hourly rain gauge data with satellite and/or radar observations convective and stratiform precipitation can be disentangled and other synoptic information will be provided about the spatial-dependent processes behind precipitation and the observed changes. Both satellite/radar observations, and model data can be tested (by comparing to the observed statistics of the in-situ data) on their ability to capture local extreme precipitation. Promising for future research is the potential to find a more regional to continental (European) signal, by applying the same kind of trend analysis on hourly data of other European station, which could reveal a North-South gradient in precipitation trends.

References

Aceituno, P. (1989). "On the functioning of the Southern Oscillation in the South American sector. Part II. Upper-air circulation". In: *Journal of Climate* 2.4, pp. 341–355.

Adams, D.K. and E.P. Souza (2009). "CAPE and convective events in the southwest during the North American monsoon". In: *Monthly Weather Review* 137.1, pp. 83–98.

Ahrens, C.D. (2012). *Meteorology today: an introduction to weather, climate, and the environment*. Cengage Learning.

Allen Myles, R. and W. J Ingram (2002). "Constraints on future changes in climate and the hydrologic cycle". In: *Nature* 419.6903, pp. 224–232.

Anagnostou, E.N. (2004). "A convective/stratiform precipitation classification algorithm for volume scanning weather radar observations". In: *Meteorological Applications* 11.4, pp. 291–300.

Artusi, R., P. Verderio, and E. Marubini (2002). "Bravais-Pearson and Spearman correlation coefficients: meaning, test of hypothesis and confidence interval". In: *Int J Biol Markers* 17.2, pp. 148–151.

Atkinson, B. W. (1989). *Meso-scale atmospheric circulations*. Academic press.

Barry, R.G. and A.M. Carleton (2001). *Synoptic and dynamic climatology*. Psychology Press.

Basist, A., G.D. Bell, and V. Meentemeyer (1994). "Statistical relationships between topography and precipitation patterns". In: *Journal of climate* 7.9, pp. 1305–1315.

Berg P., Moseley C. and J.O. Haerter (2013a). "Strong increase in convective precipitation in response to higher temperatures". In: *Nature Geoscience* 6.3, pp. 181–185.

Berg, P. and J.O. Haerter (2013b). "Unexpected increase in precipitation intensity with temperatureA result of mixing of precipitation types?" In: *Atmospheric Research* 119, pp. 56–61.

Bergeron, T. (1968). *Studies of the Orogenic Effect on the Areal fine Structure of Rainfall Distribution*. Tech. rep. 6. Uppsala University. Meteorological Institute.

Besselaar E.J.M., Klein Tank A.M.G. Van den and T.A. Buishand (2013). "Trends in European precipitation extremes over 1951–2010". In: *International Journal of Climatology* 33.12, pp. 2682–2689.

Biggerstaff, M.I. and R.A. Houze Jr (1991). "Kinematic and precipitation structure of the 10-11 June 1985 squall line". In: *Monthly weather review* 119.12, pp. 3034–3065.

Bolton, B. (1980). "The computation of equivalent potential temperature". In: *Mon. Wea. Rev.* 108, pp. 1046–1053.

Bonan, G. (2015). *Ecological climatology: concepts and applications*. Cambridge University Press.

Bosart, L.F., W.E. Bracken, and A. Seimon (1998). "A study of cyclone mesoscale structure with emphasis on a large-amplitude inertia-gravity wave". In: *Monthly weather review* 126.6, pp. 1497–1527.

Braak, C. (1945). "Influence of the wind on rainfall measurements". In: *KNMI, De Bilt, Mededelingen en Verhandelingen* 48.

Bracken, W.E. and L.F. Bosart (2000). "The role of synoptic-scale flow during tropical cyclogenesis over the North Atlantic Ocean". In: *Monthly weather review* 128.2, pp. 353–376.

Brandsma, T. (2014). "Comparison of automatic and manual precipitation networks in the Netherlands". In:

Brauer, Claudia (2007). "Relatie tussen extreme neerslag en atmosferische ciculatie". MA thesis.

Browning, K.A. (1964). "Airflow and precipitation trajectories within severe local storms which travel to the right of the winds". In: *Journal of the Atmospheric Sciences* 21.6, pp. 634–639.

Buishand T.A., De Martino G. Spreeuw J.N. and T. Brandsma (2013). "Homogeneity of precipitation series in the Netherlands and their trends in the past century". In: *International journal of climatology* 33.4, pp. 815–833.
Buishand, T.A. (1988). "Correctie pluviograafwaarnmingen". In: *KNMI Memorandum* FM-88-28.
Carvalho, L.M.V., C. Jones, and B. Liebmann (2002). "Extreme precipitation events in S.E. South America and large-scale convective patterns in the S. Atlantic convergence zone". In: *Journal of Climate* 15.17, pp. 2377–2394.
CFA. *Time-series Analysis*. https://www.google.nl/url?sa=t&rct=j&q=&esrc=s&source=web&cd=3&ved=0ahUKEwic7 (as visited on 10 June 2016).
Chok, N.S. (2010). "Pearson's versus Spearman's and Kendall's correlation coefficients for continuous data". PhD thesis. University of Pittsburgh.
Cohen, B.H. and R.B. Lea (2004). *Essentials of statistics for the social and behavioral sciences*. Vol. 3. John Wiley & Sons.
Cramer W., Yohe G.W. Auffhammer M. Huggel C. Molau U. da Silva Dias M.A.F. Solow A. Stone D.A. and L. Tibig (2014). "Detection and attribution of observed impacts". In: In: Climate Change 2014: Impacts, Adaptation, and Vulnerability. Part A: Global and Sectoral Aspects. Contribution of Working Group II to the Fifth Assessment Report of the Intergovernmental Panel on Climate Change. Cambridge University Press,Cambridge,United Kingdom and New York, NY, USA, pp. 979–1037.
Cushman-Roisin, B. and J. Beckers (2011). *Introduction to geophysical fluid dynamics: physical and numerical aspects*. Vol. 101. Academic Press.
Dai, A. (2001). "Global precipitation and thunderstorm frequencies. Part I: Seasonal and interannual variations". In: *Journal of climate* 14.6, pp. 1092–1111.
Daniels E.E., Lenderink G. Hutjes R.W.A. and A.A.M. Holtslag (2014). "Spatial precipitation patterns and trends in The Netherlands during 1951–2009". In: *International journal of climatology* 34.6, pp. 1773–1784.
Denkema, A. (1980). "Results of comparative measurements with various types of pluviometers during the period of December 1971 to January 1975 at De Bilt, Netherlands (in Dutch)". In:
— (1981). "Results of comparative measurements in the Foppenpolder (Maasland), Netherlands (in Dutch)". In:
Freitas L., Pereira-M.G.-Caramelo L. Mendes M. and L.F. Nunes (2013). "Homogeneity of monthly air temperature in Portugal with HOMER and MASH". In: *Idojaras* 117.1, pp. 69–90.
Gandu, A.W. and P.L. Silva Dias (1998). "Impact of tropical heat sources on the South American tropospheric upper circulation and subsidence". In: *Journal of geophysical research* 103.D6, pp. 6001–6015.
Grimm, A.M. and P.L. Silva Dias (1995). "Analysis of tropical-extratropical interactions with influence functions of a barotropic model". In: *Journal of the Atmospheric Sciences* 52.20, pp. 3538–3555.
Haerter, J.O. and P Berg (2009). "Unexpected rise in extreme precipitation caused by a shift in rain type?" In: *Nature Geoscience* 2.6, pp. 372–373.
Hardwick Jones R., Westra S. and A. Sharma (2010). "Observed relationships between extreme sub-daily precipitation, surface temperature, and relative humidity". In: *Geophysical Research Letters* 37.22.
Hobbs, P.V. (1993). *Aerosol-cloud-climate interactions*. Vol. 54. Academic Press.
Hobbs, P.V., R.A. Houze Jr, and T.J. Matejka (1975). "The dynamical and microphysical structure of an occluded frontal system and its modification by orography". In: *Journal of the Atmospheric Sciences* 32.8, pp. 1542–1562.
Hoerling, M.P. and A. Kumar (2000). *Understanding and predicting extratropical teleconnections related to ENSO*. Cambridge University Press.
Hoose, C. et al. (2008). "The global influence of dust mineralogical composition on heterogeneous ice nucleation in mixed-phase clouds". In: *Environmental Research Letters* 3.2, p. 025003.
Houze, R.A. (2012). "Orographic effects on precipitating clouds". In: *Reviews of Geophysics* 50.1.
Houze Jr, R.A. (1997). "Stratiform precipitation in regions of convection: A meteorological paradox?" In: *Bulletin of the American Meteorological Society* 78.10, pp. 2179–2196.

Houze Jr, R.A. (2014). *Cloud dynamics*. Vol. 104. Academic press.
Huo, L. et al. (2013). *Testing for Autocorrelation in Quantile Regression Models*. Tech. rep.
Huth, R. and M. Dubrovský (2016). "Assessing significance of trends using counts of signs of the trends as test statistic". In: *Proceedings of the 16th EMS Annual Meeting & 11th European Conference on Applied Climatology (ECAC)*. Vol. 13. 229, pp. 617–628.
Ingram, W.J. (2002). "On the robustness of the water vapor feedback: GCM vertical resolution and formulation". In: *Journal of Climate* 15.9, pp. 917–921.
IPCC (2013). *Climate Change 2013: The Physical Science Basis. Contribution of Working Group I to the Fifth Assessment Report of the Intergovernmental Panel on Climate Change*. Cambridge, United Kingdom and New York, NY, USA: Cambridge University Press, 1535 (in particular: p. 134,205,209,213). ISBN: ISBN 978-1-107-66182-0. DOI: 10.1017/CBO9781107415324. URL: www.climatechange2013.org.
Klein Tank, AMG and GP Können (2003). "Trends in indices of daily temperature and precipitation extremes in Europe, 1946-99". In: *Journal of Climate* 16.22, pp. 3665–3680.
Klein Tank A.M.G., Wijngaard J.B. Können G.P. Böhm-R. Demarée G. Gocheva A. Mileta M. Pashiardis S. Hejkrlik L. Kern-Hansen C. et al. (2002). "Daily dataset of 20th-century surface air temperature and precipitation series for the European Climate Assessment". In: *International journal of climatology* 22.12, pp. 1441–1453.
KNMI (2000a). *Handboek Waarnemingen*. http://www2.knmi.nl/samenw/hawa/pdf/Handboek_H06.pdf(as visited on 21 June 2016).
— (2000b). *Handbook for the Meteorological Observation*. http://www2.knmi.nl/samenw/hawa/pdf/Handbook_H01_H06.pdf(as visited on 22 June 2016).
Koenker, R. *Package quantreg: Quantile regression*. https://cran.r-project.org/web/packages/quantreg/quantreg.pdf (as visited on 1 June 2016).
— (2005). *Quantile regression*. 38. Cambridge university press.
Koenker, R. and G. Bassett Jr (1978). "Regression quantiles". In: *Econometrica: journal of the Econometric Society*, pp. 33–50.
Koenker, R. and V. d'Orey (1994). "Remark AS R92: A remark on algorithm AS 229: Computing dual regression quantiles and regression rank scores". In: *Journal of the Royal Statistical Society. Series C (Applied Statistics)* 43.2, pp. 410–414.
Koenker, R. and P. Ng (2005). "A Frisch-Newton algorithm for sparse quantile regression". In: *Acta Mathematicae Applicatae Sinica* 21.2, pp. 225–236.
Koenker, R.W. and V. d'Orey (1987). "Algorithm AS 229: Computing regression quantiles". In: *Journal of the Royal Statistical Society. Series C (Applied Statistics)* 36.3, pp. 383–393.
Koetse, M.J. and P. Rietveld (2009). "The impact of climate change and weather on transport: An overview of empirical findings". In: *Transportation Research Part D: Transport and Environment* 14.3, pp. 205–221.
Korolev, A. (2007). "Limitations of the Wegener-Bergeron-Findeisen mechanism in the evolution of mixed-phase clouds". In: *Journal of the Atmospheric Sciences* 64.9, pp. 3372–3375.
Korolev, A.V. and G.A. Isaac (2000). "Drop growth due to high supersaturation caused by isobaric mixing". In: *Journal of the atmospheric sciences* 57.10, pp. 1675–1685.
Krennert T., et al. (2016). *Manual of Synoptic Satellite Meteorology, Conceptual models and Case Studies*. 6.8. http://www.zamg.ac.at/docu/Manual/SatManu/main.htm?/docu/Manual/(as visited on 16 May 2016). ZAMG,KNMI,FMI,DHMZ,IM and EUMETSAT.
Lawrence, M.G. (2005). "The relationship between relative humidity and the dewpoint temperature in moist air: A simple conversion and applications". In: *Bulletin of the American Meteorological Society* 86.2, pp. 225–233.
Lee, A.C.L. (1986). "An experimental study of the remote location of lightning flashes using a VLF arrival time difference technique". In: *Quarterly Journal of the Royal Meteorological Society* 112.471, pp. 203–229.
Lenderink, G., E. van Meijgaard, and F. Selten (2009). "Intense coastal rainfall in the Netherlands in response to high sea surface temperatures: analysis of the event of August 2006 from the perspective of a changing climate". In: *Climate dynamics* 32.1, pp. 19–33.

Lenderink, G. and E. Van Meijgaard (2008). "Increase in hourly precipitation extremes beyond expectations from temperature changes". In: *Nature Geoscience* 1.8, pp. 511–514.
— (2010). "Linking increases in hourly precipitation extremes to atmospheric temperature and moisture changes". In: *Environmental Research Letters* 5.2, p. 025208.
Lenderink G., Mok H.Y. Lee T.C. and G.J. Van Oldenborgh (2011). "Scaling and trends of hourly precipitation extremes in two different climate zones–Hong Kong and the Netherlands". In: *Hydrology and Earth System Sciences* 15.9, pp. 3033–3041.
Leng, L. et al. (2007). "Ordinary least square regression, orthogonal regression, geometric mean regression and their applications in aerosol science". In: 78.1, p. 012084.
Li, Z. et al. (2011). "Long-term impacts of aerosols on the vertical development of clouds and precipitation". In: *Nature Geoscience* 4.12, pp. 888–894.
Lin, Yuh-Lang (2007). *Mesoscale dynamics*. Cambridge University Press, Cambridge.
Loriaux J.M., Lenderink G. De Roode S.R. and A.P. Siebesma (2013). "Understanding convective extreme precipitation scaling using observations and an entraining plume model". In: *Journal of the atmospheric sciences* 70.11, pp. 3641–3655.
Łupikasza, E. (2016). "The Climatology of Air-Mass and Frontal Extreme Precipitation". In:
Maddox, R.A., C.F. Chappell, and L.R. Hoxit (1979). "Synoptic and meso-α scale aspects of flash flood events". In: *Bulletin of the American Meteorological Society* 60.2, pp. 115–123.
Malik, N., B. Bookhagen, and P.J. Mucha (2016). "Spatiotemporal patterns and trends of Indian monsoonal rainfall extremes". In: *Geophysical Research Letters* 43.4, pp. 1710–1717.
Markowski, P. and Y. Richardson (2010). *Mesoscale Meteorology in Midlatitudes*. 1st ed. Willey-Blackwell.
Mason, B.J. (1972). "The Bakerian lecture, 1971: The physics of the thunderstorm". In: *Proceedings of the Royal Society of London. Series A, Mathematical and Physical Sciences* 327.1571, pp. 433–466.
McCaul Jr, E.W and M.L. Weisman (2001). "The sensitivity of simulated supercell structure and intensity to variations in the shapes of environmental buoyancy and shear profiles". In: *Monthly weather review* 129.4, pp. 664–687.
Miller, S. (2015). *Applied Thermodynamics for Meteorologists*. Cambridge University Press.
Monkam, D. (2002). "Convective available potential energy (CAPE) in Northern Africa and tropical Atlantic and study of its connections with rainfall in Central and West Africa during Summer 1985". In: *Atmospheric research* 62.1, pp. 125–147.
Morrison, H., G. Thompson, and V. Tatarskii (2009). "Impact of cloud microphysics on the development of trailing stratiform precipitation in a simulated squall line: Comparison of one-and two-moment schemes". In: *Monthly Weather Review* 137.3, pp. 991–1007.
Newton, C.W. (1950). "Structure and mechanism of the prefrontal squall line". In: *Journal of meteorology* 7.3, pp. 210–222.
Office, The Met. (1997). "Convection and Showers". In: In: UK Met Office Forecasters Reference Book. London Rd, Bracknell, Berkshire: Meteorological Office College, UK Met Office. Chap. 4.
Pall P., Allen M.R. and D.A. Stone (2007). "Testing the Clausius–Clapeyron constraint on changes in extreme precipitation under CO2 warming". In: *Climate Dynamics* 28.4, pp. 351–363.
Pierrehumbert R.T., Brogniez H. and R Roca (2007). "On the Relative Humidity of the Atmosphere". In: In: The General Circulation [Scheider, T., Sobel, A.] Princeton, NJ: Princeton University Press. Chap. 6.
Pruppacher, Hans R, James D Klett, and Pao K Wang (1998). "Microphysics of clouds and precipitation". In:
Raible, C.C. et al. (2007). "Extreme midlatitude cyclones and their implications for precipitation and wind speed extremes in simulations of the Maunder Minimum versus present day conditions". In: *Climate Dynamics* 28.4, pp. 409–423.
Rangno, A.L. and P.V. Hobbs (2005). "Microstructures and precipitation development in cumulus and small cumulonimbus clouds over the warm pool of the tropical Pacific Ocean". In: *Quarterly Journal of the Royal Meteorological Society* 131.606, pp. 639–673.

Rosenzweig C., Tubiello F.N. Goldberg R. Mills E. and J. Bloomfield (2002). "Increased crop damage in the US from excess precipitation under climate change". In: *Global Environmental Change* 12.3, pp. 197–202.

Roth M., Buishand T.A. and G. Jongbloed (2015). "Trends in Moderate Rainfall Extremes: A Regional Monotone Regression Approach". In: *Journal of Climate* 28.22, pp. 8760–8769.

Rulfová, Zuzana and Jan Kyselỳ (2013). "Disaggregating convective and stratiform precipitation from station weather data". In: *Atmospheric Research* 134, pp. 100–115.

Santer, B.D. et al. (2008). "Consistency of modelled and observed temperature trends in the tropical troposphere". In: *International Journal of Climatology* 28.13, pp. 1703–1722.

Schultz, D.M. (2005). "A review of cold fronts with prefrontal troughs and wind shifts". In: *Monthly weather review* 133.8, pp. 2449–2472.

Schultz, D.M. and G. Vaughan (2011). "Occluded fronts and the occlusion process: A fresh look at conventional wisdom". In: *Bulletin of the American Meteorological Society* 92.4, p. 443.

Schumacher, R.S. and R.H. Johnson (2005). "Organization and environmental properties of extreme-rain-producing mesoscale convective systems". In: *Monthly weather review* 133.4, pp. 961–976.

Sen Roy, S. (2009). "A spatial analysis of extreme hourly precipitation patterns in India". In: *International Journal of Climatology* 29.3, pp. 345–355.

Sen Roy, S. and R.C. Balling (2004). "Trends in extreme daily precipitation indices in India". In: *International Journal of climatology* 24.4, pp. 457–466.

Service, NOAA's National Weather. *SVR PARAMETERS*. `http://www.weather.gov/media/lmk/soo/svr_parameters.pdf`(as visited on 20 May 2016).

Shulman, M.L. et al. (1996). "Dissolution behavior and surface tension effects of organic compounds in nucleating cloud droplets". In: *Geophysical Research Letters* 23.3, pp. 277–280.

Smits A.A.K.T., Klein Tank A.M.G. and G.P. Können (2005). "Trends in storminess over the Netherlands, 1962–2002". In: *International Journal of Climatology* 25.10, pp. 1331–1344.

Smits I., Wijngaard J.B. Versteeg R.P. and M. Kok (2004). *Statistiek van extreme neerslag in Nederland*. Tech. rep. 26. `http://www2.knmi.nl/publications/fulltexts/senn_eindrapportage_20041012_copy2.pdf` (as visited on 18 May 2016. Stichting Toegepast Onderzoek Waterbeheer (STOWA), p. 94.

Srinivasan, K. "'Small Area Estimations'". http://www.isec.ac.in/small_area_est%20rev.pdf (as visited on 3 June 2016).

Sumner, G. (1988). *Precipitation, Process and Analysis*. John Wily and Sons Ltd.

Ter Maat, H.W. et al. (2013). "Exploring the impact of land cover and topography on rainfall maxima in the Netherlands". In: *Journal of Hydrometeorology* 14.2, pp. 524–542.

Thompson, R. *EXPLANATION OF SPC SEVERE WEATHER PARAMETERS*. `http://www.spc.noaa.gov/exper/mesoanalysis/help/begin.html`(as visited on 20 May 2016).

Trenberth K.E., Dai A. Rasmussen R.M. and D.B. Parsons (2003). "The changing character of precipitation". In: *Bulletin of the American Meteorological Society* 84.9, pp. 1205–1217.

Trenberth, K.E. (1999). "Conceptual framework for changes of extremes of the hydrological cycle with climate change". In: *Weather and Climate Extremes*. Springer, pp. 327–339.

— (2011). "Changes in precipitation with climate change". In: *Climate Research* 47.1, p. 123.

Velasco, I. and J.M. Fritsch (1987). "Mesoscale convective complexes in the Americas". In: *Journal of Geophysical Research: Atmospheres* 92.D8, pp. 9591–9613.

Von Storch, H. and F.W. Zwiers (1999). *Statistical analysis in climate research*. Cambridge University Press, United Kingdom and New York, NY, USA, 484 pp.

Wallace, J.M. and P.V. Hobbs (2006). *Atmospheric Science: an introductory survey*. 2nd ed. Academic Press.

Wapler, K. and T.P. Lane (2012). "A case of offshore convective initiation by interacting land breezes near Darwin, Australia". In: *Meteorology and Atmospheric Physics* 115.3-4, pp. 123–137.

Warmerdam, P.M.M. (1981). "De invloed van de wind op regenwaarnemingen: een vergelijkend regenmeteronderzoek". In: H_2O 14, pp. 16–20.

Wasko, C. and A. Sharma (2014). "Quantile regression for investigating scaling of extreme precipitation with temperature". In: *Water Resources Research* 50.4, pp. 3608–3614.

Wauben, W.M.F. (2004). *Precipitation amount and intensity measurements with the Ott Pluvio*. Koninklijk Nederlands Meteorologisch Instituut.

Weisman, M.L. and J.B. Klemp (1982). "The dependence of numerically simulated convective storms on vertical wind shear and buoyancy". In: *Monthly Weather Review* 110.6, pp. 504–520.

Wilks, D.S. (2011). *Statistical methods in the atmospheric sciences*. 2nd ed. Vol. 100. Philadelphia, United States: Elsevier, 627 pp.

Wingo, M.T. and D.J. Cecil (2010). "Effects of vertical wind shear on tropical cyclone precipitation". In: *Monthly Weather Review* 138.3, pp. 645–662.

Yue, S. et al. (2002). "The influence of autocorrelation on the ability to detect trend in hydrological series". In: *Hydrological Processes* 16.9, pp. 1807–1829.

Zhai P., Zhang X. Wan H. Pan X. (2005). "Trends in total precipitation and frequency of daily precipitation extremes over China". In: *Journal of climate* 18.7, pp. 1096–1108.

Zhang X., Vincent L.A. Hogg W.D. and A. Niitsoo (2000). "Temperature and precipitation trends in Canada during the 20th century". In: *Atmosphere-ocean* 38.3, pp. 395–429.

Zou, K.H., K. Tuncali, and S.G. Silverman (2003). "Correlation and simple linear regression 1". In: *Radiology* 227.3, pp. 617–628.